ISTANBUL TECHNICAL UNIVERSITY ★ ENERGY INSTITUTE

POROSITY GENERATION AND OPTIMIZATION OF SILICON-BASED ANODES FOR HIGH ENERGY DENSITY LITHIUM ION BATTERIES

Ph.D. THESIS

Neslihan YUCA

Energy Science and Technology Division
Energy Science and Technology Programme

JULY 2017

ISTANBUL TECHNICAL UNIVERSITY ★ ENERGY INSTITUTE

POROSITY GENERATION AND OPTIMIZATION OF SILICON-BASED ANODES FOR HIGH ENERGY DENSITY LITHIUM ION BATTERIES

Ph.D. THESIS

Neslihan YUCA
(301102006)

Energy Science and Technology Division
Energy Science and Technology Programme

Thesis Advisor: Prof. Dr. Üner ÇOLAK

JULY 2017

İSTANBUL TEKNİK ÜNİVERSİTESİ ★ ENERJİ ENSTİTÜSÜ

YÜKSEK ENERJİ YOĞUNLUKLU LİTYUM İYON BATARYALAR İÇİN SİLİSYUM BAZLI ANOTLARDA GÖZENEK GELİŞTİRİLMESİ VE OPTİMİZASYONU

DOKTORA TEZİ

Neslihan YUCA
(301102006)

Enerji Bilim ve Teknoloji Anabilim Dalı
Enerji Bilim ve Teknoloji Programı

Tez Danışmanı: Prof. Dr. Üner ÇOLAK

TEMMUZ 2017

Neslihan Yuca, a Ph.D. student of ITU Institute of Energy student ID 301102006, successfully defended the thesis entitled POROSITY GENERATION and OPTIMIZATION OF SILICON-BASED ANODES FOR HIGH ENERGY DENSITY LITHIUM ION BATTERIES", which she prepared after fulfilling the requirements specified in the associated legislations, before the jury whose signatures are below.

Thesis Advisor :   **Prof. Dr. Üner ÇOLAK**   ....
İstanbul Technical University

Jury Members :   **Prof. Dr. Hatem AKBULUT**   ....
Sakarya University

                              Prof. Dr. Sebahattin GÜRMEN   ....
İstanbul Technical University

                              Prof. Dr. Özgül KELEŞ   …..........................
İstanbul Technical University

                              Assoc. Prof. Dr. Selmiye ALKAN GÜRSEL   ....
Sabancı University

Date of Submission : 23 June 2017
Date of Defense :   31 July 2017

To science,

FOREWORD

First of all, I would like to express my special thanks of gratitude to Prof. Dr. Üner Çolak for guiding me in my dissertation with his large knowledge and experiences in material science. He always has been very positive and patient during my studentship and research. I would like to thank Dr. Gao Liu and Dr. Hui Zhao, from Lawrence Berkeley National Laboratory, who made great contribution on my thesis.

I also thank to Enwair Energy Technologies research group members, who helped and supported me all the time.

Lastly, I would like to thank my family for all their love and encouragement. For my parents, sister and brother who raised me with a love of science and supported me in all my affairs. And most of all for my loving, supportive, and encouraging husband Murat Ferhat whose faithful support during the final stages of this Ph.D. is so appreciated.

I appreciate all the people who support me to assembly 361 coin cells during my thesis.

Thank you.

June 2017   Neslihan YUCA
                                                          (Environmental Engineer, M.Sc.)

TABLE OF CONTENTS

ABBREVIATIONS

AFM	**:**	Atomic Force Microscopy
AES	**:**	Auger Electron Spectroscopy
AM	**:**	Active Material
BET	**:**	Brunauer–Emmett–Teller
CA	**:**	Carbon Additive
CE	**:**	Coulombic Efficiency
CV	**:**	Cyclic Voltammetry
CNT	**:**	Carbon Nanotubes
c-SiO	**:**	Carbon Coated Silicon
CVD	**:**	Chemical Vapor Deposition
DEC	**:**	Diethylene Carbonate
DVS	**:**	Dynamic Vapor Sorption
EC	**:**	Ethylene Carbonate
EDS	**:**	Energy Dispersive Spectroscopy
EDX	**:**	Energy Dispersive X-ray spectroscopy
EIS	**:**	Electrochemical Impedance Spectroscopy
EV	**:**	Electric Vehicle
FEC	**:**	Fluoroethylene Carbonate
FESEM	**:**	Field Emission Scanning Electron Microscopy
FIB	**:**	Focused Ion Beam
FTIR	**:**	Fourier Transform Infrared Spectroscopy
HEMM	**:**	High Energy Ball Milling
HEV	**:**	Hybrid Electric Vehicle
HOMO	**:**	Highest Occupied Molecular Orbital
IL	**:**	Ionic Liquid
LCO	**:**	Lithium Cobalt Oxide
LFP	**:**	Lithium Iron Phosphate
LIBs	**:**	Lithium Ion Batteries
LUMO	**:**	Lowest Unoccupied Molecular Orbital
MIT	**:**	Massachusetts Institute of Technology
MP	**:**	Mercury Intrusion Porosimetry
MWCNT	**:**	Multiwall Carbon Nanotubes
NMC	**:**	Nickel Manganese Cobalt
NMP	**:**	N-Methyl-2-Pyrrolidone
NMR	**:**	Nuclear Magnetic Resonance
n-PAA	**:**	Neutral Poly Acrylic Acid
OCV	**:**	Open Circuit Voltage
OM	**:**	Optical Microscopy
PAA	:	Poly Acrylic Acid
PAN	**:**	Polyacrylonitrile
PFM	**:**	Poly(9,9-dioctylfluorene-co-fluorenone-co-methylbenzoic ester
PMMA	**:**	Poly(methyl methacrylate)
PPy	**:**	Poly(1-pyrenemethyl methacrylate)

PS	**:**	Polystyrene
SEI	**:**	Solid Electrolyte Interphase
SEM	**:**	Scanning Electron Microscopy
SGF	**:**	Si Oxide Coated Graphite Flake
Si-LP	**:**	Silicon Leaf Powder
SiNPs	**:**	Silicon Nano Particulates
SiNWs	**:**	Silicon Nanowires
SP	**:**	Super P
TEM	**:**	Transmission Electron Microscopy
VC	**:**	Vinylene Carbonate
VLS	**:**	Vapor Liquid Solid
XPS	**:**	X-ray Photoelectron Spectroscopy
XRD	**:**	X-ray Diffraction Spectroscopy

LIST OF TABLES

LIST OF FIGURES

POROSITY GENERATION AND OPTIMIZATION OF SILICON-BASED ANODES FOR HIGH ENERGY DENSITY LITHIUM ION BATTERIES

SUMMARY

Energy storage systems are widely used to regulate energy grids and to rehabilitate the energy quality taken from grid by increasing grid realibility. However, at present as a result of the clean energy tendency, developments of the energy storage systems have come to forefront to be able to use for electric/hybrid vehicles and renewable energy sources. Thus, renewable energy sources such as wind energy and solar energy which are not sustainable will be stored when they are available. Then, this stored energy can be used when the energy sources has interruption. This will make it charming by providing the high realibility for renewable sources.

Energy storage technologies are in transformation that power (watt) and energy (watt-hour) can be provided seperetly while it is not possible to produce them enough at the same time. Supercapacitors can provide high power only for seconds and fuel cells can store limited energy in peak powers. This is a big challenge for the modern advanced technologies (smart phones, wearable computer, electrical vehicles etc.) which need high energy and power. Lithium ion batteries (LIB) are the very promising solution for the high energy and power applications. Because LIBs have high energy and power density and light weight when it is compared to any another rechargable batteries. These properties are the reason to use LIBs in mobile phones, laptops, digital camera/video camera and, other electronic equipments. The other advantages of LIBs, when it is compared to lead acid and metal hydride batteries, are high energy efficiency, no memory effect, and relatively long cycle life.

Lithium ion batteries are the energy storage systems which have widely application range. From consumer electronic like; smart phones, tablets, portable computers etc. to electric vehicle, from aerospace applications to military usage, they can be used as an essential equipment in social and political area. So, it has been critical field with a big competition as a result of the importance of the indigenization. Today, nearly all the lithium ion batteries used in consumer electronics, have been produced in Asia and for the electrical vehicles, new technologies are needed. The Unites States of America has been planned to be one of the leader as an electrical vehicle producer with considering the importance of being the local LIBs procuder is critical and they needed long-term plans to be in that competitive market and to be successful. In our country, a couple of universities, institutes and business firms has started to study on LIBs technologies.

The main components of lithium ion batteries are electrolyte, which provides a transferring medium for charged structures such as ions; anode, that is oxidized during the electrochemical reaction, gives electrons to the external circuit, and cathode that is reduced during the electrochemical reaction and takes electrons from external circuit. $LiPF_6$ salt is dissolved in organic solvents such as ethylene carbonate, diethyl carbonate and/or dimethyl carbonate and it is the most widely used electrolyte which is commercially available, however there are intense studies on

solid electrolytes or polymer electrolytes. The cathode materials are metal oxide structures that can react with lithium reversibly to form a host-guest compound. The most important examples that have been commercialized among these structures are lithium cobalt oxide (LCO), lithium iron phosphate (LFP) and nickel manganese cobalt (NMC) composites. At present, graphite is commercially used anode material while silicon, tin, and germanium are widely studied. The theoretical capacities are 4200 mAh/g, 1600 mAh/g, and 999 mAh/g, respectively. The fact that graphite anode active material is currently the most widely used and commercialized product, however, its limited energy density makes high-capacity silicon (Si) based materials as an alternative.

Present commercial anodes are graphite for LIBs. But limited energy density of graphite makes high capacity Si based materials an alternative electrode material. When the theoretical capacity of graphite, 372 mAh/g, is compared to Si based anode electrodes, 4200 mAh/g, it seen that Si based anodes have 11 times higher capacity than graphite. However, Si based anodes have some challenges which need to be overcome. The most important one is the volume change of Si (300% volume change) at the charge and discharge steps. As the result of this volumetric change, anode material has cracks, electrical conductivity is failed, ionic transfer, and the capacity decreases.

The problem of silicon has been tried to solve by developing silicon based composites, synthesizing porous silicon structures, studying polymer binder solutions, or by developing various production methods. Here, prospective solutions were presented with optimized and developed methods for silicon based anode active materials and by using these methods with various polymer binders.

Firstly, the calendaring process, which is an important step in anode production, was carried out for different anode porosity percentages and the most suitable ratio was tried to be found. For the c-SiO/PFM composition, 15% calendering was found as the most suitable ratio and it also studied with the Si/PAA and Si/nPAA compositions, which is a different material and polymer composition. Structural and electrochemical analyses of the obtained anodes are made and the presented contribution is explained. Pycnometry was also used to show the electrode density and pore volume change after calendering process.

Secondly, porous Si based anode was produced by a developed method. Here the main purpose is; to use the Si-based anodes for long cycles with high columbic efficiency. Today, the capacity of commercially available carbon-based anodes is not sufficient for our daily applications (mobile phones and computers) and for electric vehicles which are planned to have widespread use in the future. For this reason, it is necessary to develop high specific capacity and high energy density anodes. Here, on the other hand, it is desired to provide an anode design which can meet these requirements. The c-SiO/PFM composition is desired to be rendered porous form by adding and removing different ratios of the salt to the structure. These porosites, which are created in the anode structure, prevent the deterioration of the integrity of the structure by allowing the volumetric expansion which happens when the lithium enters into the silicon structure. Thus, more stable electrode results can be obtained over longer cycles, even though the high loading active material is coated. In the completed study, the optimum salt rate added and removed from the electrode structure was determined as 30% by weight and the study was also carried out for the Si/PPy anode composition. For the characterization of the porous electrode, SEM, EDS, AFM, pycnometry and mercury porosimeter were used.

As a result of calendering optimization, the optimum calendering ratio was found as 15%.The c-SiO/PFM anode composition reached a loading capacity of 3,5 mAh/cm^2 and a specific capacity of 1250 mAh/g after 100 cycles with 15% calendering. When the same calendaring ratio was applied to the Si/PAA and Si/nPAA anodes, the electrodes exhibited a stable cycle performance and gave a specific capacity of 511 and 1370 mAh/g at the end of the 100th cycle, respectively. Pycnometry results for c-SiO electrode showed increasing electrode density while pore volume was decreasing after increasing calendaring ratio.

In the porosity formation study we conducted, c-SiO/PFM anode working with 10% NaCl gave 3 mAh/cm^2 loading capacity and a specific capacity of 1000 mAh/g after 100 cycles. The c-SiO/PFM anode operated with 30% NaCl gave 4 mAh/cm^2 loading capacity and a specific capacity of 750 mAh/g at 100 cycles. The method was also applied to the Si/PPy anode composition using 30% NaCl. With the Si/PPy anode operating with 30% NaCl, it was reached a specific capacity of 1100 mAh/g at 100 cycles. Structure characterization results also confirmed the porous electrode formation. Under SEM top view and cross section analysis, pores were observed. EDS analysis showed the presence of Cu particles on the electrode surface after washing. AFM results indicated higher roughness value (Ra) after porosity generation. Results of pycnometry and mercury porosimeter were also claimed increasing pore volume and porosity after electrode washing process which provided pores on the electrode structure.

Considering the studies and results presented in this thesis, it is understood that the generated method and performed optimization from this thesis can shed light to commercial usage of Si based materials for lithium ion battery applications.

YÜKSEK ENERJİ YOĞUNLUKLU LİTYUM İYON BATARYALAR İÇİN SİLİSYUM BAZLI ANOTLARIN OPTİMİZASYONU VE POROZİTE OLUŞTURMA METODU

ÖZET

Enerji depolama sistemleri; enerji şebekelerini düzenlemek, şebeke güvenilirliğini artırarak şebekeden alınan elektrik enerjisinin kalitesini iyileştirmek için yaygın olarak kullanılmaktadır. Ancak temiz enerjiye yönelim nedeniyle günümüzde, elektrikli ya da hibrit elektrikli araçlar ile yenilenebilir enerji kaynakları ve bu sistemlerde kullanılacak enerji depolama sistemlerinin geliştirilmesi ön plana çıkmıştır. Bu sayede rüzgâr ve güneş gibi sürekli olarak yararlanma imkanı olmayan yenilenebilir kaynaklardan bu kaynakların mevcut olduğu zamanlarda üretilecek enerjinin depolanarak, kaynakların kesintiye uğradığı zamanlarda kullanılmasına olanak sağlayacak; böylece yenilenebilir enerjinin güvenilirliğini artırarak, kullanımını cazip hale getirecektir.

Günümüzde, enerji depolama teknolojileri ise bir dönüşüm halinde olup, güç (watt) ya da enerji (watt-saat) kolay sağlanabilirken bunların her ikisini birlikte elde etmek mümkün olamamaktadır. Süperkapasitörler, sadece birkaç saniyelik yüksek miktarlarda güç sağlayabilmekte ve yakıt hücreleri pik güçlerde sınırlı olmak şartıyla yüksek miktarda enerji depolayabilir. Bunlar birçok, yüksek miktarda güç ve enerji gerektiren, modern ileri teknolojiler (akıllı telefonlar, giysi bilgisayarlar, elektrikli araçlar gibi) için önemli sorundur. Lityum iyon bataryalar (LIB) günümüzde, yüksek güç ve enerji uygulamaları için en iyi çözümlerdir. Çünkü LIBlar yüksek enerji ve güç yoğunlukları ile diğer şarj edilebilir pillere göre daha hafif ve daha küçüktür. Bu özellikleri, cep telefonları, dizüstü bilgisayarlar, dijital kameralar/video kameralar ve taşınabilir diğer elektronik cihazlarda büyük ölçüde neden kullanıldığını açıklamaktadır. LIB'ların diğer avantajları ise, kurşun asit ve metal hidrür bataryalar ile kıyaslandığında, yüksek enerji verimi, hafıza etkisi olmaması ve kısmen uzun çevrim ömrüne sahip olmalarıdır.

LIB'lar kullanım alanı spektrumu çok geniş olan enerji depolama sistemleridir. Cep telefonları, tabletler, taşınabilir bilgisayarlar gibi tüketici elektroniğinden, elektrikli araçlara, uçak-uzay uygulamalarından askeri uygulamalara, sosyal ve politik birçok alanda önemli bir ekipman olmaktadır. Bu nedenle yerlileşmesine önemle bakılan stratejik bir konu olması nedeniyle de dünyada büyük rekabetin olduğu bir saha haline gelmiştir. Bugün, tüketici elektroniğinde kullanılan lityum iyon bataryaların yaklaşık %90'ı Asya'da üretilmekte ve geleceğin elektrikli araçları için ilave teknolojilere gerek duyulmaktadır. Amerika Birleşik Devletleri, elektrikli araç üretiminde başı çekenlerden olmayı planlaması sebebiyle, yerli bir lityum iyon batarya üreticisinin kritik olduğunu dikkate almış ve rekabetçi bir pazar içinde yeralabilmek ve başarılı olabilmek için uzun dönemli planlara ihtiyaç duymuştur. Ülkemizde de, az sayıda olmakla birlikte, üniversiteler, araştırma kurumları ve ticari firmalar, lityum iyon batarya teknolojileri üzerine çalışmalar yapmaya başlamıştır.

Lityum iyon bataryaların ana bileşenleri, dış devreye elektron sağlayan ve elektrokimyasal reaksiyon sırasında yükseltgenen **anot**, dış devreden elektron kabul eden ve elektrokimyasal reaksiyon sırasında indirgenen **katot** ve iyon gibi yüklü yapıların transferini sağlayan bir ortam olan **elektrolit**tir. Etilen karbonat, dietil karbonat ve/veya dimetil karbonat gibi organik çözücülerde çözünmüş $LiPF_6$ tuzu ticari olarak en yaygın kullanılan elektrolit olmakla birlikte, katı elektrolit ya da polimer elektrolitler üzerinde yoğun çalışmalar bulunmaktadır. Katot malzemeleri, lityumla konak-konuk bileşiği oluşturmak üzere tersinir tepkime verebilen metal oksit yapılardır. Bu yapılar arasında ticarileşmiş olan en önemli örnekleri lityum kobalt oksit (LCO), lityum demir fosfat (LFP) ve nikel mangan kobalt (NMC) kompozitleridir. Anot aktif malzemeleri ise hali hazırda ticari olarak kullanılan grafit olmakla birlikte silisyum, kalay ve germanyum üzerinde çokça çalışılan malzemelerdir. Teorik kapasiteleri ise sırasıyla 4200 mAh/g, 1600 mAh/g, 999 mAh/g'dır. Günümüzün en yaygın kullanılan ve ticarileşmiş neredeyse tek ürünü olan grafit anot aktif malzemesi enerji yoğunluğunun sınırlı olması, yüksek kapasite gösteren silisyum (Si) bazlı malzemeleri alternatif hale getirmektedir. Si bazlı negatif elektrotlar, 372mAh/g teorik kapasiteye sahip grafit anotlarla kıyaslandığında, yaklaşık olarak teorik kapasitesi 4200mAh/g olup 11 kat fazla kapasite sağlayarak ön plana çıkmıştır. Ancak Si bazlı anot malzemelerinin de aşılması gereken bazı sorunları bulunmaktadır. Bunların en önemlisi Si atomlarının şarj-deşarj sırasında Li atomları ile reaksiyonu sonucu hacimce sübvanse edilemez bir şekilde değişmesidir (%300 civarında genişleme görülmektedir.) Bu hacimsel değişiklik sonucunda anot malzemesinde çatlaklar oluşmakta, elektriksel iletkenlik kaybedilmekle beraber, iyon transferindeki azalma, kapasite kaybıyla sonuçlanmaktadır. Silisyumun sahip olduğu bu sorun, silisyum esaslı kompozitler geliştirilerek, gözenekli silisyum yapıları sentezleyerek, polimer bağlayıcı çözümleri üzerine çalışılarak ya da çeşitli üretim metotları geliştirilerek çözülmeye çalışılmaktadır. Bu çalışmada da silisyum bazlı anot aktif malzemeleri, optimize edilen ve geliştirilen yöntemler ile ve bu yöntemlerin çeşitli polimer bağlayıcılar kullanılarak çalıştırılmasına dayanılarak çözümler sunulmuştur.

İlk olarak, anot üretiminde önemli bir adım olan haddeleme prosesi farklı anot porozitesi yüzdeleri için gerçekleştirilmiş olup, en uygun oran bulunmaya çalışılmıştır. c-SiO/PFM bileşimi için en uygun bulunan %15 haddeleme oranı farklı malzeme ve polimer bileşimi olan Si/PAA ve Si/nPAA bileşimleri ile de çalışılmıştır. Elde edilen anotların yapısal ve elektrokimyasal analizleri yapılarak, sunulan katkı açıklanmıştır. Ayrıca haddeleme sonrası elektrot yoğunluğu ve por hacminin değişimi piknometre ile gösterilmiştir.

İkinci olarak ise geliştirilen bir yöntemle, poroz Si bazlı anot üretilmiştir. Buradaki ana amaç; Si bazlı anotların kapasitesini, uzun çevrim sayılarında, kulombik verimi yüksek olarak kullanabilmektir. Günümüzde ticari olarak kullanılan karbon bazlı anotların kapasitesi, günlük uygulamalarımız (cep telefonu ve bilgisayar) için ve gelecekte yaygın bir kullanımı olması planlanan elektrikli araçlar için yeterli değildir. Bu sebeple, yüksek enerji yoğunluğuna sahip ve yüksek spesifik kapasiteli anotlar geliştirilmesi gerekmektedir. Burada yapılmak istenen ise bu ihtiyaçları karşılayabilecek, anot tasarımlarını sağlamaktır. c-SiO/PFM bileşimi, farklı oranlarda tuzun yapıya eklenmesi ve uzaklaştırılması ile poroz hale getirilmek istenmiştir. Anot yapısında sağlanan bu poroziteler, lityumun silisyum yapısına girdiğinde sebep olduğu hacimsel genişlemeye izin vererek, yapının bütünlüğünün bozulmasını önlemektedir. Böylece fazla aktif malzeme yüklenmiş olmasına ragmen, daha uzun çevrimlerde, daha kararlı elektrot sonuçları elde edilebilinmiştir. Yapılan çalışmada

elektrot yapısına eklenip uzaklaştırılan en uygun tuz oranı ağırlıkça %30 olarak tespit edilmiş olup, çalışma Si/PPy anot bileşimi için de çalışılmıştır. Poroz elektrotların karakterizasyonu için SEM, EDS, AFM, piknometre and civalı porozimetre kullanılmıştır.

Haddeleme optimizasyonun sonucu olarak, en uygun hadde oranı %15 olarak bulunmuştur. c-SiO/PFM anot bileşiminin %15 hadde ile 100 çevrim sonrası 3,5 mAh/cm^2 yükleme kapasitesine ve 1250mAh/g spesifik kapasiteye ulaşılmıştır. Aynı haddeleme oranı Si/PAA ve Si/nPAA anot bileşimleri için de uygulandığında stabil bir çevrim performansı gösteren elektrot 100. çevrim sonunda sırasıyla 511 ve 1370mAh/g spesifik kapasite vermiştir. Piknometre sonuçları ise, artan haddeleme oranına bağlı olarak c-SiO elektrodun elektrot yoğunluğunun arttığını ancak por hacminin azaldığını göstermiştir.

Porozite oluşturma çalışmasında, %10 NaCl ile çalışılan c-SiO/PFM anodu 100 çevrim sonunda 3mAh/cm^2 yükleme kapasitesi ve 1000 mAh/g spesifik kapasite sağlamıştır. %30 NaCl ile çalışılan c-SiO/PFM anodu ise 100 çevrim sonunda 4mAh/cm^2 yükleme kapasitesi ve 750 mAh/g spesifik kapasite sağlamıştır. Metot, %30 NaCl Si/PPy anot bileşimi için de uygulanmıştır. %30 NaCl ile çalışılan Si/PPy anodu ile 100 çevrim sonunda 1100 mAh/g spesifik kapasiteye ulaşılmıştır. Yapısal karakterizasyon sonuçları da poroz elektrot yapısını desteklemektedir. SEM üstten vey an kesit görüntüleri porların gözlenmesini sağlamıştır. EDS analizi ile yıkama sonrası elektrot yüzeyinde çöken Cu parçacıklarının tespitini sağlamıştır. AFM sonuçları, porosite oluşturduktan sonra daha yüksek pürüzlülük değeri (Ra) göstermiştir. Piknometre ve civalı porozimetre sonuçları ise elektrot yapısında porozite sağlayan elektrotun yıkanma sonrası artan por hacmini ve poroziteyi kanıtlar niteliktedir.

Bu tezde ki çalışmalar ve sonuçları dikkate alındığında, geliştirilen metodun ve yapılan optimizasyonun, lityum iyon batarya uygulamalarında Si esaslı malzemelerinin kullanımasına ışık tutabileceği anlaşılmaktadır.

1. INTRODUCTION

Energy production from renewable sources becomes more important because of not only fossil fuels depletion but also protecting the environment. Renewable energy sources like biomass, geothermal, hydropower, solar, wave and wind, have low environmental impact and widely available. When renewable energy sources are compared to fossil fuels, it is clearly seen that fossil fuels have made our life simple in terms of sustainability. Renewable energy sources are also needed to be sustainable for widespread utilization. Namely, renewable energies should be stored to be able to use it when energy is needed but not available.

As well as the sustainability of renewable energy, energy storage is also significant öfor many applications such as consumer electronics and electric vehicles (EVs), which require high energy and power densities with longer cycle life. [1, 2]. This indicates that energy storage systems may have different characteristics according to application type and its requirements.

There are many energy storage systems, such as mechanical, electrochemical, chemical, electrical and thermal energy storage systems as shown in Figure 1.1 [3]. Among these systems, lithium ion batteries (LIBs) as an electrochemical energy storage system will be focus of this study.
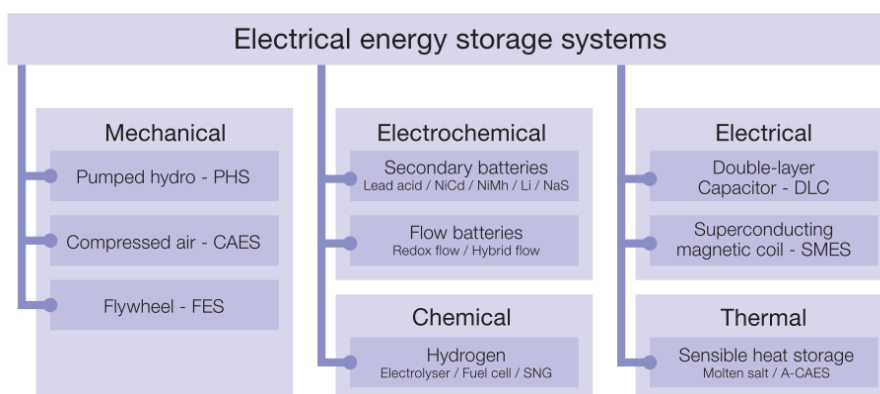
Figure 1.1 : Classification of electrical energy storage systems according to energy form [3].

Lithium-ion batteries are a popular type of rechargeable batteries used in portable electronics and electric or hybrid cars [4]. The LIBs have advantages with their excellent properties such as no memory effect, large voltage range, low self-discharge and high energy density. However, the present LIBs have developments to increase the energy density, still several challenges are needed to be resolved prior to their applications in EVs [5]. These challenges include energy and power densities, cycle life, charge-discharge rates, safety and cost of LIBs [6]. Most of these challenges are related to electrode materials. Therefore, new material compositions with new electrode designs have the serious potential to improve the energy per weight and volume at reduced cost. Nowadays an important and good example has been announced by MIT Technology Rewiev that a startup company from US developed a cheaper and faster way to make lithium-ion batteries with their new production method [7]. The investments are being made also worldwide in the development of silicon-based anodes for Li-ion batteries. On 17 February 2009, the Green Car Congress [8] reported that a spin-off company from Imperial College London received additional funding of £10 million (US$14million) for its Silicon-Based Anode Start-up project. However, the anodes for the most lithium ion batteries on the market are still carbon materials. Development of new high-capacity anode materials, such as Sn, Si, and alloy anodes, have been one of the major focus of the research in lithium-ion battery field. Although the chemical nature of all components is fixed, it still needs to fix following process parameters, which all have non-accurately known, impact on lifetime and battery performance [9]:

1. Particle size and distribution.

2. Relative amount of active material (AM), binder and conductive agent in the electrode.

3. Amount of AM per cm^2 current collector.

4. Thickness and density of the electrode.

5. Wettability process influencing active area.

In the light of these parameters, density and pore distribution of electrodes were studied to increase the performance of battery for different applications

1.1 Purpose of Thesis

As mentioned in the literature review section, silicon based materials have volume change problem during the charge/discharge processes. The drastic volume change of pure Si anode poses formidable challenges to build a thick electrode. Also, a high concentration of binder and conductive additive are typically required to achieve a satisfactory cycling performance but these inactive species (binder and carbon black) decrease the electrode level energy density to the extent that makes it less competitive than the state-of-the-art graphite electrode. A high-density lithium-ion battery leads to a high volumetric energy density, which is especially important for the application in portable electronic devices. The use of Si-containing anode such as Si/C, silicon oxide and silicon-containing alloy have intermediate capacities (800−1500 mAh/g) and volume changes (100− 150%); a high-loading electrode is easier to fabricate based on these materials due to the intrinsically smaller volume change. It is seen that there are significant studies to be able to find a sustainable solution for this problem regarding to cost, viable production methods, available materials, and high energy density. Starting with this target, in this thesis, our aim is to optimize available methods and to develop a new method to generate a highly porous electrode that can buffer the volume change of the individual c-SiO particles and help to maintain the mechanical integrity of the c-SiO electrode. The method developed here is expected to be compatible with the state-of-the-art lithium ion battery industrial fabrication processes and therefore holds great promise as a practical technique for boosting the electrochemical performance of lithium ion batteries without changing material systems. A simple, cheap, scalable, and versatile way is chosen to obtain c-SiO electrodes with high-porosity. The property gain in terms of electrochemical performance (high areal capacity with high current density) is demonstrated that a high-porosity is a key factor to improve the loading of c-SiO electrode.

When the current literature was taken into account, it was seen that silicon-based anode materials had very low loading capacities as in mAh/cm^2 or mg/cm^2. Although silicon based materials have very high specific capacity, low loading capacities are a limitation to use silicon materials commercially. In this thesis, this limitation is on the focus and it is endeavoured to become the solution for this limitations. It is aimed

to use an easy, feasible and applicable method to develop high loading capacities for high energy and power density.

Our studies in this work, which were focused on porosity and energy density of anode, can be classified for 2 purposes:

1- **Optimization of the anode porosity and electrode density with using calendering procedure** is expected to result in a better contact in electrode matrix, decreasing the contact resistance. The volume fraction of porosity decreases as the electrode density increases providing the higher specific energy density which is desired in most consumer applications, because the current requirements are the reduction of device size. Therefore to increase the energy of lithium-ion cells, we focused on increasing the active materials' volumetric energy density.

2- **Design to generate porosity in anodes** that are desired to be rendered porous form by adding and removing different ratios of the salt to the structure. This process provides a porous anode structure. This architecture may offer unique benefits, such as pores for rapid ion transport. Moreover, it helps to maintain the volumetric change of anode and prevents the deterioration of the integrity of the anode structure even allowing the dense electrode formation. Thus, more stable electrode results can be obtained over longer cycles, even though the high loading active material is coated.

As is seen aforementioned, two studies focus on the effect of electrode porosity change on cell perfromance according to applied methods for porosity. While one was decreasing the porosity to a optimum value, second was generating the enough porosity to provide available anode design for different applications.

These studies were applied for both Si and SiO materials to have some understandings about these two favored materials which have different theoratical capacity, volume change ratio and electrochemical behavior in LIBs.

2. LITHIUM ION BATTERIES

2.1 Principle of Lithium Ion Batteries

The working principle of a Li-ion cell can be explained as: Li ions move between the anode and cathode. During the discharge, Li ions deintercalate from the anode and intercalate into the cathode. Here chemical potential difference of Li ions between the two electrodes is resulted as electron leaving the anode simultaneously and flowing through the external circuit, which provides electrical energy to the load. If the process is on the opposite direction, charge step occurs. A brief overview of a lithium ion battery cell is shown in Figure 2.1.
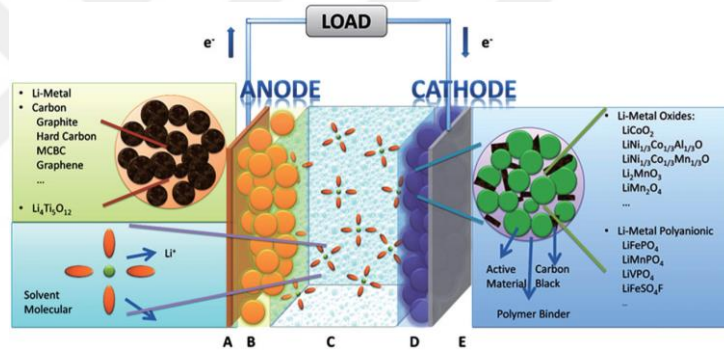
Figure 2.1 : The schematic and a brief overview of a lithium ion battery cell [10].

Li-ion cells should have thermodynamically stable configuration such a way that Goodenough et al. [11] explains it in an open-circuit energy diagram of an aqueous electrolyte systems. Figure 2.2 shows their study in a diagram. They define parameters μ_A and μ_C as anode and cathode electrochemical potentials, respectively. If a passivation layer does not create a barrier to electron transfer from the anode to the electrolyte, μ_A above the lowest unoccupied molecular orbital (LUMO) will reduce the electrolyte. If a passivation layer does not block electron transfer from the electrolyte the highest occupied molecular orbital (HOMO) to the cathode, μ_C below the HOMO will oxidize the electrolyte. μ_A and μ_C need to be within the window of the electrolyte for thermodynamic stability. This force the open circuit voltage (OCV or V_{OC}) of battery cell to being smaller than E_g :

$$eV_{OC} = \mu_A - \mu_C \leq E_g \tag{2.1}$$

where Eg is the energy difference of the electrolyte window and e is the magnitude of the electron charge. According to them, it must be designed as: (1) an anode's electrochemical potential μA needs to match to the LUMO of the electrolyte and a cathode's electrochemical potential μC needs to match to the HOMO of the electrolyte, (2) because of the electrode volume change during the charge/ discharge cycle, a stable passivating solid electrolyte interphase (SEI) layer needs to self heal itself and; the SEI layer must also permit a fast Li ion transfer between the electrode and the electrolyte without blocking electron transfer between the active particle and the current collector.
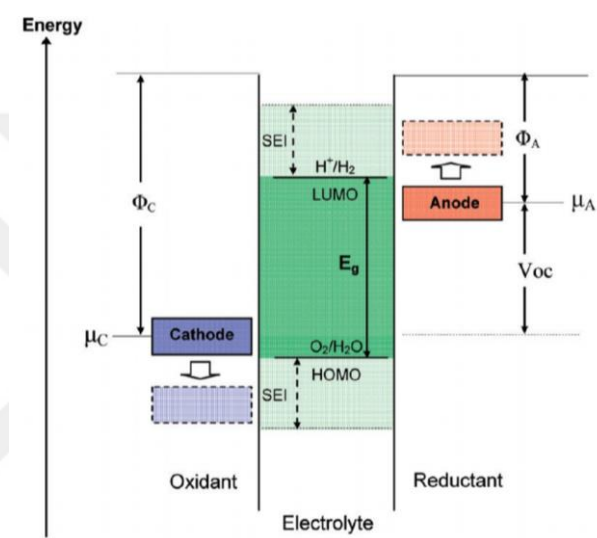
Figure 2.2 : Open-circuit energy diagram of an aqueous electrolyte systems [11].

Since OCV is the difference between the anodic and cathodic Li ion chemical potentials, or between their electronic Fermi energy levels, higher OCV can theoretically be obtained by lowering the (de)lithiation potential of the anode. Given that Li metal has the most negative standard electrode potential among the metals, it can be applied as the anode with the lowest potential for Li secondary batteries. However, when the output voltage of the anode is lower than 1 V versus Li metal anode [12], the Fermi energy level of the anode will be lower than LUMO of organic electrolytic solutions, which makes the electrolytes decompose and solid electrolyte interphase (SEI) layers form.

2.2 Anode Active Materials for LIBs

An ideal anode material for LIBs can be specified as (1) to contain elements or compounds with low atomic or formula weights, to accommodate large amounts of

Li, to be cyclable, and to have stable, and reversible gravimetric (mAh/g) and volumetric (mAh/cm^3) capacities, (2) to show a potential close to potential of Li metal and not to show large change in the potential with changes in the Li content, (3) not to be soluble in the solvents of the electrolyte and not to react chemically with the salt or solvents of the electrolyte, (4) to show good electronic and Li ionic conductivity, (5) to be cheap and environmentally friendly [13]. Additionaly, while developing new anode materials, structure, composition and morphology of anode materials should be in consideration which can be classified as insertion, alloying and conversion materials [14].

2.2.1 Insertion Based Anode Materials

Insertion process of anode materials exists with the intercalation of Li^+ at vacancies in the structure of electrode materials without destroying the crystal structure. However, minor modifications of the crystal structure can be occurred which is called as topotactic reaction. Three conditions are needed for this reaction. First one, the compound must be crystalline and there must be empty sites in the host structure. Empty sites can be in the form of isolated vacancies, 1D channels, 2D layers or channels in the 3D network. Second one, the host structure must contain a transition metal or rare earth metal. In the third condition, host structure can have unfavorable crystal structure and transition metals in low valency state resulting with no Li intercalation. Therefore, semiconducting or insulating metal oxides, transition metal ions, and 2D or 3D structures is needed for Li cycling [13].

Insertion based process provides higher rate capability, safer battery operation and longer cyclic life [15, 16].

2.2.2 Alloying-Based Anode Materials

Li can make alloys with metals/semimetals in this process with providing high capacity. For instance, alloy formation of lithium with silicon can deliver higher capacity values up to 8.5 Ah/cm or 4.2 Ah/g [17]. However, Li alloying – dealloying reactions involve large changes in the unit cell volume which is detrimental to the long-term Li cyclability. It is due to the electrochemical pulverization of the active material and loss of electrical contact between the particles and the current collector. In order to mitigate this problem; use of nanosize particles of the metals or oxides or

other compounds, incorporation of matrix elements, which are electrochemically active or inactive toward Li, starting crystal structure and morphology and lastly choice of the proper voltage range for Li cycling can be adapted.

2.2.3 Conversion Reaction-Based Anode Materials

Conversion reaction based process occurs when lithium reacts with transition metal compounds (M_aX_b, M: metal, X: O, S, F, P, N etc.) to form Li_yX. Metals are reduced to their zero oxidation state and deliver excellent capacity values [18]. However, several issues related to conversion reactions remain poorly understood, including the voltage hysteresis during charge/discharge processes. The feature of the conversion systems is the wide gap between the charge and discharge voltages and this gap has a thermodynamic origin. Recently, researchers realized that it depends on the nature of the M−X chemical bonds in the starting material (ionic vs covalent) regarding to the material electronic behavior [19-22]. For instance, the insulating CoO material shows a much wider voltage hysteresis [23] than the metallic FeP material [21] at a comparable rate.

2.3 Fabrication Process of Anode for LIBs

Lithium ion cells are fabricated with the design of materials and electrochemical couples available as the specific to their applications in terms of voltage, state of charge use, lifetime needs, and safety. The selection of electrochemical couples and the design of the cell directly affect the power, energy ratios and available energy. Therefore, it is required to preserve the mechanical integrity of electrode over numerous charge and discharge cycles despite the mechanical stress that is introduced by volumetric changes of the active material and the electrical conductivity of electrode while providing a porous structure that is favorable for ion transport. For this purpose integration of the cells requires optimized electrode manufacturing. Electrodes are coated on a current collector foil as a slurry containing composite structure of active material, binders, and conductive additives. In this process it is important to be aware of control of colloidal chemistry, adhesion, and solidification to get a formation with sufficient porosity degree and compaction in the electrode that can affect battery performance [24]. Pore structure predominantly depends on the size and shape of the applied materials such as active material

particles and additives. While mechanical integrity is attributed cohesion between particles and the adhesion of particles to the current collector [25-27], electrical conductivity is governed by the distribution of carbon black throughout the film[28].

Since we focus on the anode performance in this study, it will be detailed in terms of slurry preparation, lamination and drying of electrode preparation processes. Anode sheets are typically prepared through mixing, solving and/or dispersing active materials and additives in a solvent, casting of a homogeneous wet film on the current collector and removing the solvent by convective drying [29].

For a well prepared electrode slurry, followed procedure can be taken into account:

1- Dispersing the active material (AM)/carbon additive (CA) agglomerates,

2- Reducing the size of AM/CA aggregates as possible as.

3- To suppress the separation an agglomeration of AM, CA and a binder, arranging the most favorable composition.

4- To prevent the material degradation in the mixing, keeping the most favorable structure and composition of the AM, CA and binder.

Slurry can be prepared by different dispersing equipment showed in Figure 2.3. Slurry preparation step has the influence on electrode morphology and performance depending on the precursor slurry properties. On the other hand this process is able to modify the structure of the electrode components (AM, CA and the binder).
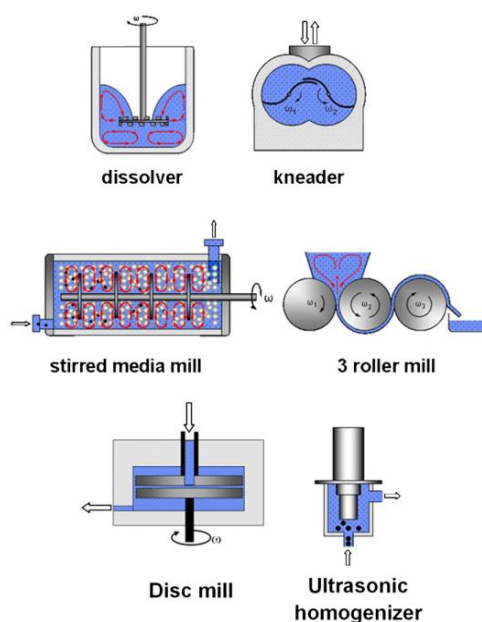
Figure 2.3 : Schematic drawings of dispersing machines [30].

A homogeneous slurry preparation is followed by electrode lamination, which is resulted not only in the cheaper production but also in superior battery capacity and cycleability. Electrode lamination is the coating of the electrode slurry on the current collector foil. There are many different methods such as chemical vapor deposition, spray deposition, laser deposition, spin coating, doctor blade coating, slot die coating etc. for lamination process. This process should be resulted with an even electrode thickness, free of coating defects and highly productive (i.e., the coating speed should be high) [24]. The distribution of the materials in the electrode constitute importance during solvent evaporation, which induces film shrinkage [31, 32] and pore formation [33]. It is known that drying process is directly have an impact on adhesion [25, 27, 34, 35], conductivity [27, 28, 35], binder distribution [34, 36-39] and electrochemical cell performance [27, 34, 35]. Many studies have been published to provide better understanding of the film solidification mechanism and the development of drying profiles [34, 37, 40, 41].

2.4 Calendering Process of Anodes for LIBs

Calendering process which is applied the electrode by pressure rollers used to form or smooth a sheet of material, has been considered to be a critical step in the production of high performance anodes [42]. Calendering is performed to change the pore structure of the electrode, which would thereby impact the electrochemical performance of the cell. Porosity and thickness of the electrode are decreased while the density of electrode is increased upon calendering.

While thin-film, solid-state batteries deliver excellent capacity retention over thousands of cycles [43], they possess very low volumetric energy densities. On the other hand, the concept of the electrode thickness and porosity can have limitations on mass transfer of Li ions which is resulted by the capacity fading of the cell due to the overpotantial that can lead to lithium plating on anode [44]. Many developing applications require batteries with high volumetric energy and power. One of the progress in this direction is the calendaring of the electrode to increase the electrode density. In addition to the increasing electrode density, calendaring generally leads to improved coating adhesion, particle interaction and electrical conductivity. However, excessive calendering, can result in very low porosities and blockage of the Li+ diffusion. As it known, low porosity is also substantial for the electrode materials

which have the volume change problem during the lithiation-delithiation process to accommodate the volume change of electrode.

Calendering process is affected by;

- Compress ratio of rolls,

- Surface of rolls,

- Applied temperature during the calendering,

- Calendering rate (m/s),

- Porosity of electrode before calendering.

2.5 Porosity Generation of Anodes for LIBs

The chemical composition and pore structures of active material directly affect the formation of the SEI layer and the diffusion of lithium ions through the anode material which is a complex mechanism [45-47]. Moreover, changes in volume occurring during the lithiation-delithiation processes can cause cell failures with long-term use [48-51]. Significant efforts have been applied to overcome the drawbacks of anodes and to improve the cycling stability of the cell through the development of material nanostructures, the application of electrolyte additives, and novel binders [52, 53]. Among these approaches several studies have focused on being able to control the pore texture of the materials and/or electrode providing large spaces that accommodate volume changes at the electrodes to improve the electrochemical performance of batteries [46, 49, 54, 55]. For example, carbon porous texture can be as xerogels, cryogels, aerogels, nano or microspheres and silicon can be in the form of nanowires [56, 57], three-dimensional porous structures [58-60], and nanocomposites [61, 62]. Although significant electrode performance has been obtained by porous material development, it is not still cost effective for commercial mass production. Therefore recent studies have been also focused on the controlling and designing of the electrode structure as an effective strategy for decreasing the volume changes during the lithiation-delithiation processes. Jeong et al. [63] presented artificially porosity-controlled composite electrodes with using PMMA pored forming agent. PMMA-treated porous electrodes exhibited an additional submicron pore distribution and greater dimensional reversibility than the untreated electrodes. Lee et al. [55] generated porous Si-based electrode by using

polystyrene (PS) beads as pore-forming agent. The electrode slurry was prepared with PS beads and after coating electrodes were heat-treated to remove PS beads. 10, 15, or 20 % PS beads were used in the slurry. They had increase in the electrode porosity for all compositions after heat treatment. The optimum results were obtained after 10% and %15 PS beads removal yielding 60.3 or 59.8 % of the initial capacity, respectively, after 100 cycles. Porosity measurement can be performed by imaging techniques and other techniques:

Imaging Methods: Image processing is a new and convenient method which is able to determine the pore size, pore size distribution and porosity. D techniques that can be used include: optical light microscopy (OM), scanning electron microscopy (SEM) with energy dispersive X-ray spectroscopy (EDX), field emission scanning electron microscopy (FESEM), focused ion beam (FIB), transmission electron microscopy (TEM). The range of 3D techniques available include: atomic force microscopy (AFM) and X-ray tomography.

- **Optical Microscopy:** Optical microscopy is a technique to viewa sample through the magnification of a lens with visible light. It is also known as a light microscope that provides a series of lenses to magnify images of small samples with visible light [64]. There are many types of optical microscopes such as: Transmitted Light Microscopy, Bright Field Microscopy, Dark Field Microscopy, Polarised Light Microscopy, Differential Interference Contrast Microscopy.

- **Scanning Electron Microscopy (SEM):** Porosity can be measured by image analysis based on scanning electronmicroscopy incorporating digital image processing. The dimension, shape and the number of pores in the sample can be inspected by image processing analysis. It is performed by some mathematical morphology algorithms for a complete pore size distribution (PSD) curve for each sample. Here the important thing is to generate a porosity threshold image to perform accurate digital porosity measurements. The advantage of the SEM to get direct and detailed structural information including the shape and size of individual pore inside the sample. The disadvantage of the SEM is underestimating the pore radius due to only working part of the pore [65].

- **Field Emission Scanning Electron Microscopy (FESEM):** A FESEM is a microscope that works with electrons instead of light. These electrons are released by a field emission source. The object is scanned by electrons according to a zig-zag pattern. It is used used to visualize very small topographic details on the surface or entire or fractioned objects [66].

- **Focused Ion Beam (FIB):** It is similar to SEM but the difference is the beam scanning the sample is ion beam instead of electron beam. The high-resolution ion beams are used and a field ionization source with a small effective source size on the order of 5 nm enables the beam to be tightly focused. As the metal ion source mostly Ga ions are used [67].

- **Transmission Electron Microscopy (TEM):** In this technique a beam of electrons is transmitted through an ultra thin sample, interacting with the it as it passes through. An image is focused onto an imaging device which is formed by the interaction of the electrons received from sample [68]. TEM provides high resolution imaging although it has operational difficulty such as high running cost, expertise requirement and difficult sample preparation [69].

- **Atomic Force Microscopy (AFM):** Atomic force microscopy (AFM) is a technique that provides images and other information from a wide variety of samples, at extremely high (nanometer) resolution. In Figure 2.4 the operation of AFM was given schematically. The advantage of AFM compared to SEM and TEM is simple operation in almost any environment, such as aqueous solutions, but also other solvents, in air, vacuum, or other gases [70].
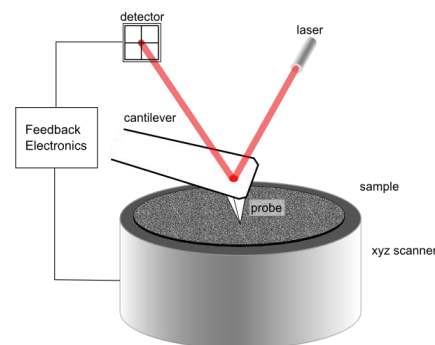
Figure 2.4 : Schematic of AFM operation.

- **X-ray Tomography:** In this technique, samples are with an X-ray beam which allows us, using an X photon detector, to record the adsorbed beam that has passed through the solid to the analyser. Image acquisition is repeated at different rotation angles and the different sections are then reconstructed using algorithms to form a three-dimensional image of the sample.X-ray Computed Tomography (CT) is a nondestructive technique which is used to visualize the interior features of solid objects, and to obtain digital information about their 3-D geometries and properties. This method provides the knowledge on the micro-structure of sample such as pore size distribution, porosity and tortuosity of the porous network [65].

Other Methods: Porosity measurements can also provided by numerical methods such as mercury intrusion porosimetry, thermoporometry, physisorption, nitrogen adsorption and BET analysis, dynamic vapour sorption and pycnometry [65].

- **Mercury Intrusion Porosimetry (MP):** Mercury porosimetry (MP) is a powerful technique to explore the pores. In MP, the volume of liquid metal that penetrates a solid is measured as a function of applied pressure. Since mercury is a hydrophobic material for most materials (its contact angle is greater than 90°), an external pressure is applied to force it into the pores of a porous solid [65].

- **Thermoporometry:** This method works due to the melting temprerature of a liquid inside the porous material providing information on the pore-size distribution [65].

- **Physisorption:** The principle of this technique is based on the measurement of amount adsorbed versus adsorptive pressure at constant temperature. It provides total surface area, mesopore and micropore volume and area, total pore volume, the distribution of pore volume and area by pore size, and surface energy distribution of a sample [65].

- **Nitrogen Adsorption And BET Analysis:** This method is generally used for the determination of adsorption isotherms of nitrogen at the temperature of liquid nitrogen (~77 K). The surface area of the sample is determined from

the measured monolayer capacity and knowledge of the cross-sectional area of the molecule being used as a probe.

- **Dynamic Vapour Sorption:** Dynamic vapour sorption (DVS) is a gravimetric technique. It measures the speed and amount of a solvent that is absorbed by a sample. In this technique, the main application is to measure water sorption isotherms. The sample is exposed to a series of step changes in relative humidity and the mass change as a function of time is monitored [65].

- **Pycnometry:** The main approximation of the pycnometry for the estimation of the sample volume is the non–ideal gas behaviour and its adsorption on to the solid material [71]. It was demonstrated that helium can be as an ideal and non-adsorbing gas at room temperature (300 K) and low pressure (< 0.5 MPa) for pycnometry measurements [72-74]. Figure 2.5 shows the schematic of helium pycnometer.
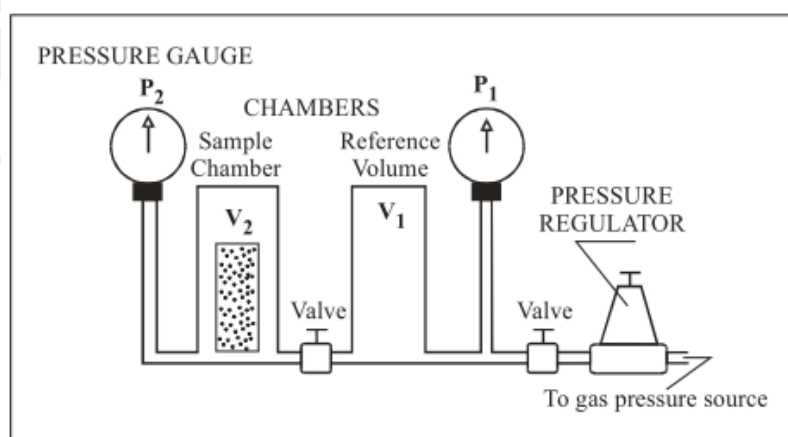
Figure 2.5 : Schematic diagram of helium porosimeter apparatus.

15

3. LITERAURE REVIEW

In the literature, various studies and strategies have been used to overcome the problem of silicon-based anodes. Some of these studies were summarized as silicon-based anodes, Si/C anodes, Si alloys/Si composites, and SiOx based anodes.

Silicon based anodes have been investigated by using; kind of silicon structure such as silicon nanotubes, silicon nanospheres, silicon flakes etc., porous silicon designs by introducing void space during synthesis to expand during lithiation with little or no change in the volume of the entire particle. Some of these silicon based anode studies were summarized in Table 3.1.

Table 3.1 : Summary of literature for silicon based anodes.

	Anode	C-Rate	Specific Capacity	Cycle Number	Year	Reference
	3D porous bulk Si	1C	2800mAh/g	100	2008	[60]
	Si nanotube	1C	3200mAh/g	200	2009	[77]
	Si thin film	0.2C	2200mAh/g	120	2012	[78]
	Ag coated hollow porous Si	500mA/g	3400mAh/g	100	2012	[79]
	3D porous Si-based multicomponent	0.1C	1600mA/h	100	2012	[80]
	Si-SiO-SiO$_2$ multicomponent	0.2C	1280mA/g	200	2012	[81]
Silicon Based Anodes	Si nanotubes	0.5C	1000mAh/g	90	2013	[82]
	Nanoporous Si network	1C	1250mAh/g	200	2013	[83]
	Mesoporous Si	400mA/g	1444mAh/g	100	2013	[84]
	Monodisperse porous Si nanospheres	1789mA/g	1500mAh/g	500	2015	[85]
	3D macroporous Si	1C	1058mAh/g	800	2016	[86]
	Nanoporous Si flakes	1C	1450mAh/g	100	2017	[87]
	Cu$_3$Si-doped porous-silicon	0.5C	2000mAh/g	100	2017	[88]

Si/C composite anodes have been intensively labored by academies and industrial companies. Today, Panasonic produces Li-ion cells for Tesla consisting of

silicon/graphite composite anode [89]. Si/C composites have advantage of both silicon and carbon. Silicon provides high specific capacity. Carbon can work as a buffer for the volume expansion, can help increase and maintain electrical contact with surrounding conducting material, and can allow decent passage of lithium ions to flow to the silicon material [90]. In Table 3.2, different carbon structures and carbon applications to improve silicon anode performance were summarized.

Table 3.2 : Summary of literature for Si/C anodes.

	Anode	C-Rate	Specific Capacity	Cycle Number	Year	Reference
	Mesoporous Si@carbon core-shell nanowire	600mA/g	2750mAh/g	80	2008	[91]
	Porous Si/C composite	180mA/g	660mAh/g	50	2009	[92]
	Carbon scaffold Si	0.05C	1280mAh/g	118	2010	[93]
	Self-supporting Si/RGO	50mA/g	786mAh/g	300	2011	[94]
	Si NWs/graphene papers	420mA/g	1400mAh/g	30	2012	[95]
	Nanoporous Si coated with C and RGO	2000mA/g	1100mAh/g	600	2013	[96]
	Carbon encapsulated Si nanoparticle	0.05C	950mAh/g	80	2014	[97]
	Si/mesoporous C composite	2000mA/g	1480mAh/g	1000	2014	[98]
Si/C Anodes	Si/void/porous carbon composite	80mA/g	980mAh/g	100	2014	[99]
	Hollow core-shell Si/C composite	100mA/g	1340mAh/g	100	2014	[100]
	Peanut shell structured carbon coated porous Si	188mA/g	1179mAh/g	120	2015	[101]
	3D interconnected porous Si/carbon	200mA/g	1552mAh/g	200	2015	[102]
	Si-porous carbon layers and graphene layers (Si-C/G)	200mA/g	760mAh/g	100	2015	[103]
	Si NPs/graphene composite	500mA/g	>1200mAh/g	600	2016	[104]
	Si NPs/rGO-hybrid	2100mA/g	1165mAh/g	100	2016	[105]
	SNPs@void@ mGra	500mA/g	1287mAh/g	500	2016	[106]
	Carbon wrapped porous Si	1000mA/g	1639mAh/g	200	2017	[107]

The volume expansion problem of silicon were also tried to suppress by Si Alloy and Si composite structures consisting of an inactive host matrix in which silicon is finely dispersed. This matrix accommodates the volume change in the Si active material, thereby preventing the pulverization of the anode. It is expected to have high mechanical strength to withstand the volume change of Si on cycling and high electronic conductivity to allow charge transfer reactions to take place [108]. Table 3.3 shows some of Si Alloys/Si composites' study as a summary.

Table 3.3 : Summary of literature for Si Alloys/Si Composites.

	Anode	C-Rate	Specific Capacity	Cycle Number	Year	Reference
Si Alloys/Si Composites	Si film deposited on a nickel substrate	2C	2200mAh/g	750	2003	[109]
	Ag coated 3D porous Si	0.2C	2500mAh/g	100	2011	[110]
	Si/NiTi	100mA/g	698mAh/g	50	2011	[111]
	Si/Ti4Ni4Si7	100mA/g	1000mAh/g	50	2012	[112]
	Sn-coated Si NWs	0.1C	1865mAh/g	100	2014	[113]
	Si@TiO_2 composite	0.1C	804mAh/g	100	2014	[114]
	Si/$FeSi_2$Ti	0.1C	620mAh/g	50	2014	[115]
	Cu coated porous Si	200mA/g	1651mAh/g	150	2015	[116]
	Titanium-silicon alloy solid core/nanoporous silicon shell	100mA/g	600mAh/g	100	2015	[117]
	Fe-Cu-Si ternary composite	210mAh/g	1261mAh/g	50	2016	[118]

The oxide form of silicon has come out as the alternative to the silicon with advantage of the specific capacity and relatively improved cycling performance. Many approaches have been reported to prepare SiO_x based materials, which include directly mixing SiO_x with carbon (e.g., graphite) or surface carbon-coating using organic sources and metal coating or metal doping. Some of example studies were given in Table 3.4.

Table 3.4 : Summary of literature for SiO_x based Anodes.

	Anode	C-Rate	Specific Capacity	Cycle Number	Year	Reference
SiO_x Based Anodes	Cr-coated SiO_x/C	0.1C	517mAh/g	100	2013	[119]
	Ball milled SiO_2/C	0.1 A/g	600mAh/g	100	2013	[120]
	Carbon-coated silicon monoxide	60mA/g	~615mAh/g	100	2013	[121]
	Diamond-like carbon/Cr double-layer coating on silicon monoxide-graphite	0.5C	490mAh/g	50	2014	[122]
	Si oxide-coated graphite flake (SGF)	2500mA/g	480mAh/g	500	2015	[123]
	F-SiO/H-rGO	120mA/g	744mAh/g	50	2015	[124]
	SiO_2–carbon composite	C/10	601mAh/g	100	2015	[125]
	Core-shell SiO_x/C	100mA/g	820mAh/g	100	2015	[126]
	Boron doped SiO	0.5C	947mAh/g	100	2015	[127]
	Hollow porous SiO_2 nanobelt	100mA/g	1012mAh/g	100	2015	[128]
	SiO_2@SnO_2/rGO	100mA/g	600mAh/g	100	2016	[129]
	SiO/graphite/amorphous carbon	100mA/g	850mAh/g	100	2016	[130]
	SiO_x/nitrogen-doped carbon composite	100mA/g	1514mAh/g	100	2016	[131]
	nano-Si@SiO_x/graphite	100mA/g	1560mAh/g	70	2016	[132]
	Si@SiO_x/Graphene hydrogel	100mA/g	1640mAh/g	140	2016	[133]
	Ball milled SiO_x	300mA/g	1184.8	100	2017	[134]

4. SILICON BASED ANODE MATERIALS FOR LIBs

4.1 Mechanism of Silicon Based Anodes

Commercial lithium-ion batteries contain graphite in the anode side, but any other anode active materials have recently come up as the promising anode materials such as Si possesses a theoretical capacity of 4200 mAh/g, while Sn has a theoretical capacity of 993 mAh/g. Especially, silicon material has the serious potential because it is the second most abundant element on the earth and has a theoretical capacity of 3580 mAh/g at room temperature, almost 10 times the capacity of graphite (372 mAh/g) [135].

In terms of advantages and properties of silicon based materials, we will focus on mechanism and experimental results of these materials in this thesis.

The voltage curve of silicon is given in Figure 4.1. A schematic phase diagram of silicon as a function of lithiation and the regions are shown in Figure 4.2. The region marked as I was determined by Obrovac and Krause [136] as the potential at which x-Si is lithiated to be precisely 170 mV. Region II indicates the electrochemical feature of $Li_{15}Si_4$ formation is an extremely small voltage plateau during lithiation found near 50 mV vs Li. Region III identifys the electrochemical feature of $Li_{15}Si_4$ delithiation is a large plateau near 0.45 V.
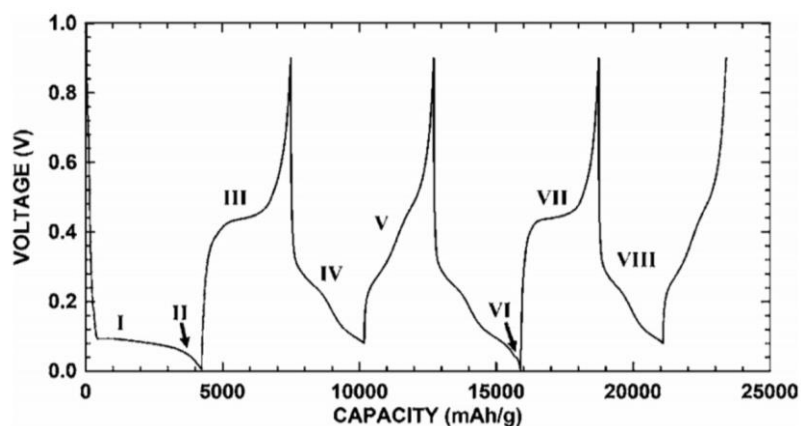
Figure 4.1 : Voltage curve of bulk Si powder [135, 136].

Region IV indicates the lithiation of a-Si in both Figure 4.1 and Figure 4.2 whereas Region V shows the delithiation of a-Li$_x$Si in Figure 4.2.
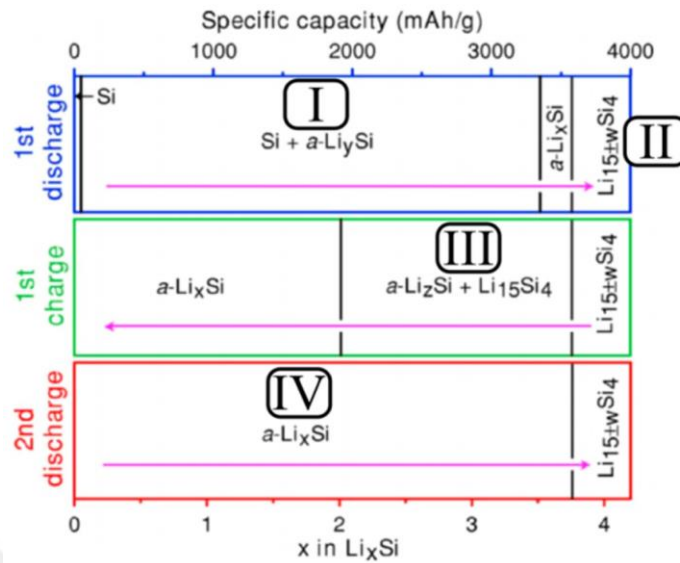
Figure 4.2 : Schematic phase diagram as a function of lithiation. Roman numerals correspond to those in Figure 4.1 [136, 137].

However, despite its remarkable high capacity and the intensive research done in the field, there have been no widespread applications of Si or Sn alloy anodes in lithium-ion cells, mostly due to the large volume change associate with lithiation and delithiation of the material. This volume change disrupts the integrity of electrode and induces excessive side reactions, leading to fast capacity fade. Because of the above mentioned problem, regardless of the high specific capacity obtained by most of the previous studies, Si normally could not reach an areal capacity above 1.5mAh/cm^2 for high C-rate. Thicker Si electrode with higher loading tends to have a more serious electrode disintegration problem; the areal capacity achieved by Si is even lower than graphite anode. Thus, more and more studies are devoted to increase the loading and specific capacities of Si anode.

Other issue for degradation of silicon-based anodes is SEI quality which directly effect cell performance, rate capability, and cyclability of the battery [138, 139]. The SEI is a layer that forms on the surface of the electrode during the first lithiation. It forms because of electrolyte decomposition and can be like a barrier between the electrolyte and the electrode. This barrier intrinsically consumes the anode and electrolyte, leading to a low efficiency and it can adjust the distribution of Li ions from the bulk electrolyte to the anode resulting with Li dentrite problem [140].

However, SEI formation prevents the electrode surface from further reacting with the electrolyte components [141]. An ideal SEI layer, should have high Li ionic conductivity, favorable thickness, and high elastic strength to inhibit the dendrite growth on Li metal anode [142].

Several attempts has recently turned to SiO_x ($0<x<2$) as the anode active material for Li-ion batteries as an alternative to pure silicon. SiO_x is also a promising material with the advantage of high abundance in the earth's crust, low discharge potential, and high initial irreversible capacity and reversible capacity of 3744 mAh/g and 1961 mAh/g, respectively [143-145]. In the past decades, silica is not generally considered to be electrochemically active for lithium storage until Gao et al. reported that commercial SiO_2 nanoparticles could react with Li between 0.0 and 1.0 V (vs. Li/Li1) with a reversible capacity of 400 mAh/g [146]. One of the first studies on SiO_x anode material aslo came from Yang et al. [147] that they tried to investigate the effect of silicon oxide powders with different oxygen contents on the electrochemical performance of the lithium ion cells. They found that a reversible capacity of SiO_x drops with the increase in the oxygen content x ($x < 1.1$) but the cyclability increases. Miyachi et. al. [145] used X-ray photoelectron spectroscopy to determine the chemical structure and electrochemical reaction of SiO with Li. They explain that a silicon-oxide bond is generally twice as strong as a Si-Si bond is one reason for good cycle performance. The reactions exist between silica and Li ions were suggested first by Fu et. al. [148]. They suggested mechanism as:

$$5SiO_2 + 4Li+ + 4e \longrightarrow 2Li_2Si_2O_5 + Si \qquad (4.1)$$

$$Si + xLi+ + xe \longrightarrow Li_xSi \qquad (4.2)$$
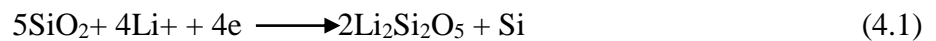
According to reaction (4.1), they calculated the theoretical discharge capacity of SiO_2 of 357.3 mAh/g. This value is found to be less than the reversible discharge capacity of 465 mAh/g. Therefore, another contribution to reversible capacity may come from Si–Li alloy/ dealloying process as described in reaction (4.2). The reactions exist between silica and Li ions were suggested by Guo et. al [143]. as:

$$SiO_2 + 4Li^+ + 4e^- \longrightarrow 2Li_2O + Si \qquad (4.3)$$

$$2SiO_2 + 4Li^+ + 4e \longrightarrow Li_4SiO_4 + Si \qquad (4.4)$$

$$Si + xLi^+ + xe^- \longleftrightarrow Li_xSi \qquad (4.5)$$
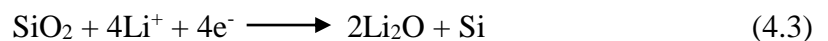
Here, the reaction generated Li_2O and Si (4.3) shows the largest reversible capacity of 1961 mAh/g. Because the SiO_2 is completely converted to Si and stored Li ions in the next process, while inactive lithium silicate is generated via other reactions (4.4) and, (4.5).

4.2 Advantage and Challenge of Silicon Based Anodes

Several types of anode materials have been studied for LIBS in the literature. A comparison of different kind of anode materials is given in Table 4.1 [149]. Among these materials Si has received great attention due to its highest theoretical capacity which is around 4200 mAh/g at fully lithiated phase ($Li_{22}Si_5$ or $Li_{4.4}Si$). Si provides over 10 times increase in anode specific capacity when it is compared to conventional graphite anode.

Table 4.1 : Comparison of different kind of anode materials for lithium-ion battery [149].

Material	Li	C	Si	Sn	Sb	Al	Mg	Bi
Density (g·cm^{-3})	0.53	2.25	**2.33**	7.29	6.7	2.7	1.3	9.78
Lithiated Phase	Li	LiC_6	**$Li_{22}Si_5$**	$Li_{22}Sn_5$	Li_3Sb	LiAl	Li_3Mg	Li_3Bi
Theoretical specific capacity (mAh·g^{-1})	3862	372	**4200**	994	660	993	3350	385
Volume change (%)	100	12	**320**	260	200	96	100	215
Potential vs. Li (V)	0	0.05	**0.4**	0.6	0.9	0.3	0.1	0.8

Although silicon's performance shows great potential for advanced lithium-ion batteries, there are some complications involving silicon's behavior. The problem is the volume change of silicon during lithiation-delithiation process, which is originated by massive quantity of lithium insertion into silicon. Since silicon has 1.46Å atomic radius while Lithium has 2.05Å, this constrained structure results in a larger volume after lithiation. Deep silicon lithiation at room temperature appears as crystalline $Li_{15}Si_4$ at below 60mV versus Li/Li$^+$ [90]. This crystalline phase turns to the amorphous Li_xSi phase during the delithiation resulting with partial irreversible charge [137]. Therefore, the cut-off voltage for anode charging is preferable to be above 70 mV to avoid the formation of the irreversible $Li_{15}Si_4$ phase.

A large volume change of the silicon during cycling is resulted with the loss of mechanical integrity, cracking, pulverization and the delamination of the active particles from the current collector [150, 151]. This leads to the increase in internal resistance and decrease in charge and discharge current causing the large irreversible capacity loss for the first several charge and discharge cycles and capacity fade for prolonged cycles.

The another issue for silicon anode is solid electrolyte interphase (SEI) layer which is form on the anode surface during the charge and discharge cycles due to electrolyte reduction and other surface reactions. The product of these reactions are basically a mixed layer of Li_2CO_3, lithium alkyl carbonates, lithium alkoxides and other salt. In Figure 4.3 an example for ethylene carbonate (EC) reduction was given [152].
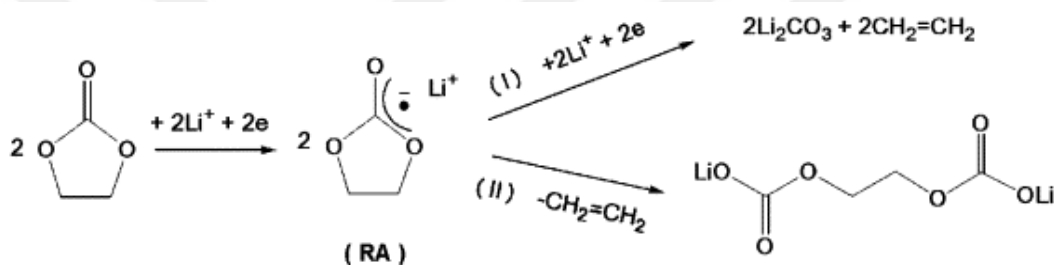
Figure 4.3 : Reaction mechanisms for SEI formation.

The properties of this layer such as thickness and stability plays an important role on the li-ion cell performance. SEI layer on the electrode/electrolyte interface can influence the kinetics of lithiation/delithiation and the interfacial stability of electrode. This layer can also help to protect the electrode surface from further reactions.

SEI layer can be detected by FTIR, XPS, Raman spectroscopy, AES, NMR etc. These techiques give limited information about SEI. However, the results collected by each characterization technique are complementary to each other.

5. EXPERIMENTAL STUDIES

Optimization of porous electrode microstructure is essentially significant for the improvement of high performance lithium-ion batteries (LIBs). In this thesis, two different approaches were performed to be able to optimize the porosity of anode. The first one is calendering process of the anode and the second one is the porosity generation on the anode by additive add/drop method. Here, our investigation was started with the carbon coated SiO (c-SiO) active material and PFM binder for both methods. Then these methods were proved with silicon active material and other binders. Silicon active material and PAA binder were used to show the workability of calendering method and silicon active material and PPy binder were used to show the workability of porosity generation method. The calendering experiments and porosity generation experiments were listed in Table 5.1 and Table 5.2, respectively.

Table 5.1 : List of calendering experiments.

Active Material	Binder	Calendering Ratio
c-SiO	PFM	10%
c-SiO	PFM	15%
c-SiO	PFM	20%
Si	PAA	15%
Si	nPAA	15%

The carbon coated SiO (c-SiO) was used as the anode material purchased from Hydro-Québec. Si nanopowder which is 30-50nm was obtained from Nanostructured & Amorphous Materials, Inc. Poly(9,9-dioctylfluorene-co-fluorenone-co-methyl benzoic ester (PFM) and Poly(1-pyrenemethyl methacrylate) (PPy) were sythesized in Dr. Gao Liu's group as the binder. PAA (Mw: 450,000) was purchased from Sigma Aldrich. Super P as the conductive additive was supplied from Gelon company. Celgard 2400 separator is obtained from Celgard. Lithium-ion electrolyte were purchased from BASF, including 1.2 M $LiPF_6$ in ethylene carbonate, diethyl carbonate (EC/DEC=3/7 w/w) containing 30 wt% fluoroethylene carbonate (FEC).

Table 5.2 : List of porosity generation experiments.

Active Material	Binder	Additive	Ratio
c-SiO	PFM	NaCl	(90:10):10
c-SiO	PFM	NaCl	(90:10):30
c-SiO	PFM	NaCl	(90:10):60
Si	Ppy	NaCl	(90:10):30

In Figure 5.1, the chemical structure of the PFM binder used in this work is given.

Figure 5.1 : The chemical structure of the PFM binder [53].

In Figure 5.2, the chemical structure of the PPy binder used in this work is given.
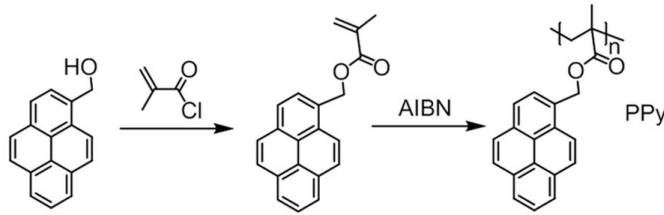
Figure 5.2 : The chemical structure of the PPy binder [153].

5.1 Fabrication of Anodes

5.1.1 Calendering process of anodes

In Figure 5.3, scheme shows that calendering makes a compact and effective electrode composed of the PFM binder and the bimodal size of carbon-coated SiO particles.
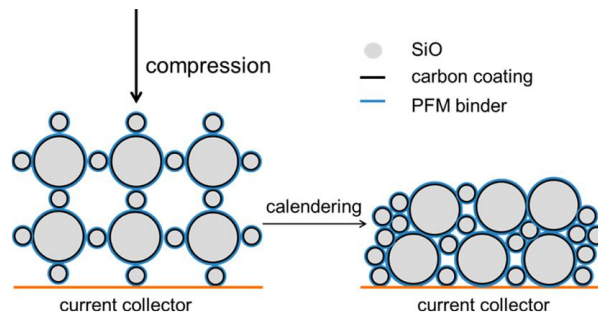
Figure 5.3 : A scheme of calendering process.

The electrodes were used to assemble the coin cells. Figure 5.4 shows schematic of coin cell parts and assembly.
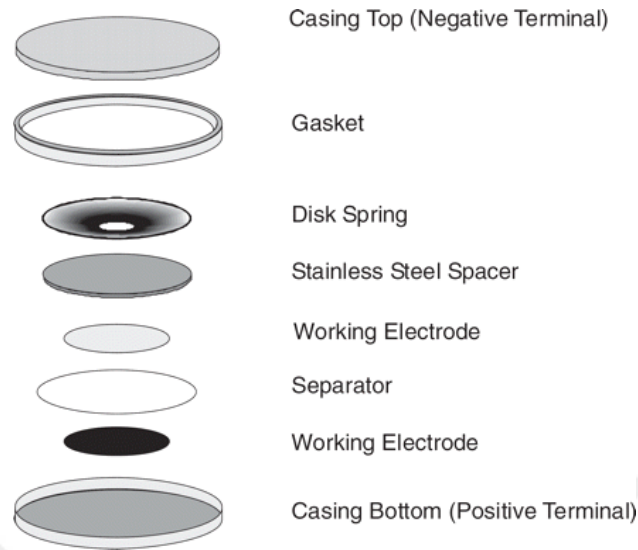
Figure 5.4 : Schematic of coin cell parts and assembly [154].

Calculation of electrode porosities and densities: Take the electrode with 10% porosity reduction as example. This electrode has a loading of 2.94 mg c-SiO/cm^2, a thickness of 30 µm. The c-SiO active material has a 10% carbon coating, meaning that this electrode has 0.294 mg carbon/cm^2 and 2.65 mg c-SiO/cm^2, and 0.327 mg PFM binder/cm^2 (the electrode is composed of 10% binder and 90% active material). The densities of the individual components are 1.9 g/cm^3 (carbon), 2.33 g/cm^3 (SiO), and 1.75 g/cm^3 (PFM polymer). Thus, the volume occupied by electrode materials is;

$$\frac{0.294}{1.9} + \frac{2.65}{2.33} + \frac{0.327}{1.75} = 1.48 \ x \ 10^{-3} cm^3$$

With a thickness of 30 µm, the volume of the electrode is 3×10^{-3} cm^3

The porosity is calculated as;

$$\frac{(3 - 1.48) x 10^3 cm^3}{3 x 10^{-3} cm^3} = 51\%$$

The electrode density is calculated as;

$$\frac{2.94}{0.9} \ x \ 10^{-3} mg \ x \ \frac{1}{3 x 10^{-3} cm^3} = 1.09 g/cm^3$$

The calculated porosities are 51%, 47% and 43% for 10%, 15% and 20% porosity reduction, respectively.

5.1.2 Calendering process of c-SiO/PFM composition

The electrode slurries were prepared for four different anode coatings. The PFM polymers were dissolved in chlorobenzene. Then, c-SiO particles were added (weight ratio of c-SiO/PFM =90/10). Slurries were mixed by using homogenizers for 1 h, and then, coated on the copper foil by using a doctor blade. The doctor blade is set to a thickness of 150 μm to coat the electrode laminate. After electrodes dried, they were calendered as ~10, 15, and 20% of the electrode thickness in roll press at 70°C. In Figure 2.3, the schematic of calendering process is shown. The electrodes were cut as disk for coin cell assembling. They were placed in the glovebox overnight and further dried in the vacuum oven at 90 °C for 16 h to completely remove the water.

5.1.2.1 Calendering process of Si/PAA and Si/nPAA compositions

PAA polymer was dissolved in water. Then, silicon nanoparticles and Super P (SP) were added (weight ratio of Si nanoparticle/polymer/SP =75/15/10). For Si/nPAA electrode, polymers were dissolved in water and 1M NaOH were added in another bottle for nPAA preparation until pH is <7. Then, again, silicon nanoparticles and super P were added as the same ratio of first slurry. Slurries were mixed by using homogenizers for 1 h, and then, coated on the copper foil by using a doctor blade. After electrodes dried, they were calendered as ~15% of the electrode thickness in roll press at 70°C. The electrodes were calendered from 32-40μm to 27-34μm (The thickness of copper foil was not added which was 16μm).

PAA which is a carboxyl-containing polymer is useful as thickeners and emulsifiers for aqueous mixtures when it is neutralized. Structure of PAA and nPAA and the reaction can be seen in Figure 5.5 (a-c). The neutralization step results in a thickening agent containing a mixture of neutralized carboxyl containing polymer and solvent. Because of these compositions absorb large quantities of water and because of their swelling properties, it is possible to get a viscous slurry, which helps to get a dense electrode coating on the copper foil [155].
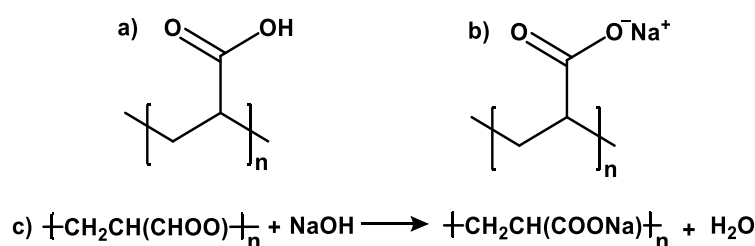
Figure 5.5 : Schematic of a) PAA and b) nPAA c) nPAA reaction.

5.1.3 Porosity generation methods of anodes

In this study, porosities were generated in the electrodes of LIBs by using and removing the additives. The electrode slurry was prepared as normal with addition of some additives and fabricated on the copper foil. The electrode laminate was dried, then washed in a solvent to to remove the additives from the electrode structure. The used solvent should be able to dissolve additives but not the polymer binder. When the additive was removed, porosities were generated from where the additives originally locate. The experiments were written step by step below:

Additive type and size: In this study, NaCl was used which is cheap and easily accessible. The NaCl which was originally 0.5-1mm was ball-milled in different times (20, 30 and 40 minutes) to optimize the size.

Salt content in the slurry: In this study used slurry content is;

active material:binder:salt= 9:1:10%(active material+binder)

active material:binder:salt= 9:1:30%(active material+binder)

active material:binder:salt= 9:1:60%(active material+binder)

5.1.3.1 Porosity generation method with c-SiO/PFM composition

- Slurry with 10% NaCl addition: 1.8g c-SiO active material, 0.2g PFM binder and 0.2g 30-minute ball milled salt in 5g chlorobenzen to make slurry in homoginizer for 1h. Then the slurry was coated on copper foil with adjusting doctor blade to 150μm thickness. Then the electrode was washed in water:methanol (1:1 wt%) solution to remove the NaCl. It was washed for a half day, 1 day and 2 days. The optimum time was selected as 1 day based on the following calculations:

Calculation 1- 200mg NaCl was used in total 2200mg slurry. Electrode weight was 26.9 and copper foil weight was 21.58mg. NaCl content in the slurry was calculated as:

$$\frac{200}{2200} x(26.90 - 21.58) = 0.48 \ mg \ NaCl$$

Electrode weight was 26.9 mg before washing and it was 26.4 mg after washing.

$$26.9 - 26.4 = 0.5mg$$

According to calculations there was 0.48mg NaCl in the electrode. It was observed that 2.5mg was removed. This difference can be the reason of solved Cu particles that will be explained in EDS results.

Calculation 2- Another calculation to obtain the remaining NaCl content was performed with conducting the Mohr method. After electrode was washed, this washing solution was titrated by 0.1N $AgNO_3$ solution. 5% K_2CrO_4 solution was prepared and 1 ml K_2CrO_4 solution was added to 10 ml NaCl solution. 0.1N $AgNO_3$ was started to drop to the NaCl solution. Since NaCl content is very limited in the solution, it was directly turned to the red-brown precipitation. This consumed $AgNO_3$ volume was noted as 0.08ml. NaCl content was calculated as:

$$1ml \ 0.1N \ AgNO_3 = 0.00585g \ NaCl$$

$$0.08ml \ AgNO_3 \ x \ 5.85mg \ NaCl = 0.468mg \ NaCl$$

Calculation 1 and 2 shows consistency for the removed NaCl content.

- **Slurry with 30% NaCl addition:** 1.8g c-SiO active material, 0.2g PFM binder and 0.6g 30-minute ball milled salt in 5g chlorobenzen to make slurry in homoginizer for 1h. Then the slurry was coated on copper foil with adjusting doctor blade to 250μm thickness. The electrode was pounched to pieces as 1.6cm^2 and dried. Then the electrode was washed in water:methanol (1:1 wt%) solution to remove the NaCl. Same calculations were performed to obtain removed NaCl content:

Calculation 1- 600mg NaCl was used in total 2600mg slurry. Electrode weight was 32.3 and copper foil weight was 21.58mg. So NaCl content in the slurry was calculated as:

$$\frac{600}{2600}x(32.3 - 21.58) = 2.47 \ mg \ NaCl$$

Electrode weight was 32.3mg before washing and it was 29.8mg after washing.

$$32.3 - 29.8 = 2.5mg$$

According to calculations there was 2.47mg NaCl in the electrode. It was observed that 2.5mg was removed. This difference can be the reason of solved Cu particles that will be explained in EDS results.

Calculation 2-According to Mohr method the consumed $AgNO_3$ volume was noted as 0.42ml. NaCl content was calculated as:

$$1mL \ 0.1N \ AgNO_3 = 0.00585g \ NaCl$$

$$0.42ml \ AgNO_3 \ x \ 5.85mg \ NaCl = 2.457mg \ NaCl$$

Calculation 1 and 2 shows consistency for the removed NaCl content.

- **Slurry with 60% NaCl addition:** 1.8g c-SiO active material, 0.2g PFM binder and 1.2g 30-minute ball milled salt in 5g chlorobenzen to make slurry in homoginizer for 1h. Then the slurry was coated on copper foil with adjusting doctor blade to 250μm thickness. The electrode was pounched to pieces as 1.6cm^2 and dried in vacuum oven for 16h at 90°C. Same calculations were performed to obtain removed NaCl content:

Calculation 1- 1200mg NaCl was used in total 3200mg slurry. Electrode weight was 33.2 and copper foil weight was 21.58mg. So NaCl content in the slurry was calculated as:

$$\frac{1200}{3200}x(33.20 - 21.58) = 4.35 \ mg \ NaCl$$

Electrode weight was 33.2mg before washing and it was 28.85mg after washing.

$$33.20 - 28.35 = 4.85mg$$

According to calculations there was 4.35mg NaCl in the electrode. It was observed that 2.5mg was removed. This difference can be the reason of solved Cu particles that will be explained in EDS results.

Calculation 2- According to Mohr method the consumed $AgNO_3$ volume was noted as 0.75ml. NaCl content was calculated as:

$$1ml\ 0.1N\ AgNO_3 = 0.00585g\ NaCl$$

$$0.75ml\ AgNO_3\ x\ 5.85mg\ NaCl = 4.38mg\ NaCl$$

Calculation 1 and 2 shows consistency for the removed NaCl content.

Table 5.3 shows the result of removed NaCl calculations in the summary.

Table 5.3 : The removed NaCl content (mg).

NaCl Content wt%	NaCl content (mg)	The removed NaCl content according to electrode weight difference between before and after washing (mg)	The removed NaCl content according to Mohr Method (mg)
10% NaCl	0.48	0.500	0.468
30% NaCl	2.47	2.500	2.457
60% NaCl	4.35	4.850	4.380

5.1.3.2 Porosity generation method with Si/PPy composition

Si was used with PPy binder. PPy was dissolved in NMP. The weight ratio of Si nanoparticle/polymer/additive =9:1:30%. NaCl was used as the additive again.

5.2 Assembling of Coin Cells

The electrodes were used to assemble the coin cells. As a counter electrode, the Li metal was used. 70µl, 1.2M lithium hexafluorophosphate ($LiPF_6$) in ethylene carbonate (EC), diethyl carbonate (DEC) (EC/DEC = 3:7 by weight), and 30% by weight of fluoroethylene carbonate (FEC) was used as the electrolyte. The performance of the assembled 2325 or 2032 coin cells was evaluated with Maccor Series 4000 Battery Test system in a thermal chamber at 30°C or Neware Battery Test system.

5.3 Electrochemical Tests

5.3.1 Calendered electrodes

The cut-off voltage of cell testing was between 1.2 V and 0.01V, assuming a theoretical value of 1,000 mAh/g for c-SiO and 4200 mAh/g for silicon. They were tested at C/25 for 2 cycles and at C/10 for further cycles. Electrochemical Impedance Spectroscopy (EIS) were conducted on a VMP galvanostat/potentiostat (Bio-Logic). Cells were cycled at C/10 for 1 cycle, the cell was brought to half lithiation at the 2nd cycle and rested for 4 hours before EIS measurement.

5.3.2 Porous electrodes

The cut-off voltage of cell testing was between 1.0 V and 0.01V, assuming a theoretical value of 1,000 mAh/g for c-SiO and 4200 mAh/g for Si. They were tested at C/25 for 2 cycles and at C/10 for further cycles. Electrochemical Impedance Spectroscopy (EIS) were conducted on a VMP galvanostat/potentiostat (Bio-Logic). Cells were cycled at C/10 for 1 cycle, the cell was brought to half lithiation at the 2nd cycle and rested for 4 hours before EIS measurement.

5.4 Characterization of Anodes Before and After Cycling

A JSM-7500F scanning electron microscope (SEM) was used to characterize the morphology of the electrode surface. ZEISS EVO LS15 scanning electron microscope (SEM) was used for cross section images and EDS-EDX measurements. Atomic force microscopy (AFM) was used for surface roughness. Micromeritics - Accupyc2 1340 Helium pycnometer and Micromeritics - Autopore 4 mercury porosimeter were used porosity measurement. Synchrotron X-ray Tomography was performed to further characterize the improved porous c-SiO electrode structure.

6. RESULTS AND DISCUSSIONS

6.1 Characterization Results of Materials

Characterization of c-SiO powder

Figure 6.1a shows the characterization of the pristine c-SiO particles, particle size analysis via light scattering of the particles dispersed in water indicates a bimodal distribution of the particle size, with a smaller particle diameter of ∼ 1.5 μm, and bigger particle diameter of ∼ 12 μm. Figure 6.1b shows the SEM image of the pristine c-SiO particles, which also reflects this biomodal particle size.
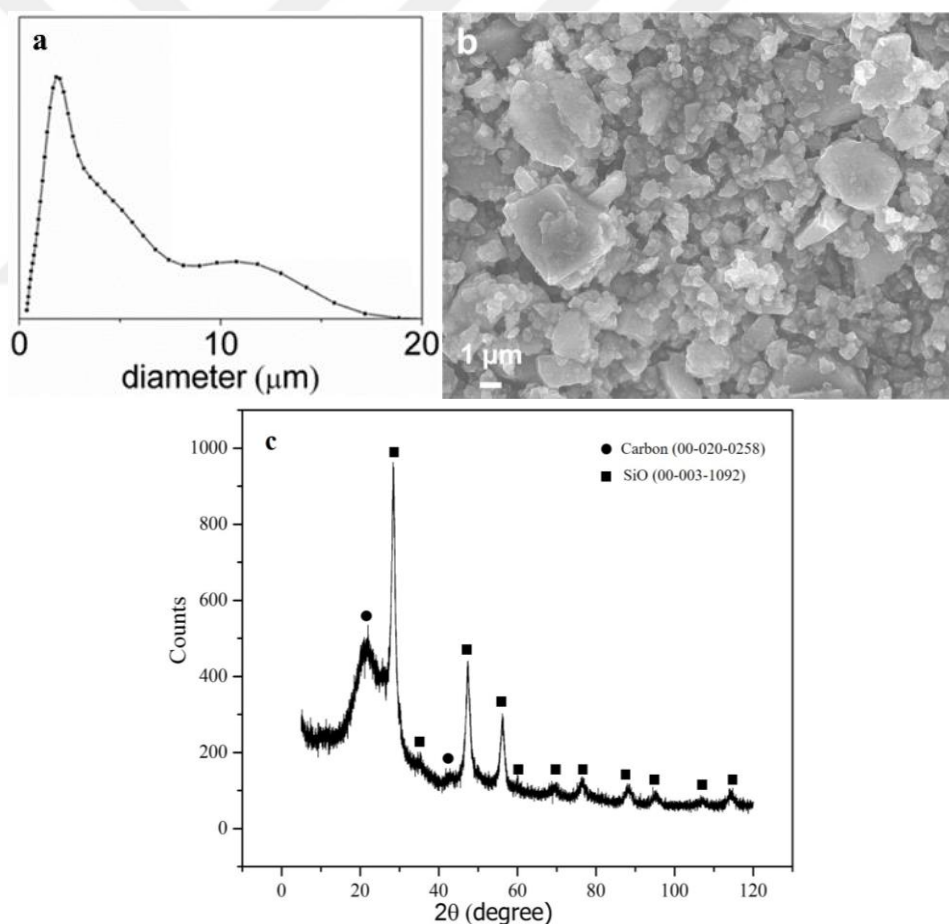
Figure 6.1 : a) particle size analysis via light scattering for the c-SiO pristine particles, embedded is the SEM image of the particles with a scale bar of 1 μ m. b) SEM image of c-SiO particles. c) XRD result od c-SiO powder.

Figure 6.1 c) shows the XRD patterns of carbon coated SiO. The wide peaks at about 22° and 43° are attributed to the carbon layer coated on SiO [156]. The peaks at around 28°, 36°, 47°, 56°, 60°, 69°, 88°, 95° and 107° were analysed by X'Pert HighScore Plus programme as SiO.

Characterization of Si nano powder

Si nanopowder was characterized by particle nanosizer and TEM (Figure 6.2). TEM image indicates that silicon nanoparticle has the diameter between 25-50nm while particle size distrubition shows the average particle diameter as 103.8nm. This difference can be explained with the agglomeration of silicon nanoparticles in water during the measurement.
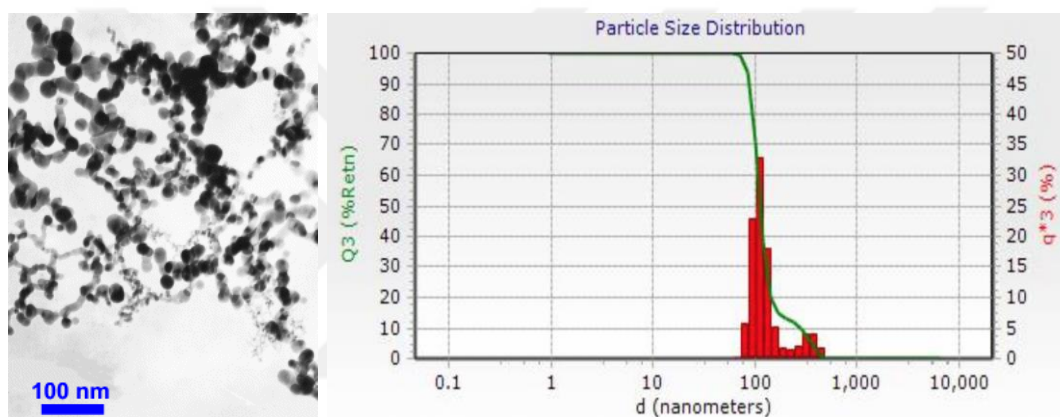
Figure 6.2 : Particle size distribution and TEM image of Si nano particle.

6.2 Characterization Results of Anodes Before Cycling

6.2.1 Characterization results of calendered c-SiO/PFM anodes

10% Calendering of c-SiO/PFM anodes

Figure 6.3 shows the surface SEM images of c-SiO/PFM uncalendered electrodes and Figure 6.4 shows the surface SEM images of 10% calendered c-SiO/PFM electrodes. According to calculation in Section 5.1.1, the uncalendered electrode has ca. 60% porosity and after 10% calendering, it becomes around 51% porosity. The particles sizes based on the SEM images indicate that the particles are not broken during calendering process.
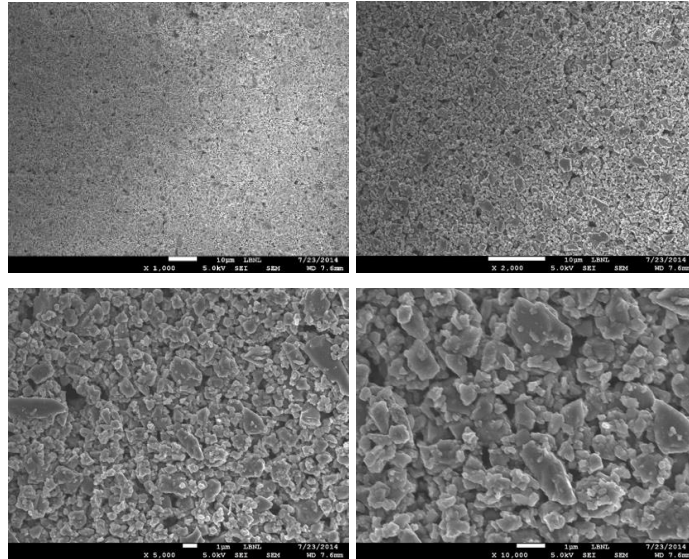
Figure 6.3 : SEM images of uncalendered anodes at different magnifications.
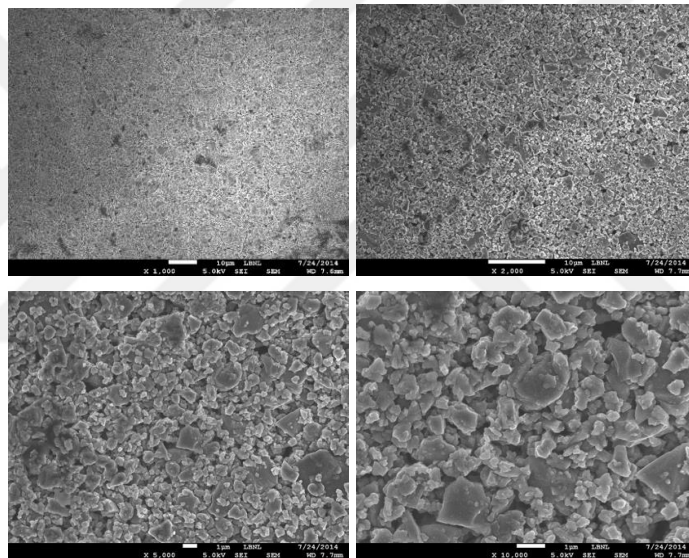
Figure 6.4 : SEM images of 10% calendered anodes at different magnifications.

15% Calendering of c-SiO/PFM anodes

Figure 6.5 shows the surface SEM images of uncalendered c-SiO/PFM electrodes and Figure 6.6 shows the surface SEM images of 15% calendered c-SiO/PFM electrodes. According to calculation in Section 5.1.1, the uncalendered electrode has ca. 62% porosity and after 15% calendering, it becomes around 47% porosity. The particles sizes based on the SEM images indicate that the particles are not broken during high-pressure calendering process. When the uncalendered electrode, with ~62% porosity and calendered electrode with 47% porosity is compared, it is seen that the number of empty spaces (pores) is reduced after calendering. Singh et al. showed the similar result [44] that electrodes were well compacted and pores were

shrinked after calendering. The morphology of the electrodes indicates that electrode porosities are successfully decreased while maintaining the c-SiO particles intact, which may lead to an improved electrochemical performance.
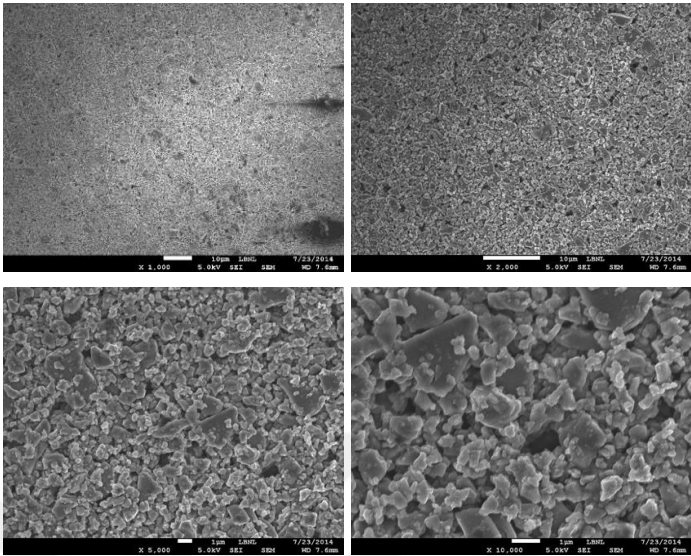
Figure 6.5 : SEM images of uncalendered anodes.
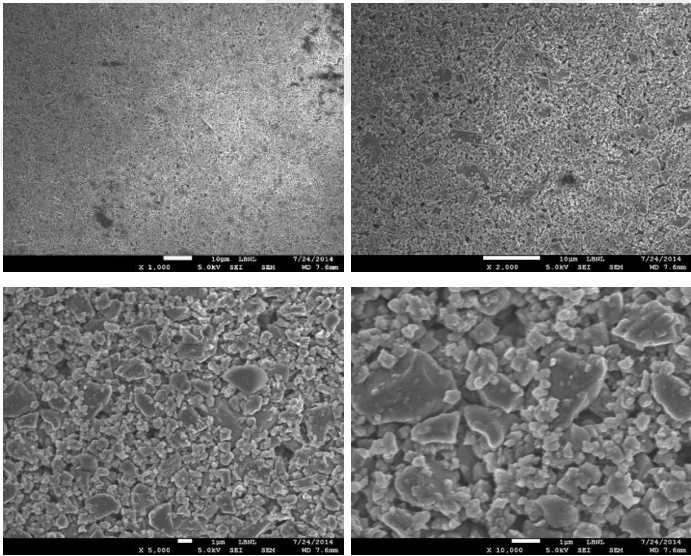
Figure 6.6 : SEM images of 15% calendered anodes.

20% Calendering of c-SiO/PFM anodes

Figure 6.7 shows the surface SEM images of uncalendered c-SiO/PFM electrodes and Figure 6.8 shows the surface SEM images of 20% calendered c-SiO/PFM electrodes. According to calculation in Section 5.1.1, the uncalendered electrode has ca. 63% porosity and after 20% calendering, it becomes around 43% porosity. The particles sizes based on the SEM images indicate that the particles are not broken during high-pressure calendering process. Here, it is seen that

after calendering, pores were decreased which provides an integrated anode structure and it may lead to an effect on electrochemical performance.
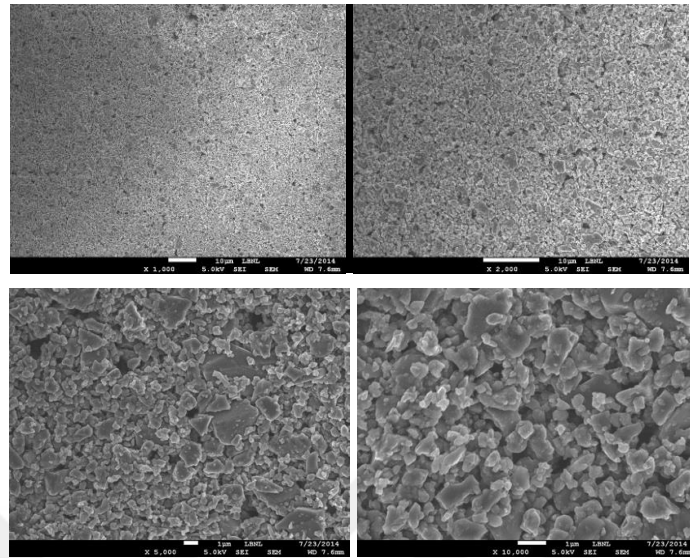
Figure 6.7 : SEM images of uncalendered anodes.
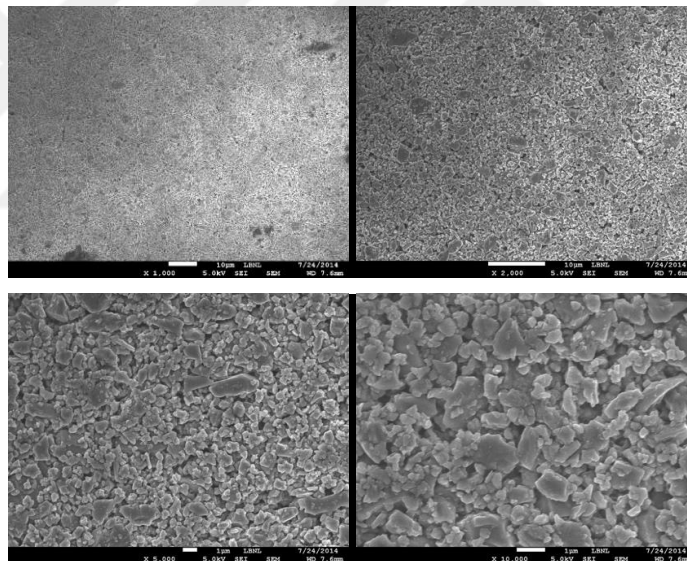
Figure 6.8 : SEM images of 20% calendered anodes.

To further understand the electrode density and porosity of electrodes after calendering, pycnometry measurements were performed. The measurements were carried out with the electrode which were coated on copper foil. Table 6.1 shows the results from pycnometer measurements. With the increasing calender ratio, electrodes have higher densities which is consistent with the view of SEM images of after calendaring of electrodes. This can be attributed to the decreasing pore volume and increasing active material density after calendering. Pore volumes were

decreased with increasing calendering ratio. This is because of the applied compress which provides compactness.

Table 6.1 : Summary of results for density and pore volume of calendered electrodes.

Sample	Density (g/cm^3)	Pore volume (cm^3/g)
Uncalendered electrode	3.17	0.63
10% calendered electrode	3.36	0.57
15% calendered electrode	4.03	0.48
20% calendered electrode	4.79	0.43

6.2.2 Characterization results of calendered Si/PAA and Si/nPAA anodes

The calendering process was also applied for Si material to understand the effect of particle intact and dense electrode feature on electrochemical performance of the cell. Figure 6.9 shows the SEM images of Si/PAA and Si/nPAA electrode surface. The spherical structure of silicon nanoparticals can be seen clearly. SEM images show that the surface is smoother on Si/PAA electrode than Si/nPAA electrode surface which is rough. This is attributed to the pores created after neutralization [158].
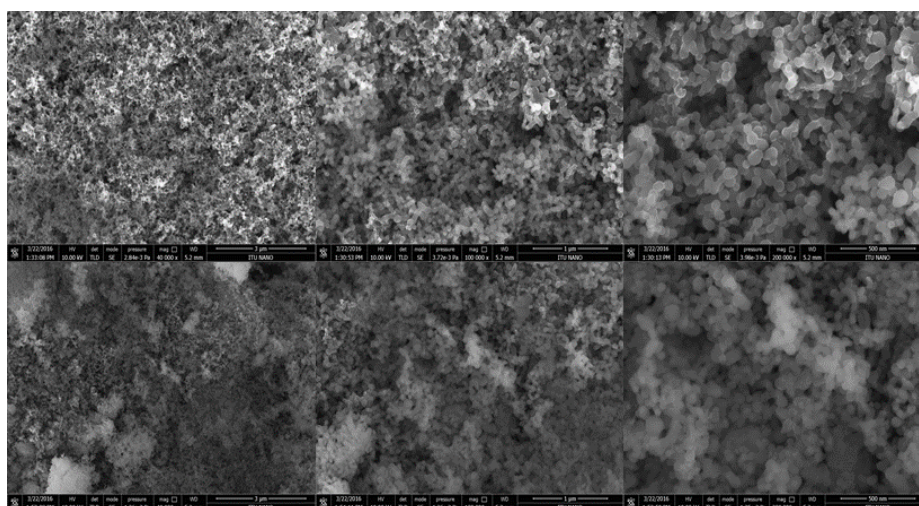
Figure 6.9 : SEM images of Si/PAA (top) and Si/nPAA electrodes before cycling (each row from left to right 40K, 100K and 200K magnification.

6.2.3 Characterization results of porous c-SiO/PFM anodes

In this study, NaCl was used which is cheap and easily accessible. The NaCl which was originally 0.5-1mm in size was ball-milled in different times (20, 30 and 40

minutes) to optimize the size. In Figure 6.10, SEM images of different sized NaCl related to ball milling time are given. 30 minute ball milled NaCl seems in homogeneous size distribution which are between 5-20 μm selected as the additive.
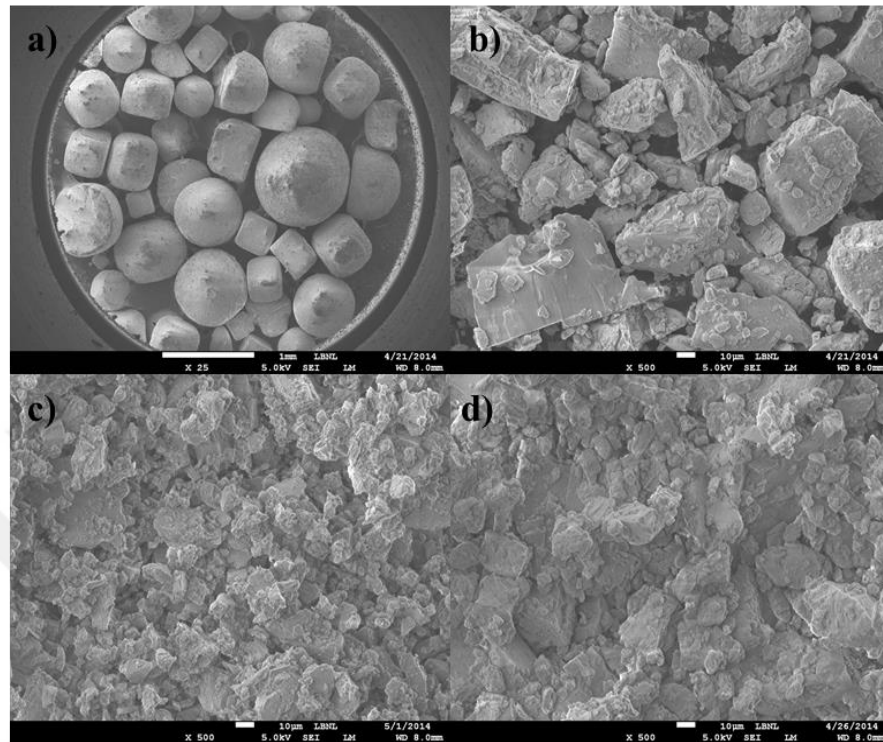
Figure 6.10 : SEM images of NaCl a) non-milled b) 20 minute milled c) 30 minute milled d) 40 minute milled.
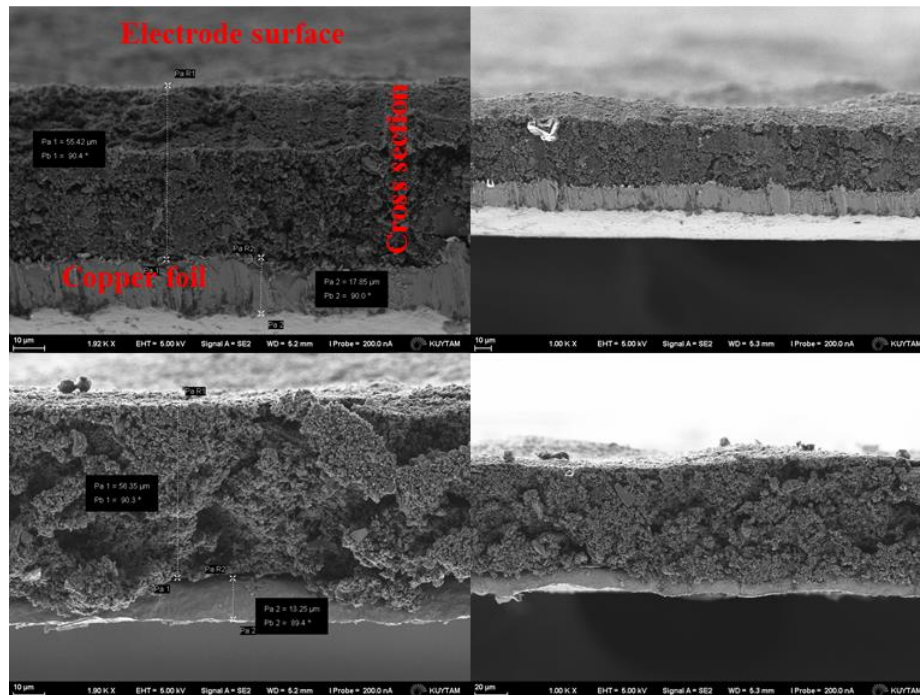
Figure 6.11 : Cross section SEM of c-SiO electrodes with 30% salt before (top) and after washing (bottom).

Characterization results of electrodes before and after washing:

To get a homogeneous electrode coating is important for the electrochemical performance of the electrode for commercial use to obtain the exact energy density. On the cross section SEM of electrode (Figure 6.11), the coatings are clearly identified as well as the copper current collector. The thickness of electrode coating and copper foil is identified. The thickness of electrode before washing is ~55µm and the thickness of electrode after washing changes between ~56µm while copper foil has the thickness between 13-17µm.

In Figure 6.12, 6.14 and 6.16, the SEM images of c-SiO/PFM electrodes are given before NaCl washing. After porosity generation using the sacrificial NaCl method, more pores are shown in the electrode (6.13, 6.15 and 6.17). Some of the high-loading Si anode studies in the literature only demonstrate cell cycling at small charge/discharge rates. For the most of the practical applications practical cycling experiments should be at higher rates. The rate capabilities of LIBs can be improved by constructing the porous electrodes conveniently, and now it is discussed the advantage and benefit of our technique from this perspective.

From dimensional analysis, the characteristic time for lithium ion diffusion through an electrode material (τeq) is determined by the following relation (6.1)

$$\tau_{eq} \approx \frac{L^2}{D} \tag{6.1}$$

where L is the diffusion length and D is the diffusion coefficient. To decrease the diffusion time and improve the rate capability of the cell, one can either decrease the diffusion length (by using electrode material particles with smaller dimensions) or increase the diffusion coefficient (by developing a better lithium ion conductor) [157].

The former approach avoids changes in the battery chemistry and has a larger effect on the diffusion time due to the exponent of the diffusion length. The use of nanomaterial particles can effectively decrease the diffusion length, although a good electrode architecture with optimized porous structure is important to utilize this nano- or microactive material particles [158].
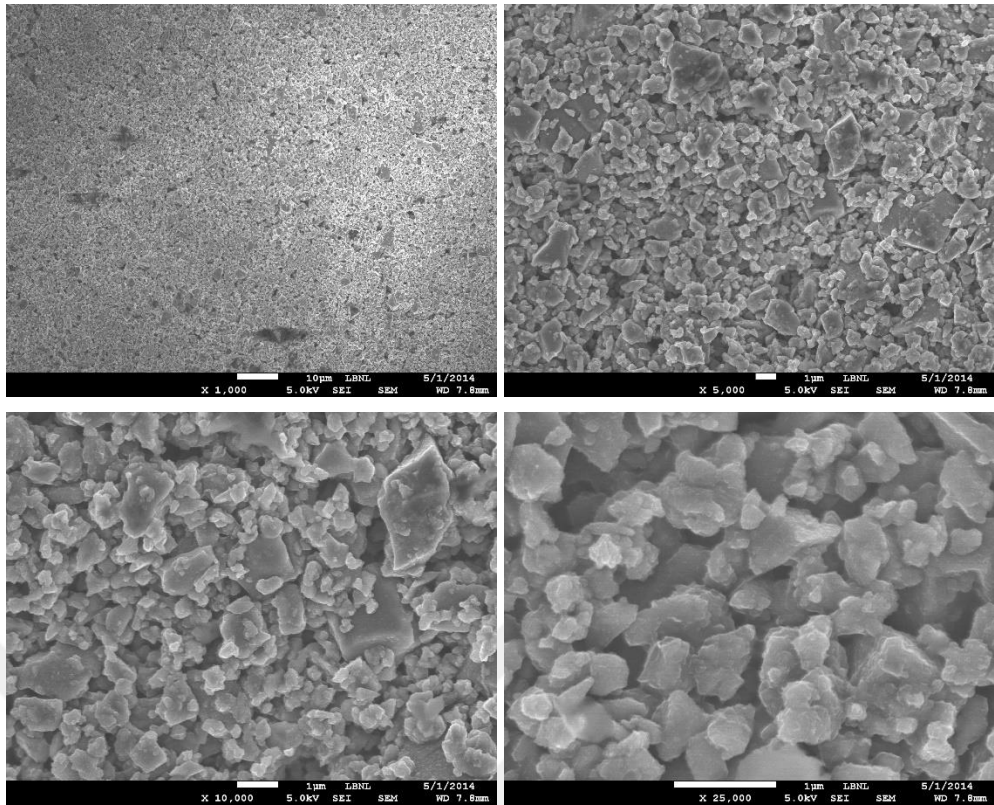
Figure 6.12 : SEM images of c-SiO electrodes with 10% salt before washing.
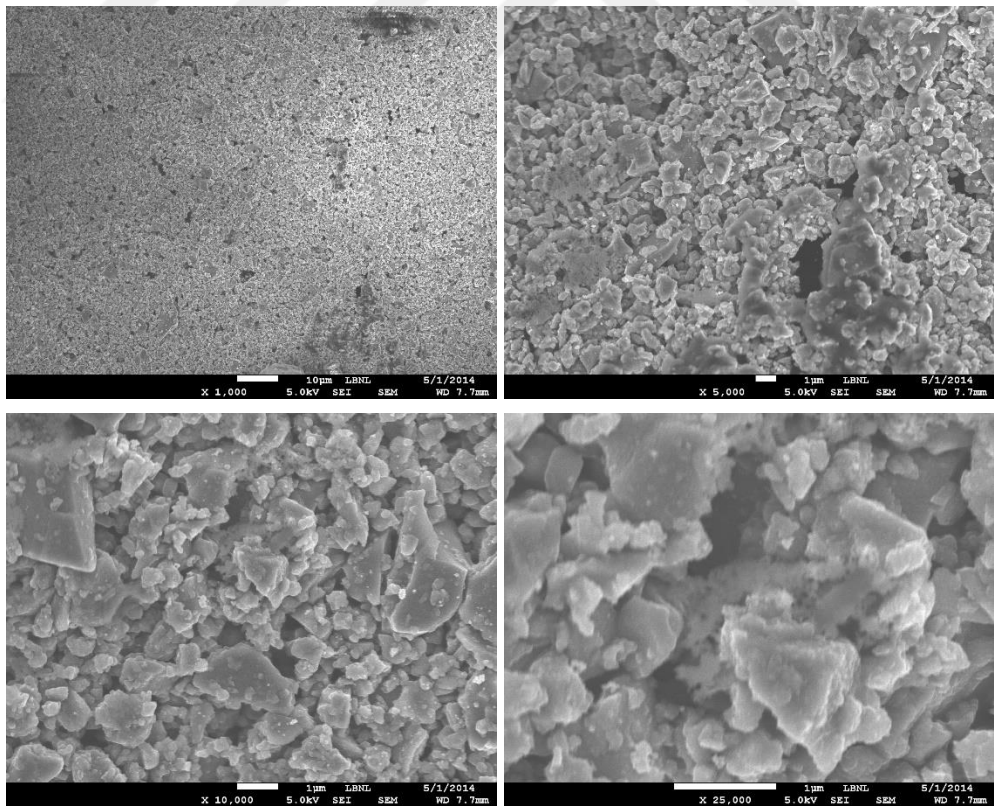
Figure 6.13 : SEM images of c-SiO electrodes with 10% salt after washing.
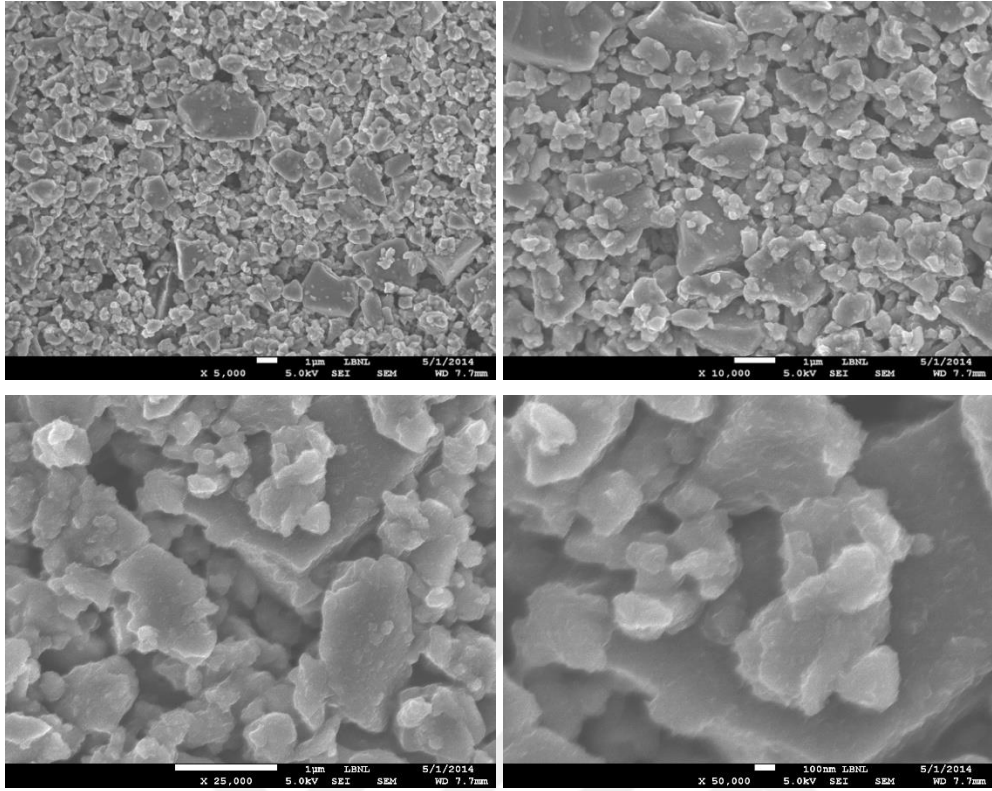
Figure 6.14 : SEM images of c-SiO electrodes with 30% salt before washing.
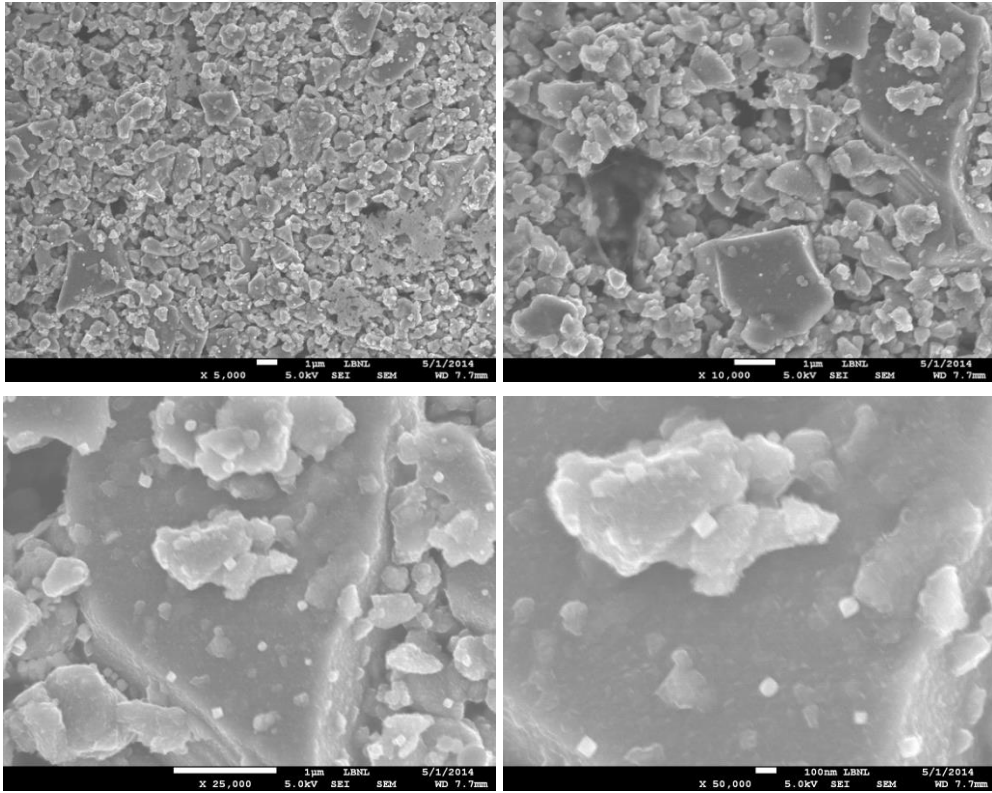
Figure 6.15 : SEM images of c-SiO electrodes with 30% salt after washing.
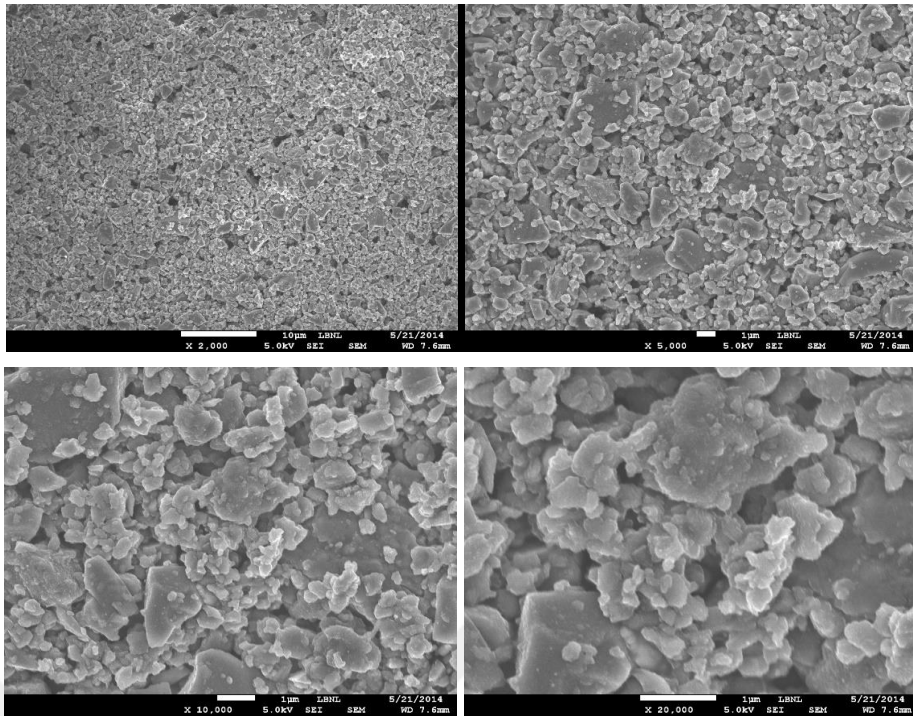
Figure 6.16 : SEM images of c-SiO electrodes with 60% salt before washing.
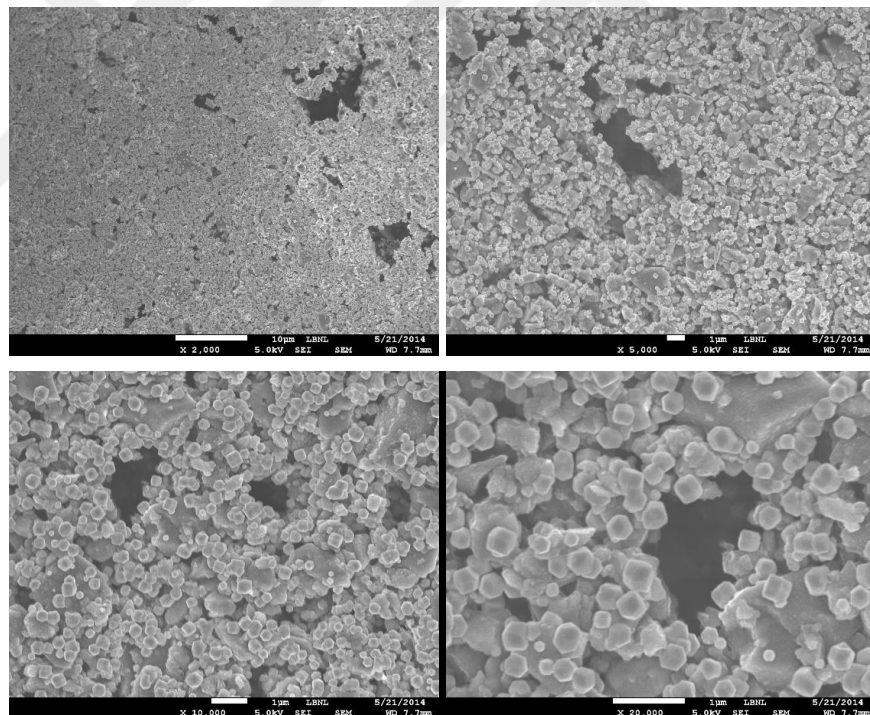
Figure 6.17 : SEM images of c-SiO electrodes with 60% salt after washing.

In order to generate porosity, a dissolvable material, i. e. NaCl, was used during the preparation of anodes. Electrodes were then washed to remove the NaCl additive to get porous structure. To further understand the electrode surface after washing, EDS mapping and EDX dot-analysis were performed. In Figure 6.18, c-SiO electrodes were shown with 30% NaCl salt before washing. In EDX spectrum, Na and Cl peaks

47

were detected which had 5-10 µm diameter under SEM image. According to EDS mapping, well dispersed Na and Cl were also observed.

In Figure 6.19, c-SiO electrodes were shown with 30% NaCl salt after washing. When SEM images of after washing electrodes (Figure 6.13, 6.15 and 6.17) were analysed, nanocubes structured materials on the electrode surface were analysed. In EDX spectrum, these nanocube structured materials revealed Cu, O, C and Si contents. According to EDS mapping, there are Cu particles on the surface of the washed electrode. This detected Cu/CuO nanocubes structures' shape are consistent with the literature [159, 160]. Cu/CuO nanocubes arise from copper current collector which is solved during the washing process of electrode.
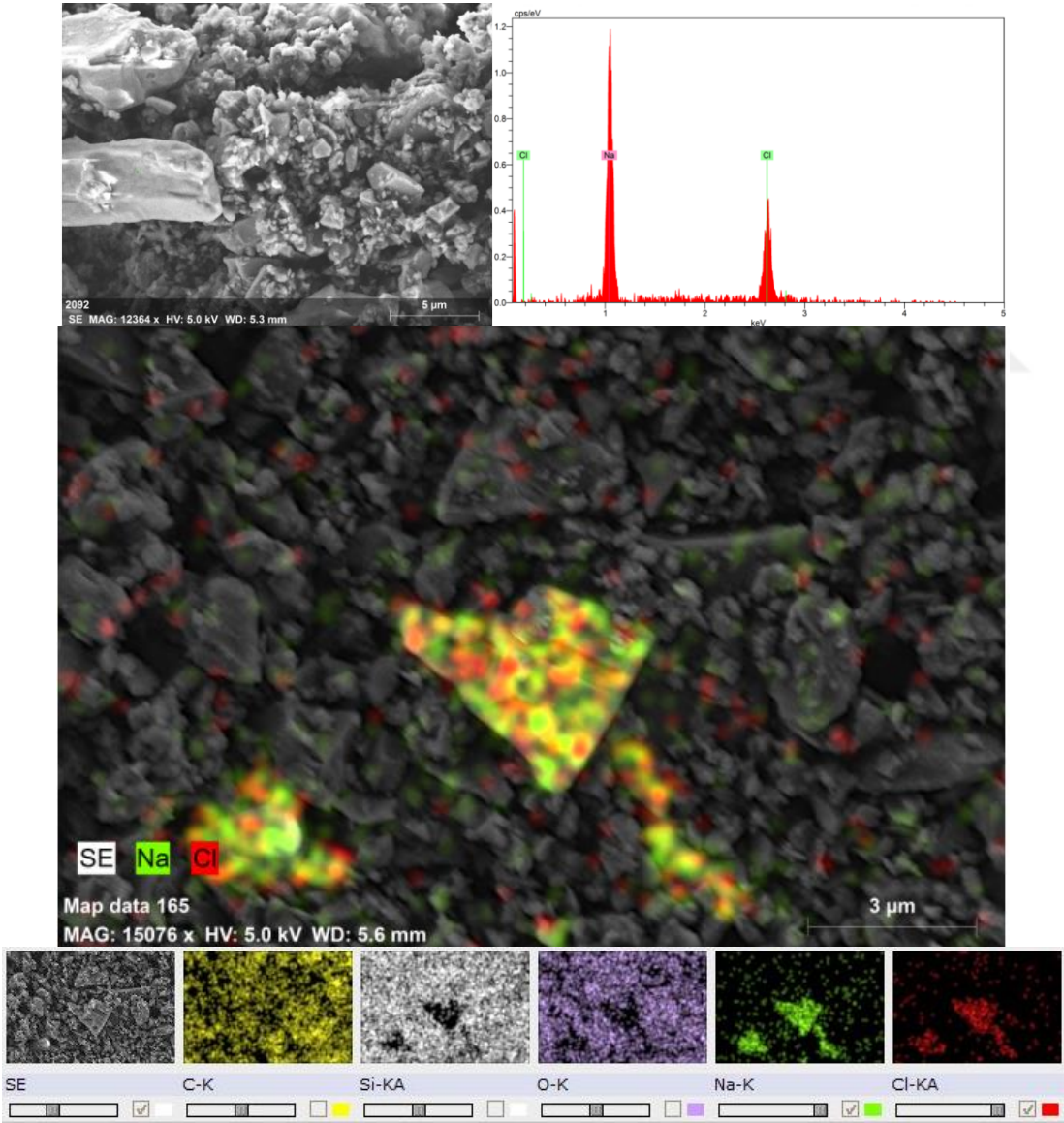
Figure 6.18 : EDS mapping and EDX of c-SiO electrodes with 30% NaCl salt before washing**.**
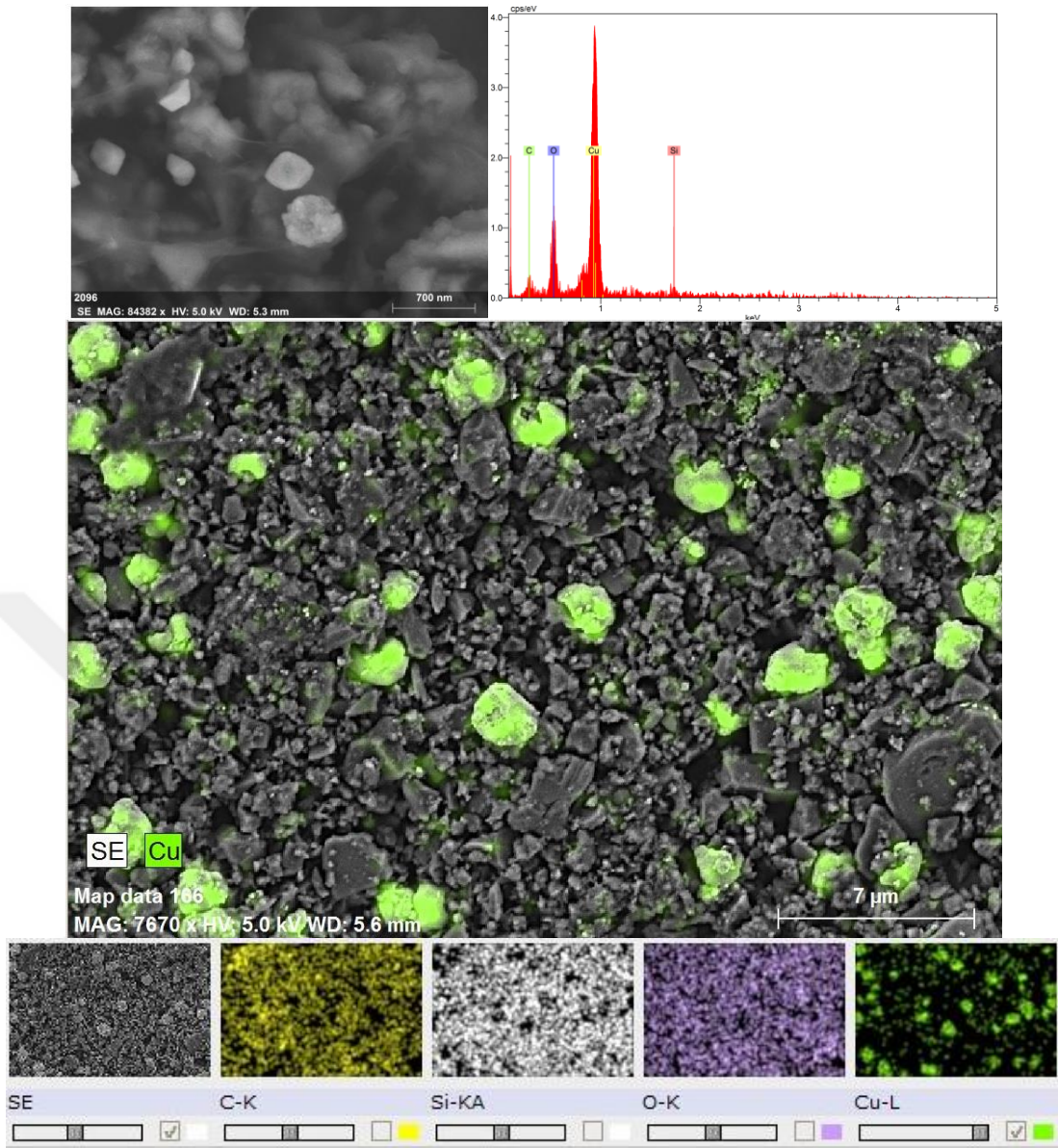
Figure 6.19 : EDS mapping and EDX of c-SiO electrodes with 30% NaCl salt after washing.

The 2D and 3D profile images with a small area of $10\mu m \times 10\mu m$ are observed with AFM in Figure 6.20 for c-SiO electrodes with 30% NaCl before washing and in Figure 6.21 for c-SiO electrodes after washing, respectively. From the AFM images, we can see that the rough structures on the copper surfaces changes depending on the porosity. In Table 6.2, Ra values of electrodes were given. The roughness of the electrode which has porosity after washing is 215 nm while electrode before washing has 144nm roughness.

Table 6.2 : Roughness (Ra) data of samples.

Sample	Ra (nm)
Electrode before washing	144
Electrode after washing	215
Copper foil	20
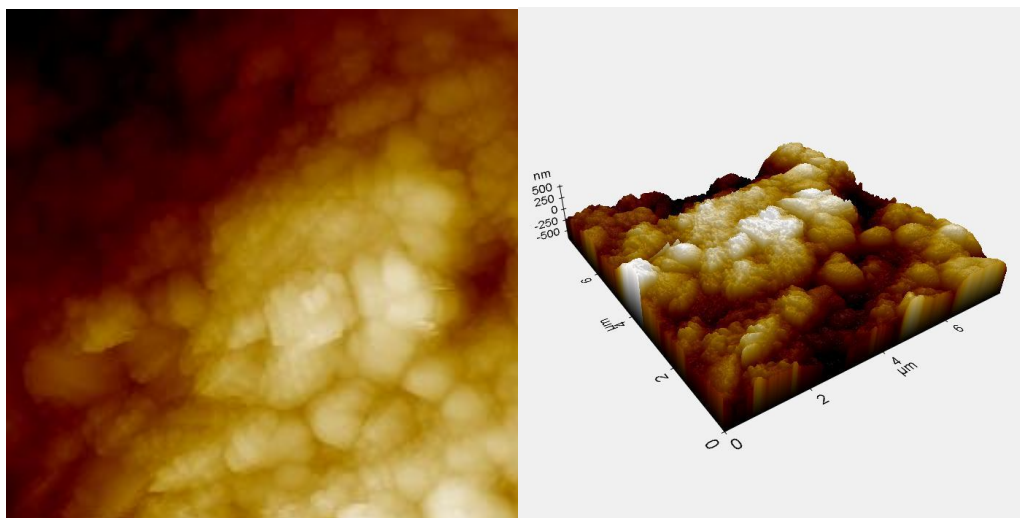
Figure 6.20 : AFM images ofc -SiO electrodes with 30% NaCl salt before washing
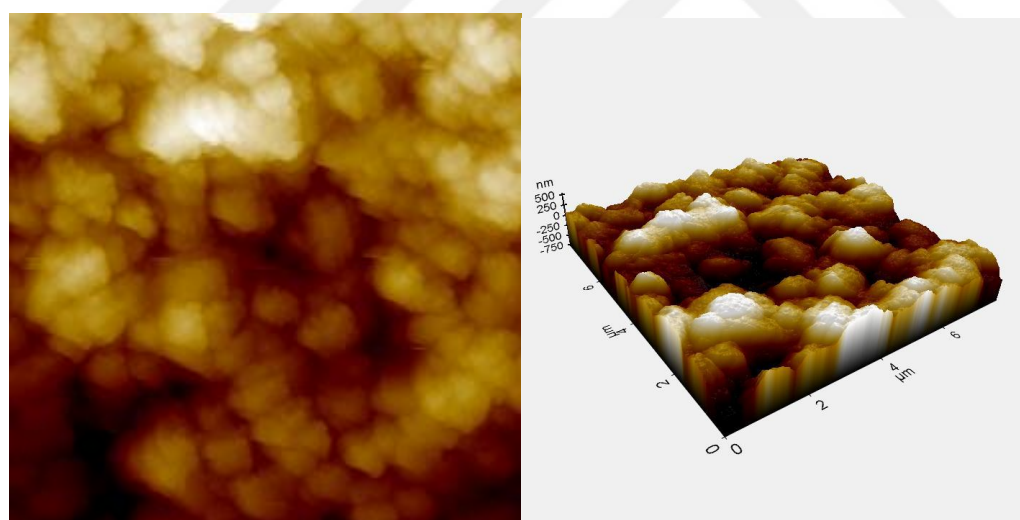
Figure 6.21 : AFM images of -SiO electrodes with 30% NaCl salt after washing.

Pycnometer measurements of c-SiO electrodes with 30% NaCl were performed to show pores volume change. In Table 6.3, results of pycnometry measurement were given with the pore volume of electrodes. In our study pore volume is increasing after NaCL removal which provides the pores on the anode structure.

Table 6.3 : Pycnometry measurement results of electrodes.

Sample	Pore volume (cm^3/g)
Electrode before washing	0.57
Electrode after washing	0.84

The porosity of the washed electrodes were calculated according to calculation given in Section 5.1.1 that c-SiO electrode with 30%NaCl had the porosity ~60% before washing and 66% porosity after washing the electrode. The mercury porosimeter analysis was performed to evaluate the porosity values with a measurement technique. Table 6.4 includes the summary of experimental data from mercury intrusion porosimetry. It was seen that before and after washing the electrode, it has the porosity of ~58% and and ~63%, respectively. These values are very close to calculated porosities that can be small difference comes from error of weight, thickness, area or density measurements. For the porosity calculation from mercury intrusion porosimetry, it was benefitted from reference [63].

Table 6.4 : The summary of experimental data from mercury intrusion porosimetry.

	non-porous electrode	porous electrode
[1]Volume of Hg intrusion per unit weight of electrode (ml g^{-1})	0.5507	0.6407
[2]Weight of electrode per unit area (g cm^{-2})	0.0159	0.0152
[3]Volume of Hg intrusion per unit area of electrode (ml cm^{-2}), (1)x(2)	0.0087	0.0097
[4]Density of composite film in electrode (g cm^{-3})	1.06	0.99
[5]Apparent volume of composite film per unit area (ml cm^{-2}) (2)/(4)	0.015	0.01535
[6]Porosity (%), (3)/(5)x100	58.3742	63.4293

To further characterize the improved porosity on c-SiO electrode structure, synchrotron X-ray microtomography was performed on electrode samples. Computed microtomography provides qualitative and quantitative 3D information [161, 162] about the morphology and transport phenomena in battery and fuel cell

materials, which traditional cross-section SEM could not achieve. In this work, the pores formed from the normal slurry preparation/lamination process are visualized in the volume rendering shown in Figure 6.22 b, c. These pores are important for electrolyte soaking and lithium ion transport, but at sizes of 1−10 μm they are not able to accommodate the 50− 100% volume changes of the c-SiO particles during lithiation/ delithiation. The extra pores generated by sacrificial NaCl particles at sizes of 10−100 μm (Figure 6.22 e,f) buffer the volume changes at the particle level, thereby enabling the improved electrochemical performance shown in Figure 6.39- Figure 6.42.
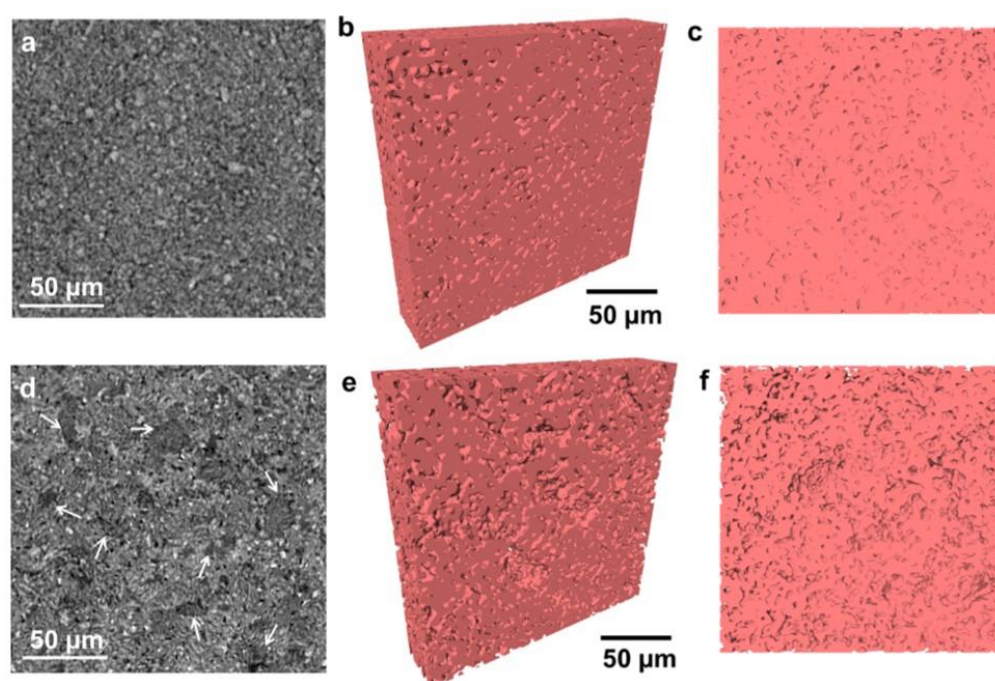
Figure 6.22 : Tomographically reconstructed cross-section and volume rendering of (a−c) the control c-SiO/PFM electrode and (d−f) the c-SiO/PFM electrode with porosity generation. The pores induced by NaCl are marked with arrows in the cross-section.

6.2.4 Characterization results of porous Si/PPy anode

The proof of the porosity generation method was performed by different anode active material such as silicon different polymer binder such as PPy. For this combination carbon black weren't used as the conductive additive since the PPy binder is conductive. In Figure 6.23 and Figure 6.24, the SEM images show the Si/PPy electrode before and after salt washing, respectively. Spherical silicon nanoparticles are very clear for both cases.
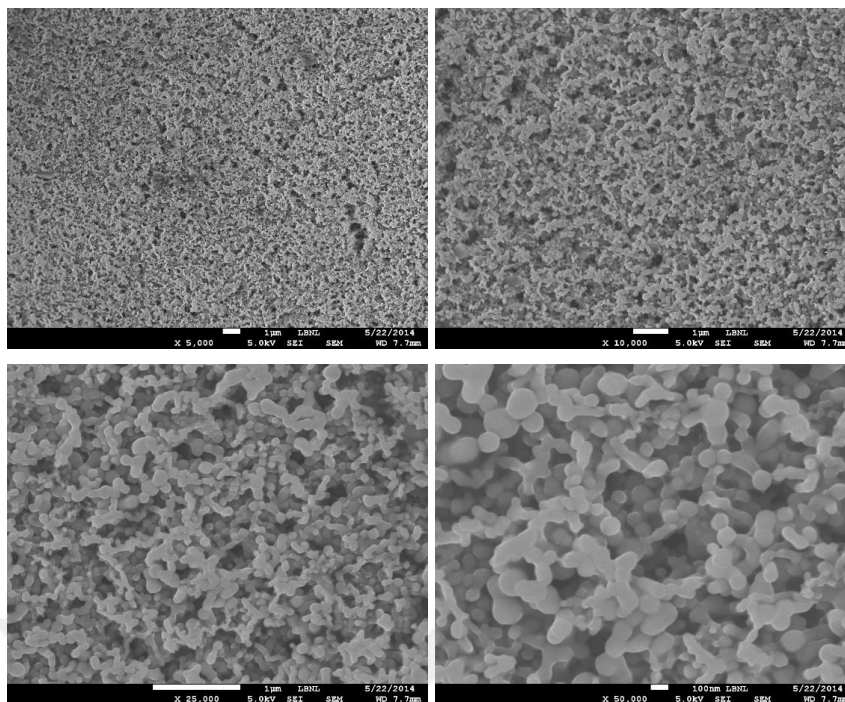
Figure 6.23 : SEM images of Si/PPy electrodes with 30% salt before washing.
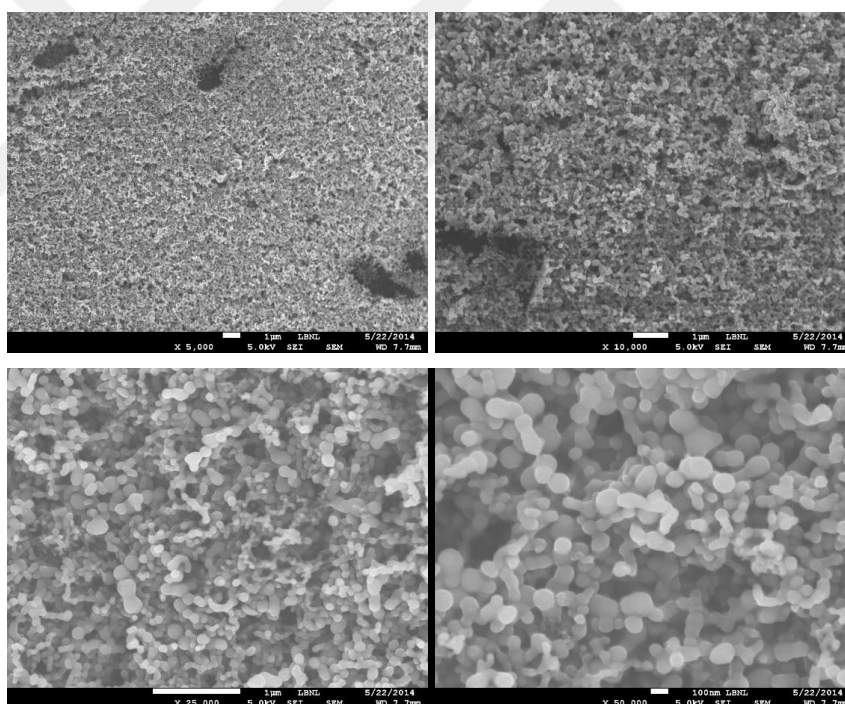
Figure 6.24 : SEM images of Si/PPy electrodes with 30% salt after washing.

In Figure 6.23, because the salt was dispersed on the anode structure, it is not distinguisable although silicon is nanoparticle and salt is micron-sized particle. So after washing the electrode and removal most of the NaCl, 1-5 micron-sized pores can be seen obviously in Figure 6.24. The density of pores and the size of the pores can be substantial for the electrochemical performance of the cells.

6.3 Electrochemical Test Results of c-SiO/PFM Anodes

As shown in Figure 6.25 the areal capacity is inversely related to the cycling performance while the specific capacities given in Figure 6.26 decrease when the mass loading increases. With c-SiO loadings below 2.5 mg/cm2, a stable cycling performance with desired specific capacities (>1000 mAh/g) is obtained. As the c-SiO area loading reaches as high as 3.39 mg/cm2, the cycling performance exhibits obvious capacity decay. This phenomenon is observed in all lithium-ion battery electrodes, but it is especially pronounced in the Si-based electrodes [165, 166]. As the loading and thickness increase, both the ion-transport distance and tortuosity of the pores in the composite electrode increase. Thus, lithium ion diffusion is inhibited. To further increase the areal capacity of the c-SiO/PFM system, the electrodes with the high loading ($\sim$3 mg c-SiO/ cm^2) are compressed into smaller porosities, as an attempt to increase electronic conductivity and facilitate the lithium ion diffusion by decreasing the ion transport distance [167-169]. As a typical micrometer-size particle-based electrode, the fabricated c-SiO/PFM has porosities in the range of 60% $\sim$ 65%. All the porosities were calculated by assuming that the weight fractions and density of each material were not changed by the fabrication process. During the calendering process, a section of electrode laminate was fed through the gap of the milling machine to compress the electrode to a desired thickness corresponding to the desired electrode porosity [170]. The electrodes are calendered into 51%, 47%, and 43% porosities, in order to investigate the relation between porosity and the electrochemical performance.
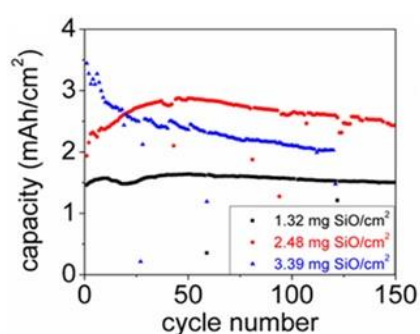
Figure 6.25 : The change of areal capacity with the number of cycles as a function of c-SiO loading at C/10 (100 mA/g).
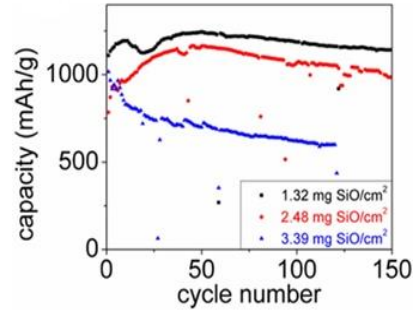
Figure 6.26 : The specific capacity with the number of cycles as a function of the c-SiO loading at C/10 (100 mA/g).

6.3.1 Electrochemical test results of calendered c-SiO/PFM anodes

The areal capacities and specific capacities are shown with half cell configuration in Figures 6.27 and 6.28. A 47% porosity is determined to deliver the best cell cycling performance, with a high Coulombic efficiency (CE, Figure 6.29). Electrodes with 51% porosity may still have too much porosity: the charge transport path is not improved to an ideal case, although the performance is indeed improved compared to the uncalendered electrode. The electrodes with 43% porosity, on the other hand, are overcompressed. The specific capacities (800−1000 mAh/g) of c-SiO correspond to a volume change of ∼100% during lithiation and delithiation. Therefore, moderate high porosity is still necessary on the electrode level to accommodate this large volume change. When overcompressed, the critical connections for electron transport such as particle/binder/particle connection, and binder adhesion on to the particle surface and current collector are also likely to be weakened, and the ion transport pathways become narrower to limit fast ion transport. It is likely that the particle/binder/particle connection is damaged during overcalendering. Binder adhesion on to the particle surface and current collector are also likely to be affected when too much compression is applied on the electrode.
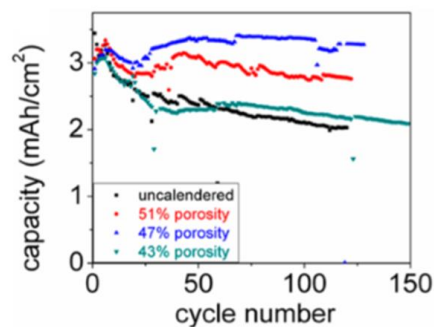
Figure 6.27 : Areal capacity of the c-SiO/PFM electrode after it was calendered into the different porosities.
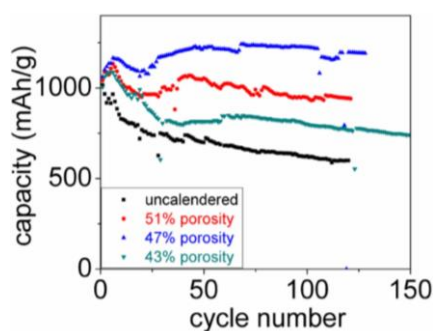
Figure 6.28 : Specific capacity of the c-SiO/PFM electrode after it was calendered into different porosities.

The galvanostatic voltage profiles are shown in Figure 6.30 (1st cycle) and Figure 6.31 (50th cycle). The voltage curves basically overlap with each other in the first cycle, indicating that the different electrode porosities do not take effect in the first lithiation/delithiation cycle. However, the voltage curves at the 50th cycle in Figure 6.31 correlate well with the cycling performance, with 47% porosity showing the lowest overpotential. With 47% porosity, the Coulombic efficiency (CE) of the cell is as high as 99.76% at the 50th cycle, compared to the CEs of electrodes with other porosities (99.33% for uncalendered sample, 99.45% for 51% porosity and 99.45% for 43% porosity, all at 50th cycle).
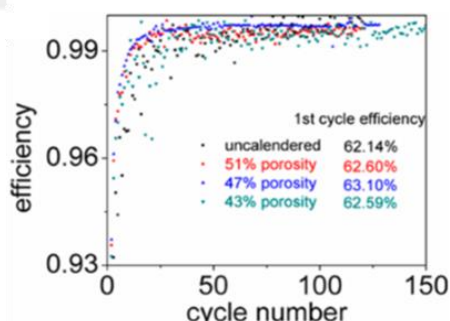
Figure 6.29 : Coulombic efficiency of the c-SiO/PFM electrode after it was calendered into different porosities, the cells were cycled at C/10 (100 mA/g).

High CE is critical for the long-term stable cycling of the anode electrode and better capacity retention at the full cell level [163, 164]. Besides the formation of SEI [165], lithium reacts and converts silicon oxide to silicate, which contributes to the large first cycle irreversible capacity [166]. A prelithiation strategy was used in a previous report to successfully solve this problem [167]. Note that the optimum electrode porosity has an electrode density of $\sim$1.2 g/cm^3 while delivering a high areal capacity of 3.5 mAh/ cm^2, which is a high-density electrode compared to most literature reports with similar high loading.
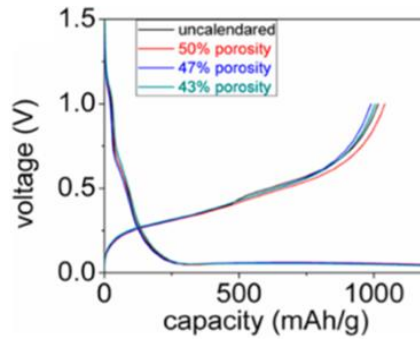
Figure 6.30 : Voltage profiles of the 1st cycle of the c-SiO/PFM electrode after it was calendered into different porosities.
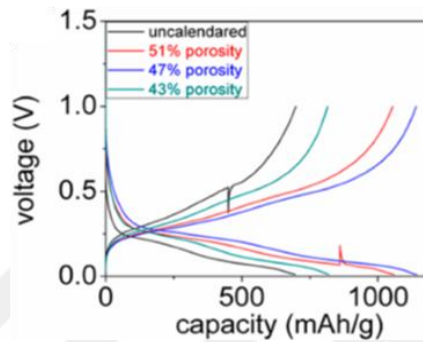
Figure 6.31 : Voltage profiles of the 50th cycle of the c-SiO/PFM electrode after it was calendered into different porosities.

The rate performance at C/2 and 1C rates in Figure 6.32 reveals that both 47% and 51% porosities improve the electrochemical performance of the c-SiO/PFM electrode. Either uncalendered electrode (63% porosity) or overcalendered (43% porosity) impairs the rate performance.
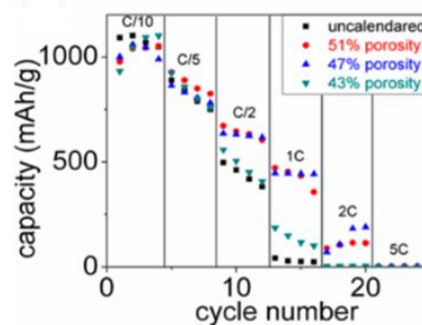
Figure 6.32 : Rate performance of the c-SiO/PFM electrode after it was calendered into different porosities.

The impedance of the half cells based on electrodes with different porosities is shown in Figure 6.33. The sample cells initially went through a formation cycle at C/10, and the impedance was measured at half lithiation, since the voltage of the cell was relatively stable at that stage. The electron conduction of a half cell can be separated

into two different ranges. Long-range conduction describes the process where the electrons move from the current collector through the bulk electrode laminate, which is inversely proportional to the high frequency intercept of the impedance sweep. Typically, long-range conductivity corresponding to high frequency impedance is not a limiting parameter for the electrode impedance. Short-range conduction corresponding to low frequency impedance describes the process is a limiting factor, which charge transfer at the electrode/electrolyte interface happens. After it was compressed into a more compact electrode architecture, the charge transfer impedance becomes lower compared to the uncalendered electrodes. This can be explained with that the pressure applied during calendering results in a better contact between the electrode matrix and the copper foil, decreasing the contact resistance and also better binding and conduction between the particles. These two effects decrease the overall cell impedance of electrodes after calendaring [9].
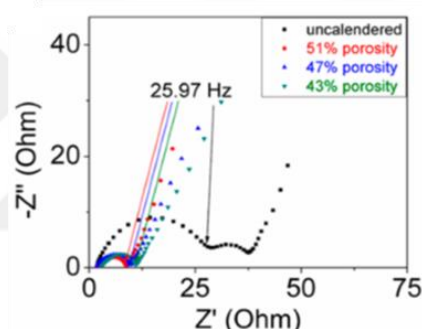
Figure 6.33 : The cell impedance based on the c-SiO/PFM electrode after it was calendered into different porosities.

6.3.2 Electrochemical test results of calendered Si/PAA anodes

Here, the effect of calendering on performance of Si/PAA and Si/nPAA electrodes was also investigated. Although Si/PAA and Si/nPAA cells showed 3120 mAh/g and 2561 mAh/g first cycle capacities, their capacities were 115 and 862mAh/g after 100 cycles, respectively. Si/PAA cell had a drastic capacity fading, however, Si/nPAA cell still had 512 mAh/g specific capacity after 250 cycles. Cycling performance of the electrodes were given in Figure 6.34.
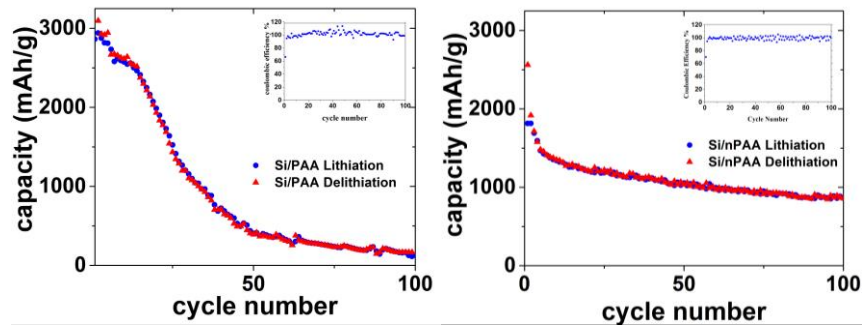
Figure 6.34 : The specific capacity of the Si/PAA and Si/nPAA.

Electrode performance of Si electrode was improved after the usage of nPAA. This results attributed to ionized groups which were identified by FTIR of nPAA improved the electrolyte swelling properties of the polymer. The improvement of swelling can be explained with the investigation of Boisvert et.al [168] that they showed the effective charge number increased when PAA was neutralized. In Figure 6.35a, FTIR spectra identify C-H bonds at around 1360 cm^{-1} and 1450 cm^{-1} for PAA. After neutralization of PAA, stretching frequencies of the carboxylate ion (COO-) were identified at 1400 and 1560. This indicated that the carboxylate functional groups of the nPAA were fully ionized. That result is very consistent with the study of Kirwan et. al [169] that they studied with PAA at different pH values. In the light of FTIR datas, the electrolyte swelling test was conducted in 1.2 M $LiPF_6$ which is in EC/DEC = 3:7 by weight, and 30% by FEC by weight. The polymer films were immersed to electrolyte for a week and got data periodically. In Figure 6.35b, it can be clearly seen that nPAA has 2.46% electrolyte uptake performance when PAA has 0.28%.
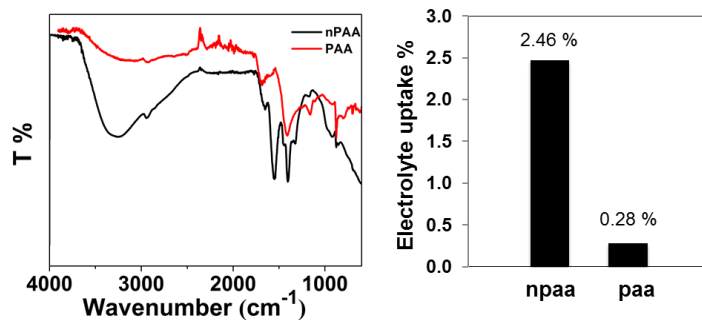
Figure 6.35 : a) FTIR peaks of PAA and nPAA b) Electrolyte swelling results of PAA and nPAA.

Since the calendering result of the c-SiO/PFM was found that 15% calendering is electrochemically the best result, Si/PAA electrode was also calendered as 15%. In

Figure 6.36, cycling data of calendered electrodes were given. When we compare the calendered electrodes data with uncalendered electrodes data (Figure 6.34), it is clearly seen that, after calendering the data are more stable because of more homogeneous and smoother electrode structure. The calendered Si/PAA electrode had 3492 mAh/g first cycle specific capacity when it is 511mAh/g after 100 cycles. In case of calendered Si/nPAA electrode, the specific capacities are 2409 and 1370 mAh/g at the first cycle and 100th cycle, respectively. As a result of observation, it was understood that electrodes are formed more homogeneous and smoother after calendering process. If porous structures are not in optimum size, volume change would cause breaks on electrode structure during lithiation-delithiation processes. Therefore, this design provided a better porosity condition as keeping the electrode structure integrity and resulted by higher specific capacity.
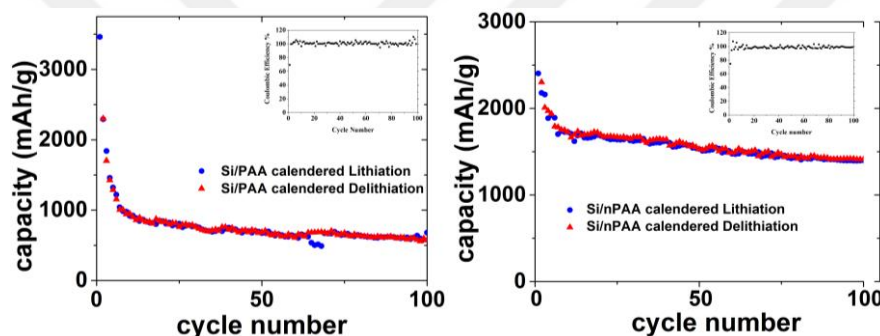
Figure 6.36 : The specific capacity of the calendered Si/PAA and Si/nPAA.

One of the challenges with Si electrodes is to increase the mass loading of electrode. It is a necessity for electric vehicles and consumer electronics to increase the areal mass loading (mg/cm^2) of electrode. It is generally below 0.3 mg/cm^2 [170]. In this study, we achieved the areal mass loading between 0.63 -0.71mg/cm^2 for Si/PAA electrode and 0.9-1.0 mg/cm^2 for Si/nPAA electrode. Figure 6.37 shows the discharge−charge profiles of the Si/PAA and Si/nPAA electrodes before and after calendering process for the first and the 100th cycle at C/10 between 0.01–2.5V. The initial delithiation and lithiation capacities of Si/PAA are 3492 mAh/g and 2418 mAh/g with a Coulombic efficiency (CE) of 66.41%. The irreversible capacity loss can be attributed to the formation of SEI layer and the irreversible reaction. Columbic efficiency at the first cycle was improved from 66.41 to 70.14 after neutralization. This result becomes more remarkable after calendering process. This is due to the Columbic efficiency at the first cycle increased from 69.25 to 74.76

after neutralization and calendering. This study shows that modification of PAA with neutralization and calendering process further enhanced the electrochemical performance of silicon anode. This result is very consistent with the literature studies [171-174] which were tried to develop electrochemical performance of silicon with different kind of modifications of PAA.
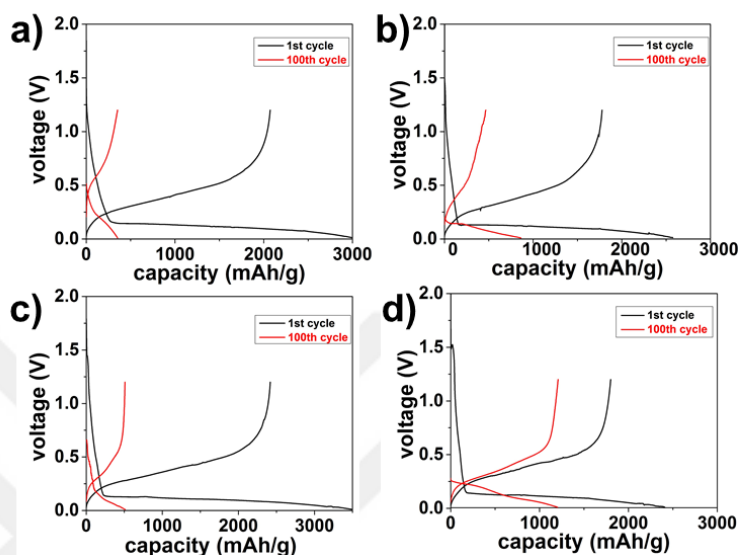
Figure 6.37 : Voltage profile of cells a) Si/PAA and b)Si/nPAA and Calendered c) Si/PAA and d) Si/nPAA.

In order to obtain information on the electrochemical reactions of the Si/nPAA and calendered Si/nPAA samples, cyclic voltammetry (CV) was performed in the potential range between 0.1 and 1.2V at a scan rate of 0.05 mV/s and electrochemical impedance spectroscopy (EIS) was performed between 100 kHz and 10mHz. In Figure 6.38a) and 6.38b), it is clearly seen that the first cycle curves of both sample are quite different from the subsequent ones. It is difficult to observe SEI peak which is consistent with voltage curves in Figure 6.37. This can be attributed to very thin SEI formation on Si anode surface. The first cycle peaks at the anodic side of both uncalendered and calendered electrodes showed the crystalline peak at around 0.6V where the uncalendered has an additionally amorphous peak at around 0.47V [175]. This can be explained the effect of particle interaction after calendering that delays the conversion of crystalline structure to amorphous. In Figure 6.38a), for following cycles, lithiation produced the sharp peaks at 0.1V in cathodic sweep and there are two peaks at 0.35 and 0.48V at the anodic sweep could be assigned to delithiation process of Li_xSi [176]. In Figure 6.38b), at the 1st cycle there is a main cathodic peak at around 0.1V, corresponding to the lithiation reaction of Si to form Li_xSi alloy,

while the two anodic peaks are at 0.33 and 0.50 V. During the following cycles, the same peaks are observed.
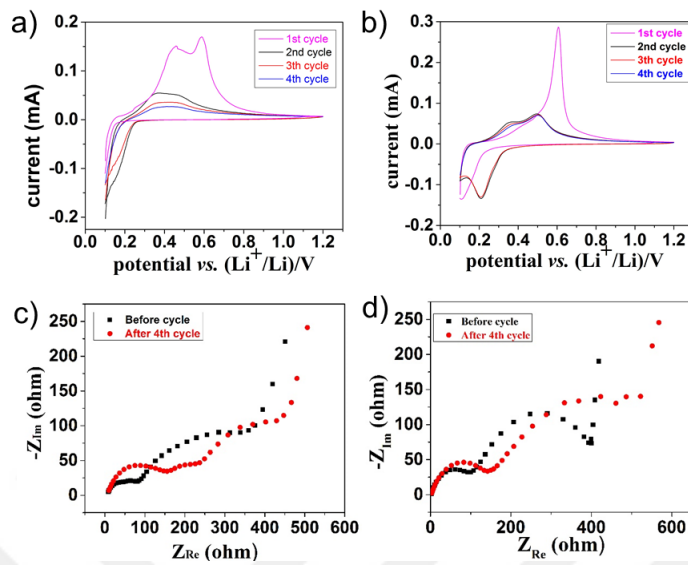
Figure 6.38 : Cyclic voltammograms of (a) Si/nPAA and (b) calendered Si/nPAA and Electrochemical impedance spectra of (c) Si/nPAA and (d) calendered Si/nPAA.

In Figure 6.38c) and 6.38d) the typical Nyquist plots (Z_{re} vs. $-Z_{im}$) of Si/nPAA and calendered Si/nPAA were compared. They were in half cells at open circuit voltage state and after 4 cycles at the delithiation state. The semicircles can be assigned to the charge transfer impedance of the electrodes. In the high-frequency and medium frequency regions, the semicircles are assigned to the SEI and impedance of the interfacial charge-transfer, respectively. The low frequency region is referred to the impedance of Li ion diffusion. As shown, both samples demonstrated similar impedance before cycling start which had very close semicircles in high frequency region. After 4 cycles, both uncalendered Si/nPAA sample and calendered Si/nPAA sample had three semicircles shown with frequencies as 2500Hz, 10Hz and 250mHz for uncalendered sample and shown with frequencies as 400Hz, 250mHz and 40mHz, respectively. While EIS curves of uncalendered Si/nPAA exhibit three semicircles for the high-to-intermediate frequency region, calendered Si/nPAA sample has additional 3rd semicircle at lower frequency. This can be explained more stable SEI layer after calendering process that increases the electrode structure integrity providing the higher electron transfer. This is also consistent with cycling performance of calendered Si/nPAA electrochemical performance which has higher performance. It is also observed that, the semicircle of calendered Si/nPAA samples was smaller than uncalendered Si/nPAA samples in the high frequency region that

62

can be assigned to electrical conductivity [177] and higher charge transfer resistance after calendering process.

6.3.3 Electrochemical test results of porous c-SiO/PFM anodes

To demonstrate the capability of our high-porosity Si-based anode toward this practical application, a high loading c-SiO/PFM anode with porosity generated by 10, 30 and 60 wt% NaCl was cycled at C/10 for 2 cycles as a formation step, and at C/3 long-term cycling was then performed. Note that the electrode was only composed of active material and polymer binder without any carbon conductive additives. Figure 6.39 and Figure 6.40 shows the influence of adding 10% NaCl on the electrochemical performance of c-SiO anode. Black-red (3.00 mg c-SiO/cm^2) and green-blue (3.39 mg c-SiO/cm^2) curves correspond to electrodes with similar loadings and show the influence of including 10wt% ball-milled NaCl. The control sample with 3.39 mg c-SiO/ cm^2 exhibits gradual capacity decay over cycling (green-blue curve). After porosity generation, 10% NaCl is enough to generate sufficient internal porosity to stabilize the cycling performance, allowing an areal capacity of above 3 mAh/cm^2 to be maintained over 100 cycles at a C/10 rate (0.3 mA/cm^2).
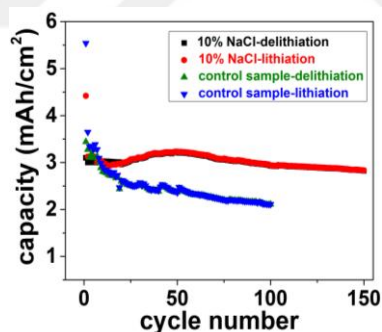
Figure 6.39 : Areal capacity of the c-SiO/PFM electrodes with 10 % NaCl and without NaCl.
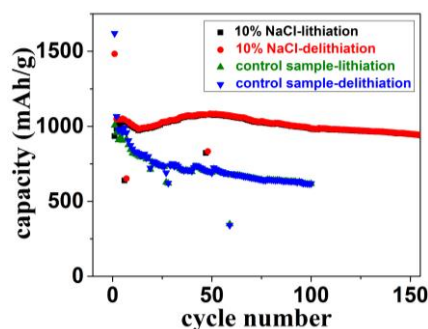
Figure 6.40 : Specific capacity of the c-SiO/PFM electrodes with 10% NaCl and without NaCl.

Figure 6.41 and Figure 6.42 shows the influence of adding 30% NaCl on the electrochemical performance of c-SiO anode. Black-red (5.26 mg c-SiO/cm^2) and green-blue (4.89 mg c-SiO/cm^2) curves have similar c-SiO loadings and show the influence of 30wt% NaCl. The control sample with active material loading as high as 4.89 mg c-SiO/cm^2 almost shows cell failure after a couple of cycles at C/10 (green-blue curve). A larger amount of NaCl (30 wt %) is added to generate more internal porosity to accommodate the volume expansion of the active material particles and facilitate lithium ion transport, allowing an areal capacity of above 4 mAh/cm^2 to be maintained over the first 30 cycles at a C/10 rate (0.49 mA/cm^2). Note that the relatively noisy data are common for the high-loading cells in this work, presumably due to the evolution of electrical contact during cell cycling.
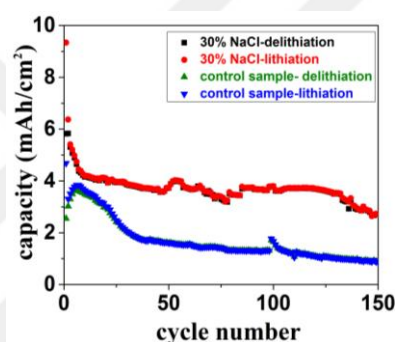
Figure 6.41 : Areal capacity of the c-SiO/PFM electrodes with 30 % NaCl and without NaCl.
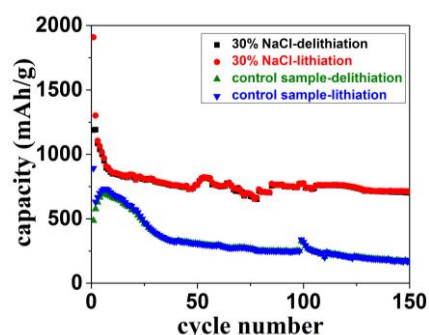
Figure 6.42 : Specific capacity of the c-SiO/PFM electrodes with 30% NaCl and without NaCl.

The voltage curves for the improvement of electrodes with a high material loading were shown in Figure 6.43 and in Figure 6.44 for 10%NaCl at 1st and 100th cycle respectively. The voltage curves of 30%NaCl sample were also given in Figure 6.45 and in Figure 6.46 at 1st and 100th cycle, respectively. The effect of porosity generation is quite clear even for the first cycle, permitting access to almost theoretical lithiation (1900 mAh/g) and delithiation (1100 mAh/g) capacities of the c-

SiO anode. A higher porosity should facilitate lithium ion transport and increase exposure of c-SiO active material particles to electrolyte solution [111]. Both factors may contribute to the successful recovery of the full capacities of the active c-SiO materials. A porous lithium-ion electrode can be described macroscopically by two important parameters, electrode tortuosity (τ) and electrode porosity (ε). High tortuosity can hinder the rate of ion transport through the porous electrode network. Bruggeman relation describes the relationship between tortuosity and porosity [178].

$$\tau = \varepsilon^{-\alpha} \tag{6.2}$$

The relation (6.2) suggests that increased porosity is associated with decreased tortuosity. Both changes should facilitate lithium ion transport during cell operation, promoting the enhanced material loading and stabilized cycling performance seen in Figure 6.39-Figure 6.42. The major electrochemical parameters of the cells are only meaningful to compare electrodes with similar loadings. Incorporating 10 wt % NaCl probably does not generate enough porosity to significantly modify the initial cycling performance of the c-SiO electrode, as the capacity decay at this loading ($\sim$3 mg c-SiO/ cm^2) only occurs after 10 cycles. Control sample and the samples with 10% NaCl show only minor differences in performance initially, although the electrode with 10% NaCl shows higher Coulombic effciency (CE) and capacity retention over the rest of the cycling process. At an active material loading as high as $\sim$5 mg c-SiO/cm^2, the sample with 30wt % NaCl shows a large difference even at the first cycle. The charge capacity is improved to 1189 mAh/g from a value of 535.6 mAh/g in control sample of 30% NaCl, presumably due to the improved access of lithium ion to the active material particles. Although it starts with a high capacity, the modified electrode is able to retain $\sim$60% of its initial capacity, compared to $\sim$30% for the control sample.
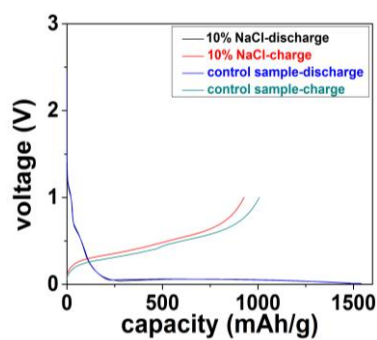
Figure 6.43 : 1st cycle voltage curves of samples with 10% NaCl and without NaCl.
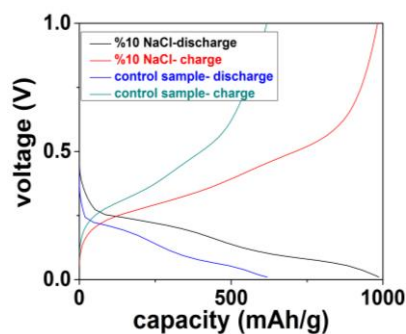
Figure 6.44 : 100th cycle voltage curves of samples with 10% NaCl and without NaCl.
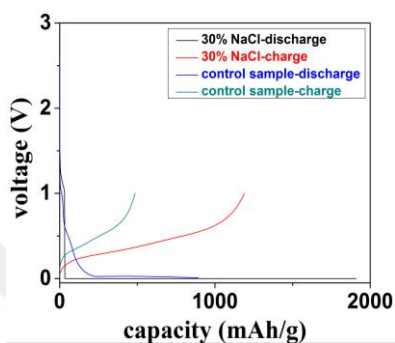
Figure 6.45 : 1st cycle voltage curves of samples with 30% NaCl and without NaCl.

Figure 6.46 : 100th cycle voltage curves of samples with 30% NaCl and without NaCl.

The study also was conducted for 60wt% NaCl. Figure 6.47 shows the cycling performance of the c-SiO/PFM electrode with 60wt% NaCl. It is seen that there is a serious capacity fade after a few cycles as the specific capacity was around 230mAh/g after 100 cycles. When it is compared to electrode with 30wt% NaCl design, it was around 750mAh/g after 100 cycles. In this design, it was probably generated too much porosity, which was, resulted the integrity loss of anode structure. This result is very consistent with the SEM image of cycled electrode which has cracks on the surface (Figure 6.55). The voltage profile in Figure 6.48 also shows the first cycle performance which has 58% CE.

Figure 6.47 : Cycling performance of the c-SiO/PFM electrodes with 60% NaCl.
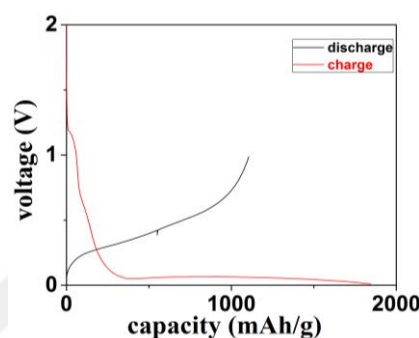
Figure 6.48 : 1st cycle voltage curves of c-SiO/PFM electrodes with 60% NaCl.

As shown in Figure 6.49a an areal capacity of 3 mAh/cm^2 was still maintained at this high current density (1.7 mA/cm^2). According to literature, this is one of the highest reported areal loadings for a Si-based anode at such a high charge/discharge rate. Note that the electrode was only composed of active material and polymer binder without any carbon conductive additives. Impedance data from the half cells based on electrodes with or without NaCl is shown in Figure 6.49b The sample cells initially went through a formation cycle at C/10, and impedance was measured at half lithiation; at this stage, cell potentials were relatively stable. There are two different ranges of the electron conduction in a lithium-ion half cell. Long-range conduction describes the process by which the electrons move from the current collector through the bulk electrode laminate, which is inversely proportional to the high-frequency intercept of the impedance sweep. Typically, long-range conductivity corresponding to high frequency impedance is not a limiting parameter for the electrode impedance. However, short-range conduction corresponding to low-frequency impedance describes the process by which charge transfer at the electrode/electrolyte interface happens, which is a limiting factor. With a higher internal porosity, the charge transfer impedance becomes smaller compared to that of the control electrodes. After washing of c-SiO/PFM electrodes with 30% NaCl, it shows

obviously the lowest interface resistance and surface charge transfer resistance, as compared to that of the control sample, which means faster Li intercalation kinetics. Here, there can be also effect of Cu particles on the electrode surface shown in SEM images (Figure 6.13, 6.15 and 6.17) and EDS mapping (Figure 6.19). Various studies in the literature have been performed with Cu and Cu_xO [179-184] that provides several advantages as:

- Improving the modulus, strength, and hardness of the electrodes due to the reinforcing effect that provides to maintain the structure integrity of the electrodes, leading to enhanced cyclic performance.

- Acting as buffer medium to absorb mechanical stress caused by the volumetric change of the silicon nanoparticles because copper possess excellent mechanical strength and ductile ability.

- Helping to build electronic transportation path along with increasing cycles due to their outstanding electron conductivity.

In our study, greater cycling performance was obtained with both 10% NaCl and 30% NaCl addition/removing process, which provided porous anode structure. The precipitated copper particles could also support the structure integrity with maintaining the ductility. The other advantage of copper particles could be the electron conductivity which decreases charge transfer impedance of the porous electrode compared to the control sample.
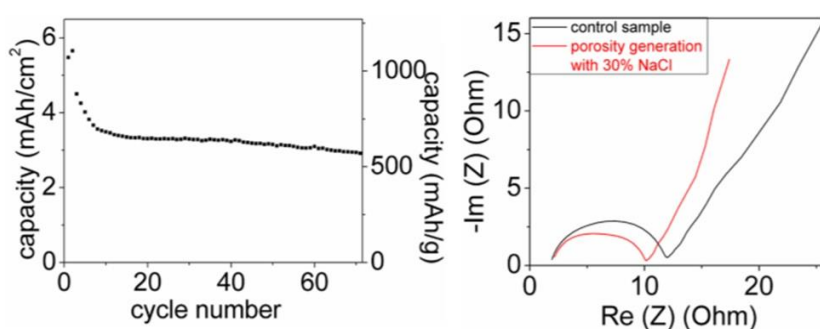
Figure 6.49 : (a)Cycling performance of the c-SiO/PFM electrodes with porosity generation, C/10 for the first two cycles then C/3 (1.7 mA/cm²). (b) Cell impedance of the c-SiO/PFM half cells with or without porosity generation using 30 wt % NaCl.

6.3.4 Electrochemical test results of porous Si/PPy anodes

Porosity generation method was performed with Si/PPy electrode design to compare it to c-SiO/PFM. The best result for c-SiO/PFM design was the case of 30% NaCl

addition. Here, this design was used. The mass loading of the electrode is 1 mg Si/cm^2. Figure 6.50 shows the cycling performance of Si/PPy electrode with 30wt% NaCl. The first cycle specific capacity is 4168 mAh/g and after 100 cycles it is 2134 mAh/g. The first cycle coulombic efficiency of the electrode is 70%. The cycling performance of the electrode seems stable after a few cycle. In consideration of the high mass loading for silicon active material, this stability can be explained with the generated pores that may provide enough volume for Silicon expansion during the lithiation process. This helps to keep the anode structure together and use the electrode for higher for cycles.
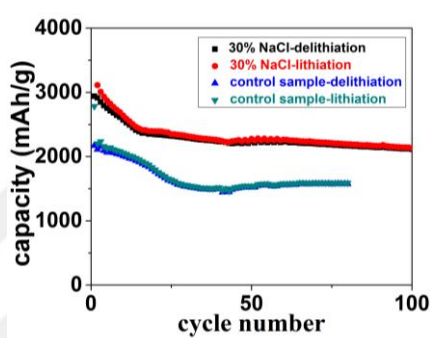
Figure 6.50 : Specific capacity of the Si/PPy electrodes with 30% NaCl and without NaCl.

The voltage curves of Si/PPy electrodes with 30% NaCl and without NaCl were shown in Figure 6.51 and in Figure 6.52 at 1st and 50th cycle, respectively. Porosity generated Si/PPy electrode shows 4168 mAh/g and 2941 mAh/g 1st cycle discharge and charge capacity, respectively while Si/PPy electrode without NaCl has 2782 mAh/g and 2170 mAh/g 1st cycle discharge and charge capacity, respectively. At 50th cycle it is obviously seen that, porosity generated Si/PPy electrode showed 2239 mAh/g delithiation capacity which was improved from 1543 mAh/g of control sample capacity.
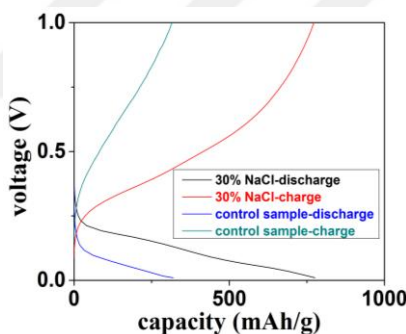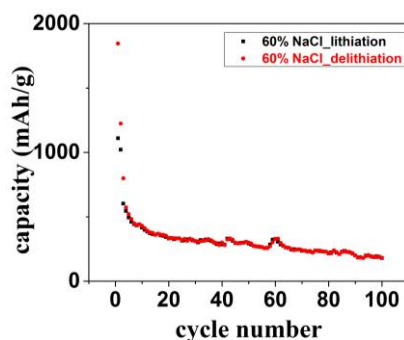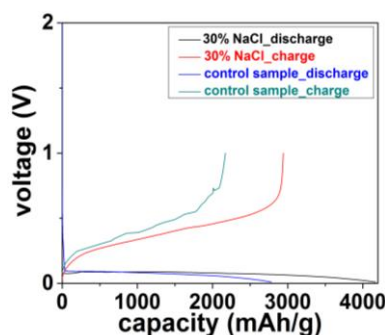

Figure 6.51 : 1st cycle voltage curves of Si/PPy samples with 30% NaCl and without NaCl.
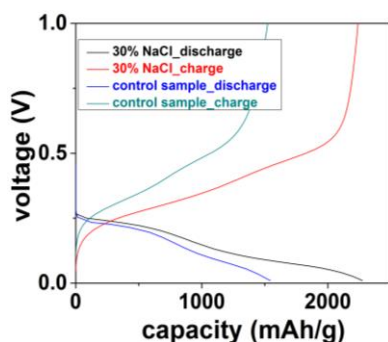
Figure 6.52 : 100th cycle voltage curves of Si/PPy samples with 30% NaCl and without NaCl.

6.4 Characterization Results of Anodes After Cycling

6.4.1 Characterization results of calendered c-SiO/PFM anodes after cycling

In Figure 6.53, SEM images of 15% calendered c-SiO/PFM electrodes after 50 cycles were given. When the SEM images of cycled electrodes were compared to Figure 6.6, it is seen that cycled electrode have more cohesive appearance. This can be explained the volume change of silicon oxide particles after cycling that fill the empty spaces.
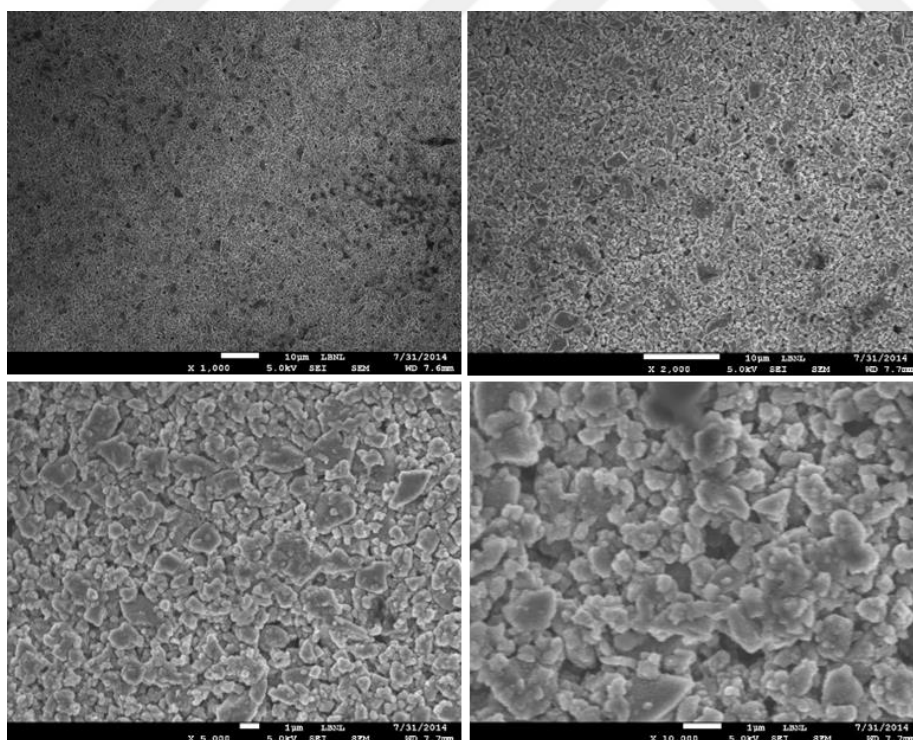
Figure 6.53 : SEM images of 15% calendered c-SiO electrodes after 50 cycles.

6.4.2 Characterization results of porous c-SiO/PFM anodes after cycling

In Figure 6.54, SEM images of c-SiO/PFM anodes with 30% NaCl process after 50 cycles were given. Although SiO particles had volume change, the pulverization and peeling off of the electrode materials, which are often observed in silicon electrodes after cycling, are not observed. Because there is not seen any cracks on the electrode structure and that means, porosities generated by our method can well accommodate the volume change of the c-SiO.
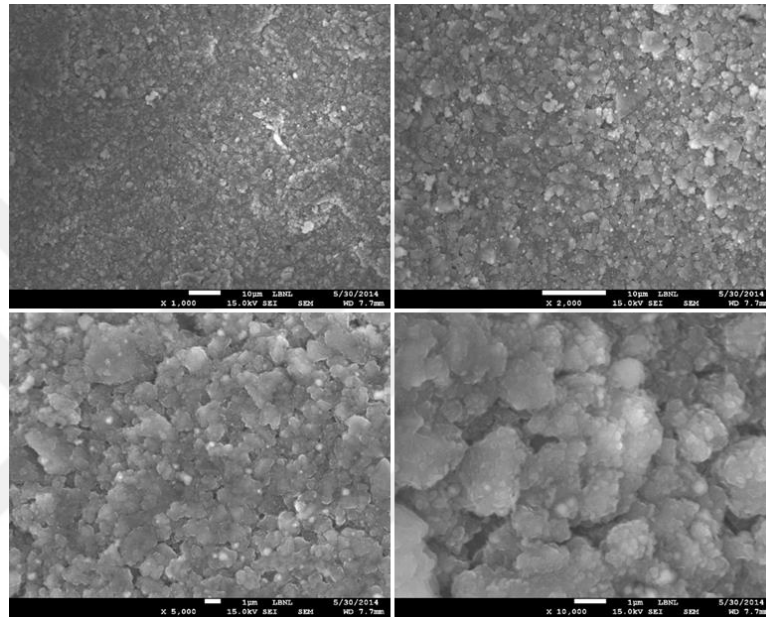
Figure 6.54 : SEM images of c-SiO electrodes with 30wt% salt process after 50 cycles.
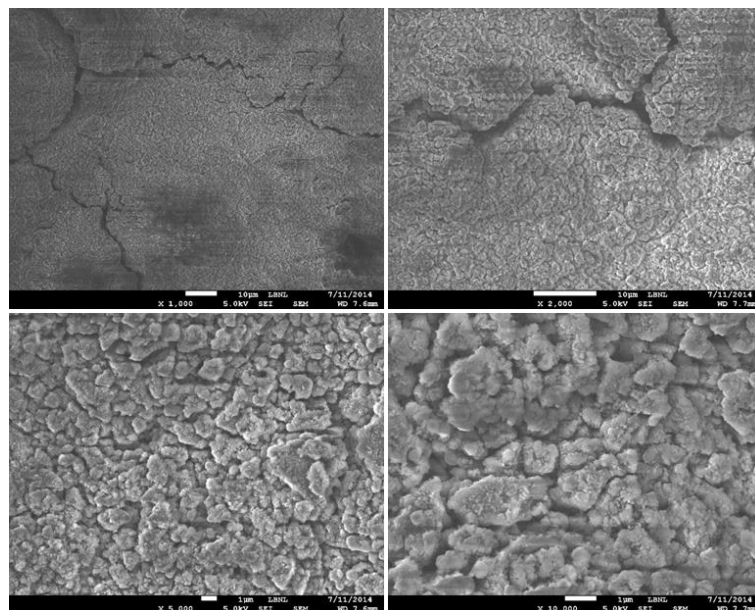
Figure 6.55 : SEM images of c-SiO electrodes with 60wt% salt process after 50 cycles.

71

In Figure 6.55 SEM images of c-SiO/PFM anodes with 60% NaCl process after 50 cycles were shown. Afer 50 cycles, the cracks are seen clearly. It is very consistent with the cycling data shown in Figure 6.47, which shows very poor cycling performance.

7. CONCLUSION AND RECOMMENDATION

Silicon is one of the most promising candidates as an anode active material because of its high theoretical capacity (more than 3579 mAh/g at room temperature) and low average discharge potential ($\sim$0.5 V vs Li/Li+). Furthermore, Si is the second most abundant element on earth and it is an environmentally benign material. Unfortunately, huge volume expansion (300% at full lithiation of Si) due to the lithium ion diffusion during the lithiation/delithiation process causes drastic capacity fade because of the high internal stresses, loss of electrical contact and the formation of non-electronic and ionic conductive passivation film between the anode surface and electrolyte.

In this thesis, solutions have been presented for problems of silicon based anode materials. High loading anodes are very important for high energy density batteries. However, because of the silicon based materials problem, it is not possible to provide a high loading anode. Here, the calendering ratio of the Si-based anodes were optimized and porosity genearation method which allows to get a high-loading electrode with good cycling performance was developed. The studies in this thesis were concluded as:

1) As a result of calendering optimization, which is the first part of our thesis work, the optimum calendering ratio was found as 15%.

2) Pycnometer measurement showed decreasing pore volume from 0.63cm^3/g to 0.57, 0.48 and 0.43 cm^3/g for 10%, 15% and 20% calendering, respectively. The electrode density was also increased by calendering from 3.17 g/cm^3 to 3.36, 4.03 and 4.79 cm^3/g for 10%, 15% and 20% calendering, respectively.

3) The c-SiO/PFM anode composition reached a loading capacity of 3.5 mAh/cm^2 and a specific capacity of 1250 mAh/g after 100 cycles with 15% calendering.

4) When the same calendering ratio was applied to the Si/PAA and Si/nPAA anode combinations, the electrode exhibited a stable cycle performance and

gave a specific capacity of 511 and 1370 mAh/g at the end of the 100th cycle, respectively.

5) In the second part of the thesis, in the porosity formation study we conducted, c-SiO/PFM anode working with 10% NaCl gave 3 mAh/cm^2 loading capacity and a specific capacity of 1000 mAh/g after 100 cycles.

6) The c-SiO/PFM anode operated with 30% NaCl gave 4 mAh/cm^2 loading capacity and a specific capacity of 750 mAh/g at 100 cycles.

7) Characterizations of electrodes before and after porosity generation were proved the generated porosities. SEM images demonstrated pores, AFM results showed higher Ra value after porosity generation and results of pycnometry and mercury porosimetry showed increased pore volume and porosity.

8) EDS mapping and EDX dot analysis showed Cu particles on the electrode surface arised from dissolution of copper current collector during the washing process.

9) The method was also applied to the Si/PPy anode composition using 30% NaCl.

10) With the Si/PPy anode operating with 30% NaCl, it was reached a specific capacity of 1100 mAh/g at 100 cycles.

When these results were compared to studies in the literature, it makes results and contribution of this thesis much remarkable. The studies in this thesis provide an easy, feasible and applicable methods to be able to use silicon based anodes which have a large advantage as the anode material. For example, Fang et.al.[113] performed a good study with SiO_2&Si nanoparticles/carbon composite films that the specific capacity of 1200mAh/g was achieved. But this was achieved when the areal capacity was 0.46mAh/cm^2. In another study, Takezawa et. al. [114] used three different oxygen containing SiO_x material which x is 0.17, 0.68 and 1.02. They reached the maximum areal capacity of 2 mAh/cm^2 with $SiO_{1.02}$ sample after 30 cycles. Marinaro et.al [115] was also studied areal capacity of Si/C composite. They reached 3.25 mAh/cm^2 areal capacity with the 900 mAh/g specific capacity. There so many examples to show the areal capacities and compare our results. As far as is known, the results of this thesis reach a very high mass loading and areal capacity for

silicon based materials. The another advantages of our results are using easy, cheap and applicable method and it is not required to change a present commercial system.

In the light of results from this study, the suggestions to develop new generation anode materials and anode production methods for lithium ion batteries were given below:

1) To develop further methods for pore sizes,

2) To generate pores on the anode under more control to specify the pores accommodation,

3) Further characterization of anode structure before and after cycling,

4) To study the effect of starting porosity, thickness, material loading and AM/binder composition in detail.

5) Applicability of the method for other type batteries such as sodium ions, magnesium ions, aluminum ions.

REFERENCES

[1] Yang, M., Zhong, Y., Ren, J., Zhou, X., Wei, J., and Zhou, Z. (2015). Electrochemical Capacitors: Fabrication of High-Power Li-Ion Hybrid Supercapacitors by Enhancing the Exterior Surface Charge Storage. *Advanced Energy Materials, 5* (17).

[2] Zhou, M., Li, X. L., Wang, B., Zhang, Y. B., Ning, J., Xiao, Z. C., Zhang, X. H., Chang, Y. H., and Zhi, L. J. (2015). High-Performance Silicon Battery Anodes Enabled by Engineering Graphene Assemblies. *Nano Letters, 15* (9)**,** 6222-6228.

[3] Url-1 <http://www.iec.ch/whitepaper/energystorage/>**,** date retrieved 12.01.2017.

[4] Tang, Y. X., Zhang, Y. Y., Li, W. L., Ma, B., and Chen, X. D. (2015). Rational Material Design for Ultrafast Rechargeable Lithium-Ion Batteries. *Chemical Society Reviews, 44* (17)*,* 5926-5940.

[5] Mahmood, N. and Hou, Y. L. (2014). Electrode Nanostructures in Lithium-Based Batteries. *Advanced Science, 1*(1), 20.

[6] Zhang, J. S., Bai, Y., Sun, X. G., Li, Y. C., Guo, B. K., Chen, J. H., Veith, G. M., Hensley, D. K., Paranthaman, M. P., Goodenough, J. B., and Dai, S. (2015). Superior Conductive Solid-Like Electrolytes: Nanoconfining Liquids within the Hollow Structures. *Nano Letters, 15* (5)**,** 3398-3402.

[7] Url-2 <https://www.technologyreview.com/s/601500/24ms-batteries-could-better harness-wind-and-solar-power/>**,** date retrieved 20.10.2016.

[8] Url-3 <http://www.greencarcongress.com/2009/02/silicon-based-a.html>**,** date ret rieved 18.10.2016.

[9] Smekens, J., Gopalakrishnan, R., Van den Steen, N., Omar, N., Hegazy, O., Hubin, A., and Van Mierlo, J. (2016). Influence of Electrode Density on the Performance of Li-Ion Batteries: Experimental and Simulation Results. *Energies, 9* (2), 104-116.

[10] Gao, J., Shi, S. Q., and Li, H. (2016). Brief Overview of Electrochemical Potential in Lithium Ion Batteries. *Chinese Physics B, 25* (1)*,* 018210-018234.

[11] Goodenough, J. B., and Kim, Y. (2010). Challenges for Rechargeable Li Batteries. *Chemistry of Materials, 22* (3), 587-603.

[12] Goodenough, J. B. (2014). Electrochemical Energy Storage in a Sustainable Modern Society. *Energy & Environmental Science, 7* (1)*,* 14-18.

[13] Reddy, M. V., Rao, G. V. S., and Chowdari, B. V. R. (2013). Metal Oxides and Oxysalts as Anode Materials for Li Ion Batteries. *Chemical Reviews, 113* (7)*,* 5364-5457.

[14] **Mahmood, N., Tang, T. Y., and Hou, Y. L.** (2016). Nanostructured Anode Materials for Lithium Ion Batteries: Progress, Challenge and Perspective. *Advanced Energy Materials, 6* (17), 1600374-1600396.

[15] **Zhang, B., Ghimbeu, C. M., Laberty, C., Vix-Guterl, C., and Tarascon, J.-M.** (2016). Correlation between Microstructure and Na Storage Behavior in Hard Carbon. *Advanced Energy Materials, 6* (1), 1501588.

[16] **Licht, S., Douglas, A., Ren, J. W., Carter, R., Lefler, M., and Pint, C. L.** (2016). Carbon Nanotubes Produced from Ambient Carbon Dioxide for Environmentally Sustainable Lithium-Ion and Sodium-Ion Battery Anodes. *Acs Central Science, 2* (3), 162-168.

[17] **Higgins, T. M., Park, S. H., King, P. J., Zhang, C., MoEvoy, N., Berner, N. C., Daly, D., Shmeliov, A., Khan, U., Duesberg, G., Nicolosi, V., and Coleman, J. N.** (2016). A Commercial Conducting Polymer as Both Binder and Conductive Additive for Silicon Nanoparticle-Based Lithium-Ion Battery Negative Electrodes. *Acs Nano, 10* (3), 3702-3713.

[18] **Rowsell, J. L. C., Pralong, V., and Nazar, L. F.** (2001). Layered Lithium Iron Nitride: A Promising Anode Material for Li-Ion Batteries. *Journal of the American Chemical Society, 123* (35), 8598-8599.

[19] **Cabana, J., Monconduit, L., Larcher, D., and Palacin, M. R.** (2010). Beyond Intercalation-Based Li-Ion Batteries: The State of the Art and Challenges of Electrode Materials Reacting through Conversion Reactions. *Advanced Materials, 22* (35), E170-E192.

[20] **Silva, D. C. C., Crosnier, O., Ouvrard, G., Greedan, J., Safa-Sefat, A., and Nazar, L. F.** (2003). Reversible Lithium Uptake by Fep2. *Electrochemical and Solid State Letters, 6* (8), A162-A165.

[21] **Boyanov, S., Bernardi, J., Gillot, F., Dupont, L., Womes, M., Tarascon, J. M., Monconduit, L., and Doublet, M. L.** (2006). Fep: Another Attractive Anode for the Li-Ion Battery Enlisting a Reversible Two-Step Insertion/Conversion Process. *Chemistry of Materials, 18* (15), 3531-3538.

[22] **Gillot, F., Monoconduit, L., Morcrette, M., Doublet, M. L., Dupont, L., and Tarascon, J. M.** (2005). On the Reactivity of Li8-Ymnyp4 toward Lithium. *Chemistry of Materials, 17* (14), 3627-3635.

[23] **Poizot, P., Laruelle, S., Grugeon, S., Dupont, L., and Tarascon, J. M. (2000).** Nano-Sized Transition-Metaloxides as Negative-Electrode Materials for Lithium-Ion Batteries. *Nature, 407* (6803), 496-499.

[24] **Kraytsberg, A., and Ein-Eli, Y.** (2016). Conveying Advanced Li-Ion Battery Materials into Practice the Impact of Electrode Slurry Preparation Skills. *Advanced Energy Materials, 6* (21), 1600655-1600678.

[25] **Baunach, M., Jaiser, S., Schmelzle, S., Nirschl, H., Scharfer, P., and Schabel, W.** (2016). Delamination Behavior of Lithium-Ion Battery Anodes: Influence of Drying Temperature During Electrode Processing. *Drying Technology, 34* (4), 462-473.

[26] Haselrieder, W., Westphal, B., Bockholt, H., Diener, A., Hoft, S., and Kwade, A. (2015). Measuring the Coating Adhesion Strength of Electrodes for Lithium-Ion Batteries. *International Journal of Adhesion and Adhesives, 60,* 1-8.

[27] Westphal, B. G., Günther, H. B., T., Haselrieder W., and Kwade, A. (2015). Influence of Convective Drying Parameters on Electrode Performance and Physical Electrode Properties *ECS Transactions, 64* (22), 57-68.

[28] Indrikova, M., Grunwald, S., Golks, F., Netz, A., Westphal, B., and Kwade, A. (2015). The Morphology of Battery Electrodes with the Focus of the Conductive Additives Paths. *Journal of the Electrochemical Society, 162* (10), A2021-A2025.

[29] Kaiser, J., Wenzel, V., Nirschl, H., Bitsch, B., Willenbacher, N., Baunach, M., Schmitt, M., Jaiser, S., Scharfer, P., and Schabel, W. (2014). Prozess- Und Produktentwicklung Von Elektroden Für Li-Ionen-Zellen. Process and Product Development of Electrodes for Lithium-Ion Cells. *Chemie Ingenieur Technik, 86* (5), 695-706.

[30] Schilde, C., Mages-Sauter, C., Kwade, A., and Schuchmann, H. P. (2011). Efficiency of Different Dispersing Devices for Dispersing Nanosized Silica and Alumina. *Powder Technology, 207* (1-3), 353-361.

[31] Komoda, Y., Kimura, R., Niga, K., and Suzuki, H. (2011). Formation of Particle Layer within Coated Slurry Characterized by Thickness Variation. *Drying Technology, 29* (9), 1037-1045.

[32] Takase, K., Miura, H., Tamon, H., and Okazaki, M. (1994). Structure Forma tion of Coated Films with Dispersed Pigments During Drying. *Drying Technology, 12* (6)*,* 1279-1296.

[33] Ma, Y., Davis, H. T., and Scriven, L. E. (2005). Microstructure Development in Drying Latex Coatings. *Progress in Organic Coatings, 52* (1)*,* 46-62.

[34] Jaiser, S., Muller, M., Baunach, M., Bauer, W., Scharfer, P., and Schabel, W. (2016). Investigation of Film Solidification and Binder Migration During Drying of Li-Ion Battery Anodes. *Journal of Power Sources, 318,* 210-219.

[35] Liu, D., Chen, L.-C., Liu, T.J., Chu, W.-B., and Tiu, C. (2017). Improvement of Lithium-Ion Battery Performance by Two-Layered Slot–Die Coating Operation. *Energy Technology, accepted manuscript.*

[36] Lim, S., Ahn, K. H., and Yamamura, M. (2013). Latex Migration in Battery Slurries During Drying. *Langmiur, 29* (26), 8233-8244.

[37] Muller, M., Pfaffmann, L., Jaiser, S., Baunach, M., Trouillet, V., Scheiba, F., Scharfer, P., Schabel, W., and Bauer, W. (2017). Investigation of Binder Distribution in Graphite Anodes for Lithium-Ion Batteries. *Journal of Power Sources, 340,* 1-5.

[38] Hagiwara, H., Suszynski, W. J., and Francis, L. F. (2014). A Raman Spectroscopic Method to Find Binder Distribution in Electrodes During Drying. *Journal of Coatings Technology and Research, 11* (1), 11-17.

[39] **Li, C. C. and Wang, Y. W.** (2011). Binder Distributions in Water-Based and Organic-Based Licoo2 Electrode Sheets and Their Effects on Cell Performance. *Journal of the Electrochemical Society, 158* (12), A1361-A1370.

[40] **Jaiser, S., Salach, N. S., Baunach, M., Scharfer, P., and Schabel, W.** (2017). The Impact of Drying Conditions and Wet Filmproperties on Adhesion and Film Solidification of Lithium Ion Battery Anodes. *Drying Technology,* 1-11.

[41] **Baunach, M., Jaiser, S., Cavadini, P., Scharfer, P. and Schabel, W.** (2015). Local Heat Transfer Characteristics of a Slot Nozzle Array for Batch Drying of Thin Films under Industrial Process Conditions. *Journal of Coatings Technology and Research, 12* (5), 915-920.

[42] **Shim, J., and Striebel, K. A.** (2003). Effect of Electrode Density on Cycle Performance and Irreversible Capacity Loss for Natural Graphite Anode in Lithium-Ion Batteries. *Journal of Power Sources, 119,* 934-937.

[43] **Dudney, N. J.** (2005). Solid-State Thin-Film Rechargeable Batteries. *Materials Science and Engineering: B, 116* (3), 245-249.

[44] **Singh, M., Kaiser, J., and Hahn, H.** (2015). Thick Electrodes for High Energy Lithium Ion Batteries. *Journal of the Electrochemical Society, 162* (7), A1196-A1201.

[45] **Collins, J., Gourdin, G., Foster, M., and Qu, D. Y.** (2015). Carbon Surface Functionalities and Sei Formation During Li Intercalation. *Carbon, 92,* 193-244.

[46] **Wang, K. X., Li, X. H., and Chen, J. S.** (2015). Surface and Interface Engineering of Electrode Materials for Lithium-Ion Batteries. *Advanced Materials, 27* (3), 527-545.

[47] **Beguin, F., Chevallier, F., Vix-Guterl, C., Saadallah, S., Bertagna, V., Rouzaud, J. N., and Frackowiak, E.** (2005). Correlation of the Irreversible Lithium Capacity with the Active Surface Area of Modified Carbons. *Carbon, 43* (10), 2160-2167.

[48] **Lee, K. T., Lytle, J. C., Ergang, N. S., Oh, S. M., and Stein, A.** (2005). Synthesis and Rate Performance of Monolithic Macroporous Carbon Electrodes for Lithium-Ion Secondary Batteries. *Advanced Functional Materials, 15* (4), 547-556.

[49] **Roberts, A. D., Li, X., and Zhang, H. F.** (2014). Porous Carbon Spheres and Monoliths: Morphology Control, Pore Size Tuning and Their Applications as Li-Ion Battery Anode Materials. *Chemical Society Reviews, 43* (13), 4341-4356.

[50] **Kakunuri, M., Vennamalla, S., and Sharma, C. S.** (2015). Synthesis of Carbon Xerogel Nanoparticles by Inverse Emulsion Polymerization of Resorcinol-Formaldehyde and Their Use as Anode Materials for Lithium-Ion Battery. *Rsc Advances, 5* (7), 4747-4753.

[51] Korsunsky, A. M., Sui, T., and Song, B. H. (2015). Explicit Formulae for the Internal Stress in Spherical Particles of Active Material within Lithium Ion Battery Cathodes During Charging and Discharging. *Materials & Design, 69,* 247-252.

[52] Chen, S. R., Gordin, M. L., Yi, R., Howlett, G., Sohn, H., and Wang, D. H. (2012). Silicon Core-Hollow Carbon Shell Nanocomposites with Tunable Buffer Voids for High Capacity Anodes of Lithium-Ion Batteries. *Physical Chemistry Chemical Physics, 14* (37), 12741-12745.

[53] Liu, G., Xun, S. D., Vukmirovic, N., Song, X. Y., Olalde-Velasco, P., Zheng, H. H., Battaglia, V. S., Wang, L. W., and Yang, W. L. (2011). Polymers with Tailored Electronic Structure for High Capacity Lithium Battery Electrodes. *Advanced Materials, 23* (40), 4679.

[54] Zhu, Y. H., Xiang, X. X., Liu, E. H., Wu, Y. H., Xie, H., Wu, Z. L., and Tian, Y. Y. (2012). An Activated Microporous Carbon Prepared from Phenol-Melamine-Formaldehyde Resin for Lithium Ion Battery Anode. *Materials Research Bulletin, 47* (8), 2045-2050.

[55] Lee, Y. J., Hwang, M., Choi, H., Baek, J., Baek, Y. K., and Choi, J. H. (2016). Fabrication of Macroporous Si Alloy Anodes Using Polystyrene Beads for Lithium Ion Batteries. *Journal of Applied Electrochemistry, 46* (6), 695-702.

[56] Chan, C. K., Peng, H. L., Liu, G., McIlwrath, K., Zhang, X. F., Huggins, R. A., and Cui, Y. (2008). High-Performance Lithium Battery Anodes Using Silicon Nanowires. *Nature Nanotechnology, 3* (1), 31-35.

[57] Peng, K. Q., Jie, J. S., Zhang, W. J., and Lee, S. T. (2008). Silicon Nanowires for Rechargeable Lithium-Ion Battery Anodes. *Applied Physics Letters, 93* (3), 033105-033109.

[58] Baggetto, L., Danilov, D., and Notten, P. H. L. (2011). HoneycombStructured Silicon: Remarkable Morphological Changes Induced by Electrochemical (De)Lithiation. *Advanced Materials, 23* (13), 1563-1566.

[59] Jia, H. P., Gao, P. F., Yang, J., Wang, J. L., Nuli, Y. N., and Yang, Z. (2011). Novel Three-Dimensional Mesoporous Silicon for High Power Lithium-Ion Battery Anode Material. *Advanced Energy Materials, 1* (6), 1036-1039.

[60] Kim, H., Han, B., Choo, J., and Cho, J. (2008). Three-Dimensional Porous Silicon Particles for Use in High-Performance Lithium Secondary Batteries. *Angewandte Chemie-International Edition, 47* (52), 10151-10154.

[61] Bae, J. (2011). Fabrication of Carbon Microcapsules Containing Silicon Nanoparticles–Carbon Nanotubes Nanocomposite by Sol–Gel Method for Anode in Lithium Ion Battery. *Journal of Solid State Chemistry, 184* (7), 1749-1755.

[62] **Zhou, X. S., Yin, Y. X., Wan, L. J., and Guo, Y. G.(** 2012). Facile Synthesis of Silicon Nanoparticles Inserted into Graphene Sheets as Improved Anode Materials for Lithium-Ion Batteries. *Chemical Communications, 48* (16)*, 2198-2200.

[63] **Jeong, G., Lee, S. M., Choi, N. S., Kim, Y. U., and Lee, C. K.** (2011). Stabilizing Dimensional Changes in Si-Based Composite Electrodes by Controlling the Electrode Porosity: An in Situ Electrochemical Dilatometric Study. *Electrochimica Acta, 56* (14)*, 5095-5101.

[64] **Url-3** <http://www.news-medical.net/life-sciences/What-is-Optical-Microscopy. aspx>, date retrieved 30.05.2017.

[65] **Lawrence, M., and Jiang, Y. (**2017). Bio-Aggregates Based Building Materials Porosity, Pore Size Distribution, *Micro-Structure*. 23, Springer.

[66] **Url-4** <http://www.vcbio.science.ru.nl/public/pdf/fesem_info_eng.pdf>, date ret rieved 30.05.2017.

[67] **Volkert, C. A., and Minor, A. M.** (2007). Focused Ion Beam Microscopy and Micromachining. *Mrs Bulletin, 32* (5)**,** 389-395.

[68] **Url-5 <**http://www.soest.hawaii.edu/HIGP/Faculty/sksharma/GG711/GG711Le c15TEM.pdf>**,** date retrieved 30.05.2017.

[69] **Url-6**<https://www.iitk.ac.in/tkic/workshop/XRD/ppt/Prof%20Anandh/TEM.pd f>date, retrieved 30.05.2017

[70] **Url-7 <**http://afmhelp.com/index.php?option=com_content&view=article&id= 51&Itemid=57>, date retrieved 30.05.2017.

[71] **Donato, I. D., and Lazzara, G.** (2012). Porosity Determination with Helium Pycnometry as a Method to Characterize Waterlogged Woods and the Efficacy of the Conservation Treatments. *Archaeometry, 54,* 906-915.

[72] **Neimark, A. V., and Ravikovitch, P. I.** (1997). Calibration of Pore Volume in Adsorption Experiments and Theoretical Models. *Langmuir, 13* (19)*, 5148-5160.

[73] **Talu, O., and Myers, A. L.** (2001). Molecular Simulation of Adsorption: Gibbs Dividing Surface and Comparison with Experiment. *Aiche Journal, 47* (5)*, 1160-1168.

[74] **Weber, J., and Bastick, M.** (1968). Influence De La Température Sur La Détermination De La Masse Volumique De Divers Carbones Par Pycnométrie Dans L'helium. *Bulletin de la Société Chimique de France, 7,* 2702-2706.

[75] **Liang, B., Liu, Y. P., and Xu, Y. H.** (2014). Silicon-Based Materials as High Capacity Anodes for Next Generation Lithium Ion Batteries. *Journal of Power Sources, 267,* 469-490.

[76] **Zuo, X. X., Zhu, J., Muller-Buschbaum, P., and Cheng, Y. J.** (2017). Silicon Based Lithium-Ion Battery Anodes: A Chronicle Perspective Review. *Nano Energy, 31,* 113-143.

[77] **Park, M. H., Kim, M. G., Joo, J., Kim, K., Kim, J., Ahn, S., Cui, Y., and Cho, J.** (2009). Silicon Nanotube Battery Anodes. *Nano Letters, 9* (11), 3844-3847.

[78] **Abel, P. R., Lin, Y. M., Celio, H., Heller, A., and Mullins, C. B.** (2012). Improving the Stability of Nanostructured Silicon Thin Film Lithium-Ion Battery Anodes through Their Controlled Oxidation. *Acs Nano, 6* (3), 2506-2516.

[79] **Chen, D. Y., Mei, X., Ji, G., Lu, M. H., Xie, J. P., Lu, J. M., and Lee, J. Y.** (2012). Reversible Lithium-Ion Storage in Silver-Treated Nanoscale Hollow Porous Silicon Particles. *Angewandte Chemie-International Edition, 51* (10), 2409-2413.

[80] **Lee, J. I., Lee, K. T., Cho, J., Kim, J., Choi, N. S., and Park, S.** (2012). Chemical-Assisted Thermal Disproportionation of Porous Silicon Monoxide into Silicon-Based Multicomponent Systems. *Angewandte Chemie-International Edition, 51* (11), 2767-2771.

[81] **Lee, J. I., Choi, N. S., and Park, S.** (2012). Highly Stable Si-Based Multicomponent Anodes for Practical Use in Lithium-Ion Batteries. *Energy & Environmental Science, 5* (7), 7878-7882.

[82] **Wen, Z. H., Lu, G. H., Mao, S., Kim, H., Cui, S. M., Yu, K. H., Huang, X. K., Hurley, P. T., Mao, O., and Chen, J. H.** (2013). Silicon Nanotube Anode for Lithium-Ion Batteries. *Electrochemistry Communications, 29,* 67-70.

[83] **Zhu, J., Gladden, C., Liu, N. A., Cui, Y., and Zhang, X.** (2013). Nanoporous Silicon Networks as Anodes for Lithium Ion Batteries. *Physical Chemistry Chemical Physics, 15* (2), 440-443.

[84] **Liu, N. A., Huo, K. F., McDowell, M. T., Zhao, J., and Cui, Y.** (2013). Rice Husks as a Sustainable Source of Nanostructured Silicon for High Performance Li-Ion Battery Anodes. *Scientific Reports, 3,* 1919-1926.

[85] **Wang, W., Favors, Z., Ionescu, R., Ye, R., Bay, H. H., Ozkan, M., and Ozkan, C. S.** (2015). Monodisperse Porous Silicon Spheres as Anode Materials for Lithium Ion Batteries. *Scientific Reports, 5,* 8781-8787.

[86] **Wu, H., Du, N., Shi, X. X., and Yang, D. R.** (2016). Rational Design of Three-Dimensional Macroporous Silicon as High Performance Li-Ion Battery Anodes with Long Cycle Life. *Journal of Power Sources, 331,* 76-81.

[87] **Kim, Y. Y., Lee, J. H., and Kim, H. J.** (2017). Nanoporous Silicon Flakes as Anode Active Material for Lithium-Ion Batteries. *Physica E-Low-Dimensional Systems & Nanostructures, 85,* 223-226.

[88] **Woo, J.-Y., Kim, A. Y., Kim, M. K., Lee, S.-H., Sun, Y.-K., Liu, G., and Lee, J. K.** (2017). Cu3si-Doped Porous-Silicon Particles Prepared by Simplified Chemical Vapor Deposition Method as Anode Material for High-Rate and Long-Cycle Lithium-Ion Batteries. *Journal of Alloys and Compounds, 701,* 425-432.

[89] **Url-8 <**https://www.technologyreview.com/s/601178/the-tesla-model-3-may-depend-on-this-battery-breakthrough/>**,** date retrieved 07.02.2017.

[90] Casimir, A., Zhang, H. G., Ogoke, O., Amine, J. C., Lu, J., and Wu, G. (2016). Silicon-Based Anodes for Lithium-Ion Batteries: Effectiveness of Materials Synthesis and Electrode Preparation. *Nano Energy, 27,* 359-376.

[91] Kim, H., and Cho, J. (2008). Superior Lithium Electroactive Mesoporous Si@Carbon Core-Shell Nanowires for Lithium Battery Anode Material. *Nano Letters, 8* (11)*,* 3688-3691.

[92] Liu, Y., Wen, Z. Y., Wang, X. Y., Hirano, A., Imanishi, N., and Takeda, Y. (2009). Electrochemical Behaviors of Si/C Composite Synthesized from F-Containing Precursors. *Journal of Power Sources, 189* (1)*,* 733-737.

[93] Guo, J. C., Chen, X. L., and Wang, C. S. (2010). Carbon Scaffold Structured Silicon Anodes for Lithium-Ion Batteries. *Journal of Materials Chemistry, 20* (24), 5035-5040.

[94] Tao, H. C., Fan, L. Z., Mei, Y. F., and Qu, X. H. (2011). Self-Supporting Si/Reduced Graphene Oxide Nanocomposite Films as Anode for Lithium Ion Batteries. *Electrochemistry Communications, 13* (12), 1332-1335.

[95] Lu, Z. Y., Zhu, J. X., Sim, D., Shi, W. H., Tay, Y. Y., Ma, J., Hng, H. H., and Yan, Q. Y. (2012). In Situ Growth of Si Nanowires on Graphene Sheets for Li-Ion Storage. *Electrochimica Acta, 74,*176-181.

[96] Ge, M., Lu, Y., Ercius, P., Rong, J., Fang, X., Mecklenburg, M., and Zhou, C. (2013). Large-Scale Fabrication, 3d Tomography, and Lithium-Ion Battery Application of Porous Silicon. *Nano letters, 14* (1), 261-268.

[97] Li, X. J., Lei, G. T., Li, Z. H., Zhang, Y., and Xiao, Q. Z. (2014). Carbon-Encapsulated Si Nanoparticle Composite Nanofibers with Porous Structure as Lithium-Ion Battery Anodes. *Solid State Ionics, 261,* 111-116.

[98] Zhang, R., Du, Y., Li, D., Shen, D., Yang, J., Guo, Z., Liu, H. K., Elzatahry, A. A., and Zhao, D. (2014). Highly Reversible and Large Lithium Storage in Mesoporous Si/C Nanocomposite Anodes with Silicon Nanoparticles Embedded in a Carbon Framework. *Advanced Materials, 26* (39)*,* 6749-6755.

[99] Yue, L., Zhang, W., Yang, J., and Zhang, L. (2014). Designing Si/Porous-C Composite with Buffering Voids as High Capacity Anode for Lithium-Ion Batteries. *Electrochimica Acta, 125,* 206-217.

[100] Tao, H., Fan, L.-Z., Song, W.-L., Wu, M., He, X., and Qu, X. (2014). Hollow Core–Shell Structured Si/C Nanocomposites as High-Performance Anode Materials for Lithium-Ion Batteries. *Nanoscale, 6* (6), 3138-3142.

[101] Han, X., Chen, H., Liu, J., Liu, H., Wang, P., Huang, K., Li, C., Chen, S., and Yang, Y. (2015). A Peanut Shell Inspired Scalable Synthesis of Three-Dimensional Carbon Coated Porous Silicon Particles as an Anode for Lithium-Ion Batteries. *Electrochimica Acta, 156,* 11-19.

[102] **Li, Q., Yin, L., and Gao, X.** (2015). Reduction Chemical Reaction Synthesized Scalable 3d Porous Silicon/Carbon Hybrid Architectures as Anode Materials for Lithium Ion Batteries with Enhanced Electrochemical Performance. *RSC Advances, 5* (45), 35598-35607.

[103] **Wu, J. X., Qin, X. Y., Zhang, H. R., He, Y. B., Li, B. H., Ke, L., Lv, W., Du, H. D., Yang, Q. H., and Kang, F. Y.** (2015). Multilayered Silicon Embedded Porous Carbon/Graphene Hybrid Film as a High Performance Anode. *Carbon, 84,* 434-443.

[104] **Huang, Y.-H., Bao, Q., Duh, J.-G., and Chang, C.-T.** (2016). Top-Down Dispersion Meets Bottom-up Synthesis: Merging Ultranano Silicon and Graphene Nanosheets for Superior Hybrid Anodes for Lithium-Ion Batteries. *Journal of Materials Chemistry A, 4* (25)*,* 9986-9997.

[105] **Kannan, A. G., Kim, S. H., Yang, H. S., and Kim, D.-W.** (2016). Silicon Nanoparticles Grown on a Reduced Graphene Oxide Surface as High-Performance Anode Materials for Lithium-Ion Batteries. *RSC Advances, 6* (30), 25159-25166.

[106] **Ding, X., Liu, X., Huang, Y., Zhang, X., Zhao, Q., Xiang, X., Li, G., He, P., Wen, Z., Li, J., and Huang, Y.** (2016). Enhanced Electrochemical Performance Promoted by Monolayer Graphene and Void Space in Silicon Composite Anode Materials. *Nano Energy, 27,* 647-657.

[107] **Gao, P. B., Tang, H., Xing, A., and Bao, Z. H.** (2017). Porous Silicon from the Magnesiothermic Reaction as a High-Performance Anode Material for Lithium Ion Battery Applications. *Electrochimica Acta, 228,* 545-552.

[108] **Kasavajjula, U., Wang, C. S., and Appleby, A. J.** (2007). Nano- and Bulk-Silicon-Based Insertion Anodes for Lithium-Ion Secondary Cells. *Journal of Power Sources, 163* (2), 1003-1039.

[109] **Ohara, S., Suzuki, J., Sekine, K., and Takamura, T.** (2003). Li Insertion/Extraction Reaction at a Si Film Evaporated on a Ni Foil. *Journal of Power Sources, 119,* 591-596.

[110] **Liu, Y., Chen, B., Cao, F., Chan, H. L. W., Zhao, X., and Yuan, J.** (2011). One-Pot Synthesis of Three-Dimensional Silver-Embedded Porous Silicon Micronparticles for Lithium-Ion Batteries. *Journal of Materials Chemistry, 21* (43)*,* 17083-17086.

[111] **Jung, H., Kim, Y.-U., Sung, M.-S., Hwa, Y., Jeong, G., Kim, G.-B., and Sohn, H.-J.** (2011). Nanosize Si Anode Embedded in Super-Elastic Nitinol (Ni-Ti) Shape Memory Alloy Matrix for Li Rechargeable Batteries. *Journal of Materials Chemistry, 21* (30)*,* 11213-11216.

[112] **Son, S.-B., Kim, S. C., Kang, C. S., Yersak, T. A., Kim, Y.-C., Lee, C.-G., Moon, S.-H., Cho, J. S., Moon, J.-T., Oh, K. H., and Lee, S.-H.** (2012). A Highly Reversible Nano-Si Anode Enabled by Mechanical Confinement in an Electrochemically Activated $Li_x ti_4 ni4 si7$ Matrix. *Advanced Energy Materials, 2* (10), 1226-1231.

[113] Kohandehghan, A., Cui, K., Kupsta, M., Memarzadeh, E., Kalisvaart, P., and Mitlin, D. (2014). Nanometer-Scale Sn Coatings Improve the Performance of Silicon Nanowire Lib Anodes. *Journal of Materials Chemistry A, 2* (29)*,* 11261-11279.

[114] Fang, S., Shen, L. F., Xu, G. Y., Nie, P., Wang, J., Dou, H., and Zhang, X. G. (2014). Rational Design of Void-Involved Si@Tio2 Nanospheres as High-Performance Anode Material for Lithium-Ion Batteries. *Acs Applied Materials & Interfaces, 6* (9), 6497-6503.

[115] Jo, M. R., Heo, Y. U., Lee, Y. C., and Kang, Y. M. (2014). A Nano-Si/Fesi2ti Hetero-Structure with Structural Stability for Highly Reversible Lithium Storage. *Nanoscale, 6* (2), 1005-1010.

[116] Li, C. L., Zhang, P., and Jiang, Z. Y. (2015). Effect of Nano Cu Coating on Porous Si Prepared by Acid Etching Al-Si Alloy Powder. *Electrochimica Acta, 161,* 408-412.

[117] Park, J.-B., Ham, J.-S., Shin, M.-S., Park, H.-K., Lee, Y.-J., and Lee, S.-M. (2015). Synthesis and Electrochemical Characterization of Anode Material With titanium–Silicon Alloy Solid Core/Nanoporous Silicon Shell Structures for Lithium Rechargeable Batteries. *Journal of Power Sources, 299,* 537-543.

[118] Du, Z. J., Ellis, S. N., Dunlap, R. A., and Obrovac, M. N. (2016). Nixsi1-X Alloys Prepared by Mechanical Milling as Negative Electrode Materials for Lithium Ion Batteries. *Journal of the Electrochemical Society, 163* (2)*,* A13-A18.

[119] Hwang, S. W., Lee, J. K., and Yoon, W. Y. (2013). Electrochemical Behavior of Carbon-Coated Silicon Monoxide Electrode with Chromium Coating in Rechargeable Lithium Cell. *Journal of Power Sources, 244,* 620-624.

[120] Lv, P. P., Zhao, H. L., Wang, J., Liu, X., Zhang, T. H., and Xia, Q. (2013). Facile Preparation and Electrochemical Properties of Amorphous Sio2/C Composite as Anode Material for Lithium Ion Batteries. *Journal of Power Sources, 237,* 291-294.

[121] Kim, K. W., Park, H., Lee, J. G., Kim, J., Kim, Y. U., Ryu, J. H., Kim, J. J., and Oh, S. M. (2013). Capacity Variation of Carbon-Coated Silicon Monoxide Negative Electrode for Lithium-Ion Batteries. *Electrochimica Acta, 103,* 226-230.

[122] Lee, J. K., Lee, J. H., Kim, B. K., and Yoon, W. Y. (2014). Electrochemical Characteristics of Diamond-Like Carbon/Cr Double-Layer Coating on Silicon Monoxide-Graphite Composite Anode for Li-Ion Batteries. *Electrochimica Acta, 127,* 1-6.

[123] Yang, N.-H., Wu, Y.-S., Chou, J., Wu, H.-C., and Wu, N.-L. (2015). Silicon Oxide-on-Graphite Planar Composite Synthesized Using a Microwave-Assisted Coating Method for Use as a Fast-Charging Lithium-Ion Battery Anode. *Journal of Power Sources, 296,* 314-317.

[124] **Yuan, X. Q., Xin, H. X., Qin, X. Y., Li, X. J., Liu, Y. F., and Guo, H. F.** (2015). Self-Assembly of Sio/Reduced Graphene Oxide Composite as High-Performance Anode Materials for Li-Ion Batteries. *Electrochimica Acta, 155,* 251-256.

[125] **Kim, J. Y., Nguyen, D. T., Kang, J. S., and Song, S. W.** (2015). Facile Synthesis and Stable Cycling Ability of Hollow Submicron Silicon Oxide-Carbon Composite Anode Material for Li-Ion Battery. *Journal of Alloys and Compounds, 633,* 92-96.

[126] **Lv, P. P., Zhao, H. L., Gao, C. H., Zhang, T. H., and Liu, X.** (2015). Highly Efficient and Scalable Synthesis of Siox/C Composite with Core-Shell Nanostructure as High-Performance Anode Material for Lithium Ion Batteries. *Electrochimica Acta, 152,* 345-351.

[127] **Woo, J., Baek, S. H., Park, J. S., Jeong, Y. M., and Kim, J. H.** (2015). Improved Electrochemical Performance of Boron-Doped Sio Negative Electrode Materials in Lithium-Ion Batteries. *Journal of Power Sources, 299,* 25-31.

[128] **Wang, H., Wu, P., Shi, H. M., Tang, W. Z., Tang, Y. W., Zhou, Y. M., She, P. L., and Lu, T. H.** (2015). Hollow Porous Silicon Oxide Nanobelts for High-Performance Lithium Storage. *Journal of Power Sources, 274,* 951-956.

[129] **Xu, X. F., Zhang, H. Y., Chen, Y. M., Li, N., Li, Y. Y., and Liu, L. Y.** (2016). Sio2@Sno2/Graphene Composite with a Coating and Hierarchical Structure as High Performance Anode Material for Lithium Ion Battery. *Journal of Alloys and Compounds, 677,* 237-244.

[130] **Wu, W. J., Liang, Y. H., Ma, H. Y., Peng, Y., and Yang, H. B.** (2016). Insights into the Conversion Behavior of Sio-C Hybrid with Pre-Treated Graphite as Anodes for Li-Ion Batteries. *Electrochimica Acta, 187,* 473-479.

[131] **Shi, L., Wang, W. K., Wang, A. B., Yuan, K. G., Jin, Z. Q., and Yang, Y. S.** (2016). Scalable Synthesis of Core-Shell Structured Siox/Nitrogen-Doped Carbon Composite as a High-Performance Anode Material for Lithium-Ion Batteries. *Journal of Power Sources, 318,* 184-191.

[132] **Gu, J. W., Zeng, Y., Feng, X. F., Wu, X. M., Zeng, C. M., and Li, M. Q.** (2016). Synthesis of Nanosilicon@Nonstoichiometric Silicon Oxide from Bulk Silicon Dioxide and Its Lithium Storage Properties. *Journal of Alloys and Compounds, 662,* 185-192.

[133] **Bai, X. J., Yu, Y. Y., Kung, H. H., Wang, B., and Jiang, J. M.** (2016). Si@SiOx/Graphene Hydrogel Composite Anode for Lithium-Ion Battery. *Journal of Power Sources, 306,* 42-48.

[134] **Zhang, J. Y., Zhang, C. Q., Liu, Z., Zheng, J., Zuo, Y. H., Xue, C. L., Li, C. B., and Cheng, B. W.** (2017). High-Performance Ball-Milled SiOx Anodes for Lithium Ion Batteries. *Journal of Power Sources, 339,* 86-92.

[135] Obrovac, M. N., and Krause, L. J. (2007). Reversible Cycling of Crystalline Silicon Powder. *Journal of the Electrochemical Society, 154* (2), A103-A108.

[136] Obrovac, M. N., and Chevrier, V. L. (2014). Alloy Negative Electrodes for Li-Ion Batteries. *Chemical Reviews, 114* (23), 11444-11502.

[137] Li, J., and Dahn, J. R. (2007). An in Situ X-Ray Diffraction Study of the Reaction of Li with Crystalline Si. *Journal of the Electrochemical Society, 154* (3), A156-A161.

[138] Agubra, V. A., and Fergus, J. W. (2014). The Formation and Stability of the Solid Electrolyte Interface on the Graphite Anode. *Journal of Power Sources, 268,* 153-162.

[139] Verma, P., Maire, P., and Novak, P. (2010). A Review of the Features and Analyses of the Solid Electrolyte Interphase in Li-Ion Batteries. *Electrochimica Acta, 55* (22), 6332-6341.

[140] Peled, E. (1979). The Electrochemical Behavior of Alkali and Alkaline Earth Metals in Nonaqueous Battery Systems—the Solid Electrolyte Interphase Model. *Journal of the Electrochemical Society, 126* (12), 2047-2051.

[141] Arora, P., White, R . E., and Doyle, M., (1998). Capacity Fade Mechanisms and Side Reactions in Lithium-Ion Batteries. *Journal of the Electrochemical Society, 145* (10), 3647-3667.

[142] Cheng, X. B., Zhang, R., Zhao, C. Z., Wei, F., Zhang, J. G., and Zhang, Q. (2016). A Review of Solid Electrolyte Interphases on Lithium Metal Anode. *Advanced Science, 3* (3), 1500213-1500233.

[143] Guo, B. K., Shu, J., Wang, Z. X., Yang, H., Shi, L. H., Liu, Y. N., and Chen, L. Q. (2008). Electrochemical Reduction of Nano-Sio2 in Hard Carbon as Anode Material for Lithium Ion Batteries. *Electrochemistry Communications, 10* (12), 1876-1878.

[144] Yaroshevsky, A. A. (2006). Abundances of Chemical Elements in the Earth's Crust. *Geochemistry International, 44* (1), 48-55.

[145] Miyachi, M., Yamamoto, H., Kawai, H., Ohta, T., and Shirakata, M. (2005). Analysis of Sio Anodes for Lithium-Ion Batteries. *Journal of the Electrochemical Society, 152* (10), A2089-A2091.

[146] Gao, B., Sinha, S., Fleming, L., and Zhou, O. (2001). Alloy Formation in Nanostructured Silicon. *Advanced Materials, 13* (11), 816.

[147] Yang, J., Takeda, Y., Imanishi, N., Capiglia, C., Xie, J. Y., and Yamamoto, O. (2002). SiOx-Based Anodes for Secondary Lithium Batteries. *Solid State Ionics, 152,* 125-129.

[148] Sun, Q., Zhang, B., and Fu, Z.-W. (2008). Lithium Electrochemistry of Sio2 Thin Film Electrode for Lithium-Ion Batteries. *Applied Surface Science, 254* (13), 3774-3779.

[149] Xu, W. (2011). Silicon Nanowire Anode for Lithium-Ion Batteries: Fabrication, Characterization and Solid Electrolyte Interphase. PhD, Louisiana State University and Agricultural and Mechanical College.

[150] **Beaulieu, L. Y., Eberman, K. W., Turner, R. L., Krause, L. J., and Dahn, J. R.** (2001). Colossal Reversible Volume Changes in Lithium Alloys. *Electrochemical and Solid State Letters, 4* (9), A137-A140.

[151] **Ulldemolins, M., Le Cras, F., Pecquenard, B., Phan, V. P., Martin, L., and Martinez, H.** (2012). Investigation on the Part Played by the Solid Electrolyte Interphase on the Electrochemical Performances of the Silicon Electrode for Lithium-Ion Batteries. *Journal of Power Sources, 206,* 245-252.

[152] **Zhang, S. S.** (2006). A Review on Electrolyte Additives for Lithium-Ion Batteries. *Journal of Power Sources, 162* (2), 1379-1394.

[153] **Park, S. J., Zhao, H., Ai, G., Wang, C., Song, X. Y., Yuca, N., Battaglia, V. S., Yang, W. L., and Liu, G.** (2015). Side-Chain Conducting and Phase-Separated Polymeric Binders for High-Performance Silicon Anodes in Lithium-Ion Batteries. *Journal of the American Chemical Society, 137* (7), 2565-2571.

[154] **Burns, J. C., Krause, L. J., Le, D. B., Jensen, L. D., Smith, A. J., Xiong, D. J., and Dahn, J. R.** (2011). Introducing Symmetric Li-Ion Cells as a Tool to Study Cell Degradation Mechanisms. *Journal of the Electrochemical Society, 158* (12), A1417-A1422.

[155] **Quigley, V. P., and Richard, J. J. I. I**. (1989). Process for Neutralizing Crosslinked Poly (Acrylic Acid). In Google Patents.

[156] **Yao, Y., Zhang, J., Xue, L., Huang, T., and Yu, A.** (2011). Carbon-Coated SiO_2 Nanoparticles as Anode Material for Lithium Ion Batteries. *Journal of Power Sources, 196* (23), 10240-10243.

[157] **Etacheri, V., Haik, O., Goffer, Y., Roberts, G. A., Stefan, I. C., Fasching, R., and Aurbach, D.** (2012). Effect of Fluoroethylene Carbonate (Fec) on the Performance and Surface Chemistry of Si-Nanowire Li-Ion Battery Anodes. *Langmuir, 28* (1), 965-976.

[158] **Vu, A., Qian, Y. Q., and Stein, A.** (2012). Porous Electrode Materials for Lithium-Ion Batteries - How to Prepare Them and What Makes Them Special. *Advanced Energy Materials, 2* (9), 1056-1085.

[159] **Bhosale, M. A., and Bhanage, B. M.** (2017). A Simple, Additive Free Approach for Synthesis of Cu/Cu_2o Nanoparticles: Effect of Precursors in Morphology Selectivity. *Journal of Cluster Science, 28* (3), 1215-1224.

[160] **Song, J. L., Xu, W. J., Lu, Y., and Fan, X. J.** (2011). Rapid Fabrication of Superhydrophobic Surfaces on Copper Substrates by Electrochemical Machining. *Applied Surface Science, 257* (24), 10910-10916.

[161] **Harry, K. J., Hallinan, D. T., Parkinson, D. Y., MacDowell, A. A., and Balsara, N. P.** (2014). Detection of Subsurface Structures Underneath Dendrites Formed on Cycled Lithium Metal Electrodes. *Nature Materials, 13* (1), 69-73.

[162] **Weber, A. Z., Borup, R. L., Darling, R. M., Das, P. K., Dursch, T. J., Gu, W. B., Harvey, D., Kusoglu, A., Litster, S., Mench, M. M., Mukundan, R., Owejan, J. P., Pharoah, J. G., Secanell, M., and Zenyuk, I. V.** (2014). A Critical Review of Modeling Transport Phenomena in Polymer-Electrolyte Fuel Cells. *Journal of the Electrochemical Society, 161* (12), F1254-F1299.

[163] **Dai, Y. L., Cai, L., and White, R. E.** (2014). Simulation and Analysis of Stress in a Li-Ion Battery with a Blended $LiMn_2O_4$ and $LiNi_{0.8}Co_{0.15}Al_{0.05}O_2$ Cathode. *Journal of Power Sources, 247,* 365-376.

[164] **Dai, Y. L., Cai, L., and White, R. E.** (2014). Simulation and Analysis of Inhomogeneous Degradation in Large Format $LiMn_2O_4$/Carbon Cells. *Journal of the Electrochemical Society, 161* (8), E3348-E3356.

[165] **Zhao, H., Park, S. J., Shi, F. F., Fu, Y. B., Battaglia, V., Ross, P. N., and Liu, G.** (2014). Propylene Carbonate (Pc)-Based Electrolytes with High Coulombic Efficiency for Lithium-Ion Batteries. *Journal of the Electrochemical Society, 161* (1), A194-A200.

[166] **Chang, W. S., Park, C. M., Kim, J. H., Kim, Y. U., Jeong, G., and Sohn, H. J.** (2012). Quartz (SiO_2): A New Energy Storage Anode Material for Li-Ion Batteries. *Energy & Environmental Science, 5* (5), 6895-6899.

[167] **Zhao, H., Wang, Z. H., Lu, P., Jiang, M., Shi, F. F., Song, X. Y., Zheng, Z. Y., Zhou, X., Fu, Y. B., Abdelbast, G., Xiao, X. C., Liu, Z., Battaglia, V. S., Zaghib, K., and Liu, G.** (2014). Toward Practical Application of Functional Conductive Polymer Binder for a High-Energy Lithium-Ion Battery Design. *Nano Letters, 14* (11), 6704-6710.

[168] **Boisvert, J.-P., Malgat, A., Pochard, I., and Daneault, C.** (2002). Influence of the Counter-Ion on the Effective Charge of Polyacrylic Acid in Dilute Condition. *Polymer, 43* (1), 141-148.

[169] **Kirwan, L. J., Fawell, P. D., and van Bronswijk, W.** (2003). In Situ Ftir-Atr Examination of Poly(Acrylic Acid) Adsorbed onto Hematite at Low Ph. *Langmuir, 19* (14), 5802-5807.

[170] **Leveau, L., Laik, B., Pereira-Ramos, J. P., Gohier, A., Tran-Van, P., and Cojocaru, C. S.** (2016). Silicon Nano-Trees as High Areal Capacity Anodes for Lithium-Ion Batteries. *Journal of Power Sources, 316,* 1-7.

[171] **Han, Z. J., Yabuuchi, N., Hashimoto, S., Sasaki, T., and Komaba, S.** (2013). Cross-Linked Poly(Acrylic Acid) with Polycarbodiimide as Advanced Binder for Si/Graphite Composite Negative Electrodes in Li-Ion Batteries. *Ecs Electrochemistry Letters, 2* (2), A17-A20.

[172] **Nguyen, C. C., Yoon, T., Seo, D. M., Guduru, P., and Lucht, B. L.** (2016). Systematic Investigation of Binders for Silicon Anodes: Interactions of Binder with Silicon Particles and Electrolytes and Effects of Binders on Solid Electrolyte Interphase Formation. *Acs Applied Materials & Interfaces, 8* (19), 12211-12220.

[173] **Bie, Y. T., Yang, J., Liu, X. L., Wang, J. L., Nuli, Y. N., and Lu, W.** (2016). Polydopamine Wrapping Silicon Cross-Linked with Polyacrylic Acid as High-Performance Anode for Lithium-Ion Batteries. *Acs Applied Materials & Interfaces, 8* (5), 2899-2904.

[174] **Song, J. X., Zhou, M. J., Yi, R., Xu, T., Gordin, M. L., Tang, D. H., Yu, Z. X., Regula, M., and Wang, D. H.** (2014). Interpenetrated Gel Polymer Binder for High-Performance Silicon Anodes in Lithium-Ion Batteries. *Advanced Functional Materials, 24* (37), 5904-5910.

[175] **Yoon, T., Nguyen, C. C., Seo, D. M., and Lucht, B. L.** (2015). Capacity Fading Mechanisms of Silicon Nanoparticle Negative Electrodes for Lithium Ion Batteries. *Journal of the Electrochemical Society, 162* (12), A2325-A2330.

[176] **Luo, J. Y., Zhao, X., Wu, J. S., Jang, H. D., Kung, H. H., and Huang, J. X.** (2012). Crumpled Graphene-Encapsulated Si Nanoparticles for Lithium Ion Battery Anodes. *Journal of Physical Chemistry Letters, 3* (13), 1824-1829.

[177] **Li, Y., Xu, G. J., Xue, L. G., Zhang, S., Yao, Y. F., Lu, Y., Toprakci, O., and Zhang, X. W.** (2013). Enhanced Rate Capability by Employing Carbon Nanotube-Loaded Electrospun Si/C Composite Nanofibers as Binder-Free Anodes. *Journal of the Electrochemical Society, 160* (3), A528-A534.

[178] **Bruggeman, D. A. G.** (1935). Berechnung Verschiedener Physikalischer Konstanten Von Heterogenen Substanzen. I. Dielektrizitätskonstanten Und Leitfähigkeiten Der Mischkörper Aus Isotropen Substanzen. *Annalen der Physik, 416* (7), 636-664.

[179] **Han, P., Yuan, T., Yao, L., Han, Z., Yang, J. H., and Zheng, S. Y.** (2016). Copper Nanoparticle-Incorporated Carbon Fibers as Free-Standing Anodes for Lithium-Ion Batteries. *Nanoscale Research Letters, 11* (1), 172.

[180] **Li, C.-H., Sengodu, P., Wang, D.-Y., Kuo, T.-R., and Chen, C.-C.** (2015). Highly Stable Cycling of a Lead Oxide/Copper Nanocomposite as an Anode Material in Lithium Ion Batteries. *RSC Advances, 5* (62), 50245-50252.

[181] **Polat, B. D., Keles, O., and Amine, K.** (2015). Silicon-Copper Helical Arrays for New Generation Lithium Ion Batteries. *Nano Letters, 15* (10), 6702-6708.

[182] **Zhang, J. Y., Zhang, C. Q., Wu, S. M., Liu, Z., Zheng, J., Zuo, Y. H., Xue, C. L., Li, C. B., and Cheng, B. W.** (2016). $Cu_2^{+1}O$ Coated Polycrystalline Si Nanoparticles as Anode for Lithium-Ion Battery. *Nanoscale Research Letters, 11* (1), 214.

[183] **Fang, K., Wang, M., Xia, Y., Li, J., Ji, Q., Yin, S., Xie, S., Ban, J., Wang, X., Qiu, B., Liu, Z., Chen, C., and Cheng, Y. J.** (2017). Facile Fabrication of Silicon Nanoparticle Lithium-Ion Battery Anode Reinforced with Copper Nanoparticles. *Digest Journal of Nanomaterials & Biostructures (DJNB), 12* (2), 243-253.

[184] Suk, J., Kim, D. Y., Kim, D. W., and Kang, Y. (2014). Electrodeposited 3d Porous Silicon/Copper Films with Excellent Stability and High Rate Performance for Lithium-Ion Batteries. *Journal of Materials Chemistry A, 2* (8), 2478-2481.

CURRICULUM VITAE

Name Surname: Neslihan Yuca

Place and Date of Birth: Istanbul, 16.02.1986

E-Mail: nyuca@itu.edu.tr

EDUCATION:

B.Sc.: Environmental Engineering, Cukurova University, 2008

M.Sc.: Energy Science and Technology, Energy Institute, ITU, 2010

PROFESSIONAL EXPERIENCE AND REWARDS:

- CEO, Enwair Energy Technologies Corp., 2015-
- Visiting Researcher, Lawrence Berkeley National Laboratory, CA, ABD, 2013-2014.
- Research Assistant, Energy Institute, Istanbul Technical University, 2010-2016.
- Assistant Engineer, UNIDO ICHET, 2009-2010.

PUBLICATIONS ON THE THESIS:

- Hui Zhao, **Neslihan Yuca**, Ziyan Zheng, Yanbao Fu, Vincent S. Battaglia, Guerfi Abdelbast, Karim Zaghib, and Gao Liu, (2015). High capacity and high density functional conductive polymer and SiO anode for high-energy lithium-ion batteries, ACS Applied Materials & Interfaces, *7 (1)*, 862-866.

- Sang-Jae Park, Hui Zhao, Guo Ai, Cheng Wang, Xiangyun Song, **Neslihan Yuca**, Vincent S. Battaglia, Wanli Yang and Gao Liu, (2015). Side-chain conducting and phase-separated polymeric binders for high-performance silicon anodes in lithium-ion batteries, Journal of the American Chemical Society, *137 (7),* 2565-2571.

- Hui Zhao, Qing Yang, **Neslihan Yuca,** Min Ling, Kenneth Higa, Vincent Battaglia, Dilworth Parkinson, Venkat Srinivasan, Gao Liu, (2016). A convenient and versatile method to control the electrode microstructure toward high-energy lithium-ion batteries, Nano Letters, *16 (7),* 4686–4690.

- **Neslihan Yuca**, Üner Çolak, (2016). A facile and functional process to enhance electrochemical performance of silicon anode in lithium ion batteries, Electrochimica Acta, *222,* 1538-1544.

OTHER PUBLICATIONS, PRESENTATIONS AND PATENTS :

SCI Publications:

- Yasin Karagöz, **Neslihan Yuca**, Tarkan Sandalcı, A. Selim. Dalkılıç, Effect of hydrogen and oxygen addition as a mixture on emissions and performance characteristics of a gasoline engine, International Journal of Hydrogen Energy, 2016, 40 (28), pp. 8750–8760.

- **Neslihan Yuca**, Hui Zhao, Xiangyun Song, Murat Ferhat Dogdu, Wen Yuan, Yanbao Fu, Vincent S. Battaglia, Xingcheng Xiao, and Gao Liu. A systematic investigation of polymer binder flexibility on the electrode performance for lithium-ion batteries, ACS Applied Materials & Interfaces, 2014, 6, 17111−17118.

- Hui Zhao, Xin Zhou, Sang-Jae Park, Feifei Shi, Yanbao Fu, Min Ling, **Neslihan Yuca,** Vincent Battaglia, Gao Liu, A polymerized vinylene carbonate anode binder enhances performance of lithium-ion batteries, Journal Of Power Sources, 263, 288–295, 2014.

- **Neslihan Yuca,** Nilgün Karatepe, Yakuphanoğlu F., Hepuzer. G. Y., Thermal and Electrical Properties of Carbon Nanotube Based Materials, Acta Physica Polonica A, 2013, 123 (2), 352-354.

- Nilgün Karatepe, **Neslihan Yuca**, B. Filiz Şenkal, Synthesis of Carbon Based Nano Materials for Hydrogen Storage, Fullerens, Nanotubes and Carbon nanostructures, 2013, 21 (1), 31-46.

- Nilgün Karatepe, **Neslihan Yuca**, Hydrogen Adsorption on Carbon Nanotubes Purified By Different Methods, International Journal of Hydrogen Energy, 2011, 36 (17), 11467-11473.

Other Publications:

- **Neslihan Yuca,** Hıi Zhao, Ziyan Zheng, Vincent Battaglia, Karim Zaghib, and Gao Liu, High Capacity and High Density Sio Anode for High-Energy Lithium-Ion Batteries, 227th ECS Meeting, May 24-28, 2015, Chicago, IL, USA.

- **Neslihan Yuca**, Hui Zhao, Murat Ferhat Dogdu, Vincent S. Battaglia, Gao Liu. Effect of flexible polymer binders on electrochemical performance of graphite negative electrode for lithium ion batteries. 248th ACS National Meeting & Exposition, August 10-14, 2014, San Francisco, CA, USA.

- **Neslihan Yuca**, Hui Zhao, Murat Ferhat Dogdu, Vincent S. Battaglia, Gao Liu. An Improved Flexible Binder for Graphite Anode in Li-Ion Battery: Toward a Better Binding Performance, 225th ECS Meeting, May 11-15, 2014, Orlando, FL, USA.

- **Neslihan Yuca**, Zeyneb Camtakan, Nilgün Karatepe, Different Techniques for Characterizing Single-Walled Carbon Nanotube Purity, SPIE NanoScience + Engineering, Carbon Nanotubes, Graphene, and Associated Devices, August 24-30, 2013 San Diego, CA, USA.

- **Neslihan Yuca**, Fatih Gümüş, Nilgün Karatepe, The Role of H_2 Reduction in the Growth of Single-Walled Carbon Nanotubes, SPIE NanoScience + Engineering, Carbon Nanotubes, Graphene, and Associated Devices, August 24-30, 2013, San Diego, CA, USA.

- Fatih Gümüş, **Neslihan Yuca**, Nilgün Karatepe, Carbon nanotube synthesis with different support materials and catalysts, SPIE NanoScience + Engineering, Carbon Nanotubes, Graphene, and Associated Devices, August 24-30, 2013, San Diego, CA, USA.

- **Neslihan Yuca**, Nilgün Karatepe, Hydrogen Adsorption Properties Of Carbon Nanotubes Synthesized At Different Temperatures, Global Conference on Global Warming-2012 (GCGW-12), July, 8-12, 2012, Istanbul, Turkey.

- Ayşenur Örs, **Neslihan Yuca**, Nilgün Karatepe, B. Filiz Şenkal, Synthesis And Thermal Properties of Boric Acid Doped Polyaniline/Carbon Nanotube Composites, Academic Journal of Science, 1(3), pp. 49–57, 2012.

- Mustafa Can Çelebi, **Neslihan Yuca**, Nilgün Karatepe, Investigation of Thermal Decomposition Behavior Of Olive Cake, Academic Journal of Science, 1(3), pp. 59-65, 2012.

- Nazlı Çınar, **Neslihan Yuca**, Nilgün Karatepe, "Effect of H_2 reduction on Carbon Nanotube Synthesis", TOJSAT : The Online Journal of Science and Technology, 2 (2), pp. 20-25, 2012.

- **Neslihan Yuca**, Nilgün Karatepe, "Hydrogen Storage In Single-Walled Carbon Nanotubes Purified By Microwave Digestion Method", World Academy of Science, Engineering and Technology 79 , pp. 605-610, 2011.

- **Neslihan Yuca**, Nilgün Karatepe, Fahrettin Yakuphanoğlu, "Thermal and Electrical Properties of Carbon Nanotubes Purified by Acid Digestion", World Academy of Science, Engineering and Technology 79 , pp. 611-616, 2011.

International Presentations:

- **Neslihan Yuca**, Hui Zhao, Murat Ferhat Dogdu, Vincent S. Battaglia, Gao Liu. Effect of flexible polymer binders on electrochemical performance of graphite negative electrode for lithium ion batteries. 248th ACS National Meeting & Exposition, August 10-14, 2014, San Francisco, CA, USA.

- **Neslihan Yuca**, Hui Zhao, Murat Ferhat Dogdu, Vincent S. Battaglia, Gao Liu. An Improved Flexible Binder for Graphite Anode in Li-Ion Battery: Toward a Better Binding Performance, 225th ECS Meeting, May 11-15, 2014, Orlando, FL, USA,

- **Neslihan Yuca**, Nilgün Karatepe, "Hydrogen Adsorption Properties of Carbon Nanotubes Synthesized at Different Temperatures", Global Conference on Global Warming 2012 (GCGW-12), 8-12 Temmuz, 2012, İstanbul, Türkiye.

- Nilgün Karatepe, **Neslihan Yuca**, B. Filiz Şenkal, Hydrogen Storage In Carbon Based Nano Structures. 5th International Ege Energy Symposium and Exhibition (IEESE-5), 27-30 Haziran, 2010 Denizli, Türkiye.

- **Neslihan Yuca**, Nilgün Karatepe, Purification Techniques for Carbon Nanotubes. International Conference on Nanomaterials and Nanosystems, 10-13 Ağustos, 2009 İstanbul, Türkiye.

National Presentations:

- **Neslihan Yuca,** Candeniz Seçkin, Ayşenur Örs, Nilgün Karatepe, Karbon Nanotüp Üretimi Ve Hidrojen Depolamada Kullanılabilirliğinin İncelenmesi. IV. Ulusal Hidrojen Enerjisi Kongresi, 15-16 Ekim, 2009 Kocaeli, Türkiye.

Patents:

- İletken Ve Esnek Polimerlerin Lityum Bataryalarda Kullanılması, TPE, Dosya No: 2016/00220 (applied).

- Usage of Conductive and Flexible Polymers in Lithium Batteries, PCT, Application No: 050518 (applied).